Cranfield University

MICHAIL TSENTSERIS

ARES: MILITARY AIRCRAFT PROPULSION INTEGRATION

SCHOOL OF ENGINEERING

MPhil THESIS

Cranfield University

School of Engineering

Department of Power Engineering and Propulsion

MPhil THESIS

Academic Year 2012-2013

MICHAIL TSENTSERIS

ARES: Military Aircraft Propulsion Integration

Supervisor: Pr P. PILIDIS

February 2013

ABSTRACT

The combat aircraft and the gas turbine engine interact with one another. These interactions have become of even greater significance than previously due to the fact that the modern aircraft have increased requirements in terms of thrust, efficiency, reliability and ease of maintenance. Issues that affect the performance and operational capability of combat aircraft are the aircraft aerodynamic characteristics, propulsion system performance and the airframe/engine matching.

This study focuses on the evaluation of the propulsion system of modern jet powered combat aircraft and combines computations with the existing integration methodology. The main objective of this study is the update of ARES method (aircraft-engine performance tool for combat aircraft) so as to be feasible the incorporation of new data in the calculations of the program. The update contains:

- the establishment of a procedure that can be used for the calculation of the additional drag that a external load (tanks, bombs, missiles, pods) contribute in the total aircraft drag,
- the modification of ARES method in order to integrate the additional drag of the external loads in the program calculations,
- the creation of a procedure that will be used for the calculation of the thrust deductions due to installation effects.

The information that can be received from this study are valuable because can be used in the evaluation of the engine performance, can give the opportunity for further engine studies such as the structural and thermal analysis, component sizing and geometry, life consumption and of course can make apparent if a specific aircraft-engine system is capable of accomplishing a demanded operating requirement.

The final results of the study led to the general conclusion that the total aircraft drag and the demanded uninstalled net thrust increased with the addition of external tanks in the aircraft. The fuel consumption was higher for the configuration with the two tanks and was noticed an increase of the TET which is proportional to the number of the used external tanks (max TET increases at least 0.8% per tank). Additionally was extracted the conclusion that the addition of an external wing tank increases the amount of the consumed fuel at least 3.5%.

Table of Contents

Table of Figures

List of Tables

Nomenclature

NOTATION

A_1	Annulus Area
AC	Capture Area
A_{ef}	Engine Face Gross Area
A_H	Highlight Area
Ath	Throat Area
Dnac,ref	Nacelle Reference Drag
FN	Net Thrust
$F_{N,installed}$	Installed Net Thrust
$F_{N,uninstalled}$	Uninstalled Net Thrust
Lduct	Diffuser Length
M	Mach Number
M_{throat}	Throat Mach number
p	Static Pressure
P	Total Pressure
$P_{t,engine\ face(ef)}$	Absolute Pressure at Engine Face
P_{to}	Pressure at Sea Level Static
q	Dynamic Pressure
qo	Flight Dynamic Head
R	Gas Constant
T	Thrust
t	Static Temperature

T	Total Temperature
Tamb	Ambient Temperature
W	Aircraft Weight or Mass Flow
Wc_{ef}	Engine Corrected Mass Flow
Wc_{th}	Corrected Throat Flow
ΔCD	Spillage Drag Coefficient
$\Delta Dspill$	Spillage Drag
$\Delta F_{N,bleed}$	Thrust Loss from the Air Bleed
$\Delta F_{N,dist}$	Thrust Loss from the Effects of Intake Flow Distortion
$\Delta F_{N,ni}$	Thrust Loss from the Actual Pressure Recovery
$\Delta F_{N,pot}$	Thrust Loss from the Power Extraction
$\Delta \Phi a$	Afterbody Force
$\delta_{t,ef}$	Non-dimensional Total Pressure
α	Speed of Sound
γ	Specific Heat Ratio
θ_t	Non-dimensional Total Temperature
ρ	Density

Chapter 1 Introduction

1.1 General Approach

During the development of a combat aircraft there are a lot of parameters that the designer has to take into account. One of them is to ensure the best aircraft/engine integration. The performance of the aircraft and the accomplishment of the demanded operating requirements connected directly with the aircraft/engine compatibility and for this reason these two parts must be designed together and fully integrated in all respects.

The major distinction of the highly integrated aircraft is that the nacelle of the engine is the aircraft itself due to the fact that the engine is buried in the fuselage. Because of this distinction the way that the overall performance of the engine is accounted, is extremely different from the one which is used for the podded systems.

The interactions of interest to airframe/engine integration are between the inlet and engine airflow and between the afterbody and exhaust jet flow. The major considerations arising from these interactions are the spillage drag, the engine performance and stability and the afterbody/nozzle performance.

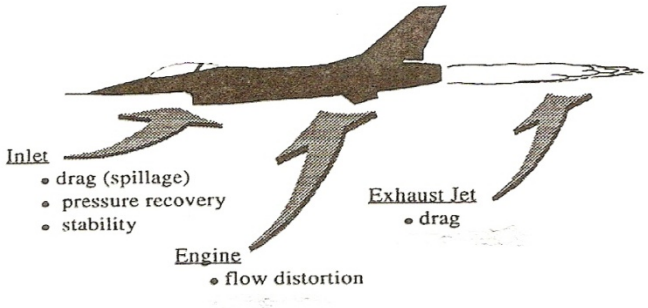

Figure 1-1: Concerns of Aircraft/Engine Integration [11]

The spillage drag is connected directly with the reduction of the mass flow that can lead to an engine thrust loss and for this reason influences the aircraft performance. The character of the flow [11] at the compressor face determines the engine performance and is the underlying reason of the relation between the inlet and the engine output. The pressure recovery influences also the performance of the power plant system because the higher the recovery, the less energy lost to drag and consequently the less energy is demanded for the compress of the air.

The jet gases at the engine exhaust alter the air flow about the aft part of the aircraft. This change affects the trim properties of the aircraft and simultaneously has as result the change of the aircraft drag. The magnitude of these particular changes is a function of the nozzle pressure ratio and nozzle geometry and undeniably can influence the aircraft performance and cause thrust losses.

The combat aircraft and the gas turbine engine interact with one another and an appropriate aircraft/engine matching is demanded for the accomplishment of an aircraft mission with specific requirements.

The study of a combat flight mission can lead to valuable results and findings that can help firstly in the decision of the aircraft/engine configuration which has the best performance, secondly in the estimation of the exact cost of each mission (cost of the fuel that is needed for the completion of the mission), thirdly in the calculation of the payload (missiles, external fuel tanks etc.) and range of the aircraft and finally in the prediction of the environmental effects that can cause each flight.

ARES [23] method as an integrated aircraft-engine performance tool for combat aircraft takes into account the way that all the aforementioned parameters affect the aircraft/engine performance and evaluate the engine performance for a specific flight mission. The method was built in such a way that allows different combinations of combat aircraft/engine to model by altering appropriate input data such as aircraft data, geometric details and mission specifications. The model [23] is able to calculate aircraft and engine performance data such as drag and lift coefficient, spillage drag, installed and uninstalled net thrust, net propulsive force, the fuel consumption, distance covered and finally to specify the maximum payload and the fuel load that is required for the

accomplishment of a mission. The study of a military flight mission can lead to valuable results and findings. ARES, through the mission analysis results and the gas turbine performance evaluation, will give the opportunity for further engine studies such as the structural and thermal analysis, component sizing and geometry and of course life consumption.

However, there are more parameters that affect the engine performance and their influence is not included in ARES calculations. The maldistribution of flow is described from the variation of the total pressure across the engine face and more specifically at the aerodynamic interface plane [5] between the intake and the engine. The flow distortion affects the engine stability and consequently causes variation in its performance. Additionally, the external stores (bombs, various missiles, pods and external tanks) and stores loading combinations that an combat aircraft is capable of carrying also affects the final engine performance.

1.2 Aim and Objectives of this Study

The update of ARES method by integrating the influence of the flow distortion effect and external stores in the aircraft/ engine performance is necessary. This upgrade will improve the accuracy of the final results and will transform ARES in an innovated, powerful and very useful military aircraft-engine performance tool.

The aim of this study is the modification of ARES method in order to integrate in the program calculations, the additional drag of the external tanks. Moreover, a further requirement is the development of a procedure that will be used for the calculation of the thrust deductions due to installation effects. The objectives of this study are the following:

1. Development of a wing-tank model, with the use of Gambit software, which will be used for the calculation of the drag which is contributed from an external wing tank,

2. Development of a CFD study with objective the calculation of the aforementioned drag in different flight conditions and angle of attacks,

3. Modification of ARES FORTAN code so as to include in the software calculations the drag data from the CFD simulations,

4. Development of an aircraft model, with the use of Gambit software, which will be used to study the way that the performance of a fully integrated (buried) propulsion system is eroded by the loss of total pressure in the long and curved intake and by the effect of flow distortion on the engine in different operational conditions,

5. Testing and assessment of the performance of the aircraft/engine configuration over a range of operational conditions.

Chapter 2 Literature Review

2.1 Introduction

The aircraft/engine integration affects the operation and the final performance of a military aircraft. A lot of reasons such as the various operating conditions, the sudden accelerations - decelerations, the large range of speed, the different external configurations (missiles, external tanks etc) and the degree, to which the engine is integrated in the airframe, play a vital role in the aircraft/engine integration.

The major feature [6] of the highly-integrated aircraft (military) is that the nacelle of the engine is the aircraft itself. For this reason the overall performance of the engine is accounted in a quite different way from that which is used for podded systems.

2.2 Mass Flow Ratio

The basic function of an air intake is to supply properly the aircraft engine with air, under all aircraft operating conditions. As it is apparent from the Figure 2-1, the aerodynamic duct [7],

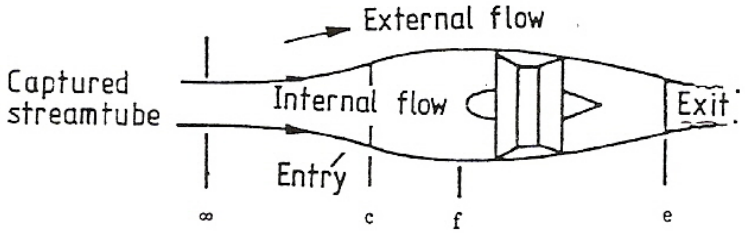

Figure 2-1: Engine nacelle in an airstream [5]

captures a certain streamtube of air which is divided into internal and external flow. The internal flow gives the demanded air to the engine and the external flow preserve

the good aerodynamics of the airframe. Station ∞ is in the undisturbed flow, station c is at the duct entry, station f is at the engine face and station e is at duct exit. As Mass Flow ratio (capture area ratio) is defined the actual flow related to full flow

$$\text{Mass Flow ratio (capture area ratio)} = \frac{A\infty}{Ac} \qquad (2.1)$$

As it is obvious from the following Figure at subsonic flight [5] speeds the value is unity at full flow and greater than 1.0 (maximum flow ratio) when the stream tube is larger than A_c. For supersonic flight speeds [5] the full flow is succeeded when the external shock is matched exactly to the area A_c and the maximum flow ratio is always less than or equal 1.0.

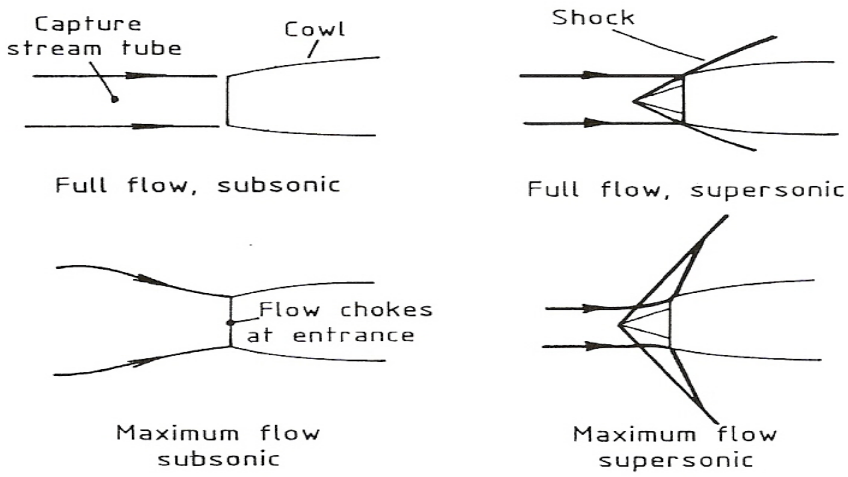

Figure 2-2: Maximum and Full flow [5]

2.3 Inlet/Engine Integration

The interaction between the inlet and the engine is of great importance firstly for the operational capability and efficiency of a combat aircraft and secondly for the engine performance.

Due to the fact that a combat aircraft should face a compact layout so as to minimise radar cross section, the engine is located inside the fuselage (central/ aft buried location) of the aircraft. This configuration is also preferable because can reduce

the installation drag and simultaneously to increase the payload and the range of the aircraft (available space for external tanks). Nevertheless, the powerplant can be affected from the flow around the aircraft and for this reason a bent or long intake is required. Vital role in the Inlet/Engine integration plays the:

- Intake design and sizing
- Spillage drag calculation

2.3.1 Intake design and sizing

The intake design and sizing for a compact aircraft based on performance requirements and simultaneously is a compromise between the operation at subsonic and supersonic speeds. The initial step is the sizing of the intake –duct flow area so as to be matched with the engine mass-flow demand at maximum-flow conditions for a given engine-face area, A_{ef}. The demanded calculations for this specific task are:

- the lip contraction ratio (Highlight/Throat area ratio)
- the throat area (Ath)
- the diffuser geometry

In the following Figure there is a detailed illustration of the general definitions that will be used in this chapter.

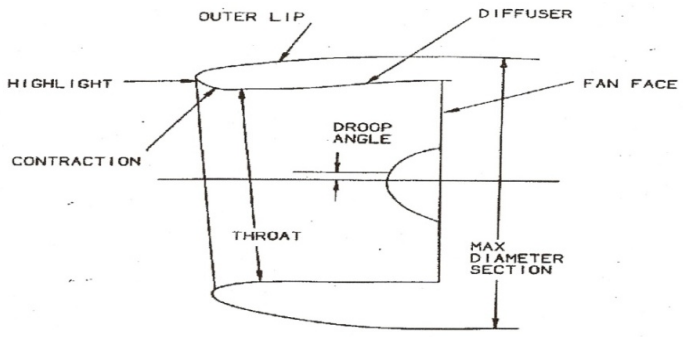

Figure 2-3: General Definitions of inlet [8]

The general procedure, as is referred also in the MSc thesis [9] of the author, that can be followed for the completion of the intake design- sizing of a combat aircraft consist of the next steps:

- The intake type

The requirements for increased reliability, manoeuvrability and ease of maintenance affect directly the intake design of a combat aircraft and the intake/airframe integration. The major difficulty is the fact that the final configuration must fulfills the previous requirements and simultaneously to achieve low drag, good efficiency and low weight and cost. Some of the most common airframe-inlet configurations for combat aircraft are illustrated in the following Figure

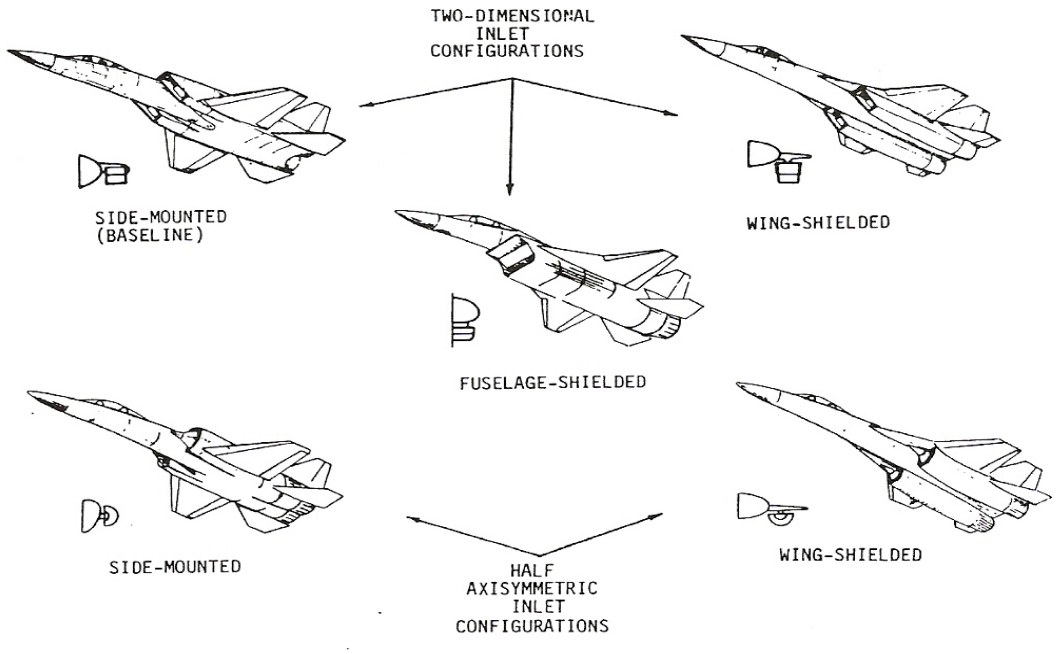

Figure 2-4: Airframe-inlet configurations [5]

The intake type depends on the shape (rectangular, half cone and pitot) and the internal configuration. For supersonic speeds [5] the variable geometry (Figure 2-5) is demanded and compression angles (ramp or cone designs) are preferable for maximum pressure recovery.

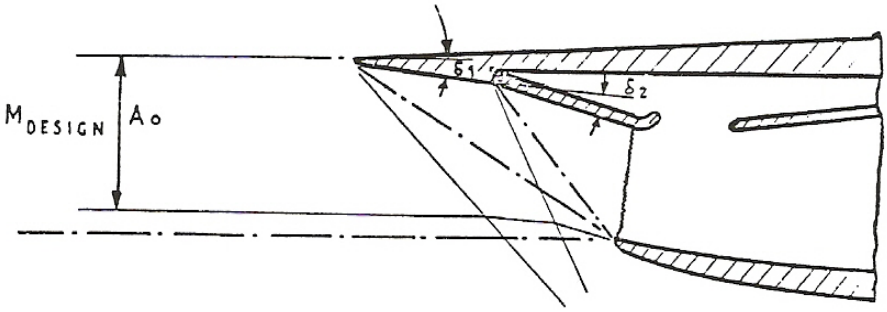

Figure 2-5: Variable geometry for a supersonic intake [5]

The cowl position is also very significant so as to avoid problems that could arise from ingestion of ramp or cone shocks.

- Throat size

Typically the intake throat sized to Mach number (M_{throat}) equal to 0.75 due to the fact that the flow path curvature and the boundary layer growth lead to a initial reduction of the Mach number (0.85 - 0.9) and continuously [10] , a secondary reduction of the Mach number (0.75) is necessary because a reduction of the total pressure recovery and an increase of the diffuser flow distortion can be caused for even small increase in flow demand. The necessary equations [6] for this part of the calculations, as referred also in the MSc thesis [9] of the author, are the following:

$$Wc_{ef} = \frac{W\sqrt{\theta t}}{\delta_{t,ef}} \qquad (2.2)$$

where Wc_{ef} is the engine corrected mass-flow, W the engine mass-flow, $\delta_{t,ef}$ is the non-dimensional total pressure and θ_t is the non-dimensional total temperature. The $\delta_{t,ef}$ and θ_t are expressed from the following equations:

$$\delta_{t,ef} = \frac{P_{t,engineface(ef)}}{P_{t,0}} \qquad (2.3)$$

$$\theta_t = \frac{T_t}{288.2} \qquad (2.4)$$

where $P_{t,\text{engine face(ef)}}$ is the absolute pressure at the engine face, P_{to} is the pressure at sea level static (SLS) and T_t is the total temperature at the engine face. Moreover, the corrected throat flow Wc_{th} can be expressed from the following equation:

$$Wc_{th} = \frac{W\sqrt{\theta t}}{\delta_{t,th}} \qquad (2.5)$$

For the Lip Design [6] the typical intake contraction ratio (Highlight/Throat area ratio), $\frac{A_H}{A_{th}}$ is equal to 1.14 for military aircraft without auxiliary intakes for take-off or 1.0 (sharp lip) for intake with auxiliary doors. The Capture Area Ratio [6] $\frac{A_C}{A_{th}}$, depends on the design choice and the geometry calculation, and a typical value for a ramp inlet is 1.3.

- Diffuser Design

For the diffuser design the demanded parameters are the Diffuser Length (L_{duct}) and the Engine Face Gross Area [6] (D_{ef}). Knowing the specific characteristics and configuration of the intake easily can be calculated the ratio $\frac{L_{duct}}{D_{ef}}$ that can be used from other equations later on.

- Intake Total Pressure Recovery

The Mach number [5] that a gas turbine engine accepts air into the compressor is around 0.4-0.5. The role of the intake for Mach number above the values of 0.4-0.5 is to act as a form of compressor so as to reduce the speed of the flow and to increase the static pressure and for Mach number below those values (0.4-0.5) is to accelerate the air so as to reach the engine face with the demanded velocity. For a practical measure of

efficiency the total pressure is preferred to static pressure. The term of pressure recovery is related to these changes in pressure.

The pressure recovery is defined as the ratio $\frac{Pt_{ef}}{Pt_0}$. The change of total pressure cause change in pressure recovery and consequently change in engine thrust. The change of total pressure can be caused [5]:

- by shock waves
- from turbulent mixing
- by friction on the duct walls and on other external surfaces that wetted by the air which afterwards goes into the intake.

At subsonic flight conditions typical variation of the $\frac{Pt_{ef}}{Pt_0}$, based on the previous expressions is given from the following equation [6] :

$$\frac{Pt_{ef}}{Pt_0} = 1 - 0.328\ (Q_{ef})^2 \qquad (2.6)$$

where $Q_{ef} = \frac{W\sqrt{\theta t}}{\delta_{t,ef} A_{ef}}$ is the corrected engine mass-flow at the engine face divided by the engine-entry gross flow area.

The usual process for sizing the intake involves choosing a design point flight condition and fixing the geometry at that flight condition. The Ath, A_H and Ac that were calculated at the design point flight condition are kept constant and are used for the next calculations.

2.3.2 Spillage Drag

As referred to the Airframe Engine Integration [6] notes, 'The intake spillage drag is a result of the failure of the intake cowl to fully balance or "recover" the pre-entry

force'. The spillage drag is connected directly with the reduction of the mass flow that can lead to an engine thrust loss and can be expressed with the following equation:

$$\Delta Dspill = qo\ \Delta CD\ Ac \qquad (2.7)$$

where Ac is the capture area, ΔCD is the incremental spillage drag coefficient and qo is the flight dynamic head can be expressed as:

$$qo = 0.7\ p_{so} M_o^2 \qquad (2.8)$$

where p_{so} is the ambient static pressure and M_o is the flight Mach number

The incremental spillage drag coefficient ΔCD can be estimated by using charts of the ΔCD versus mass flow ratio for different Mach numbers. A sample of this kind of charts is illustrated in the Figure 2-6.

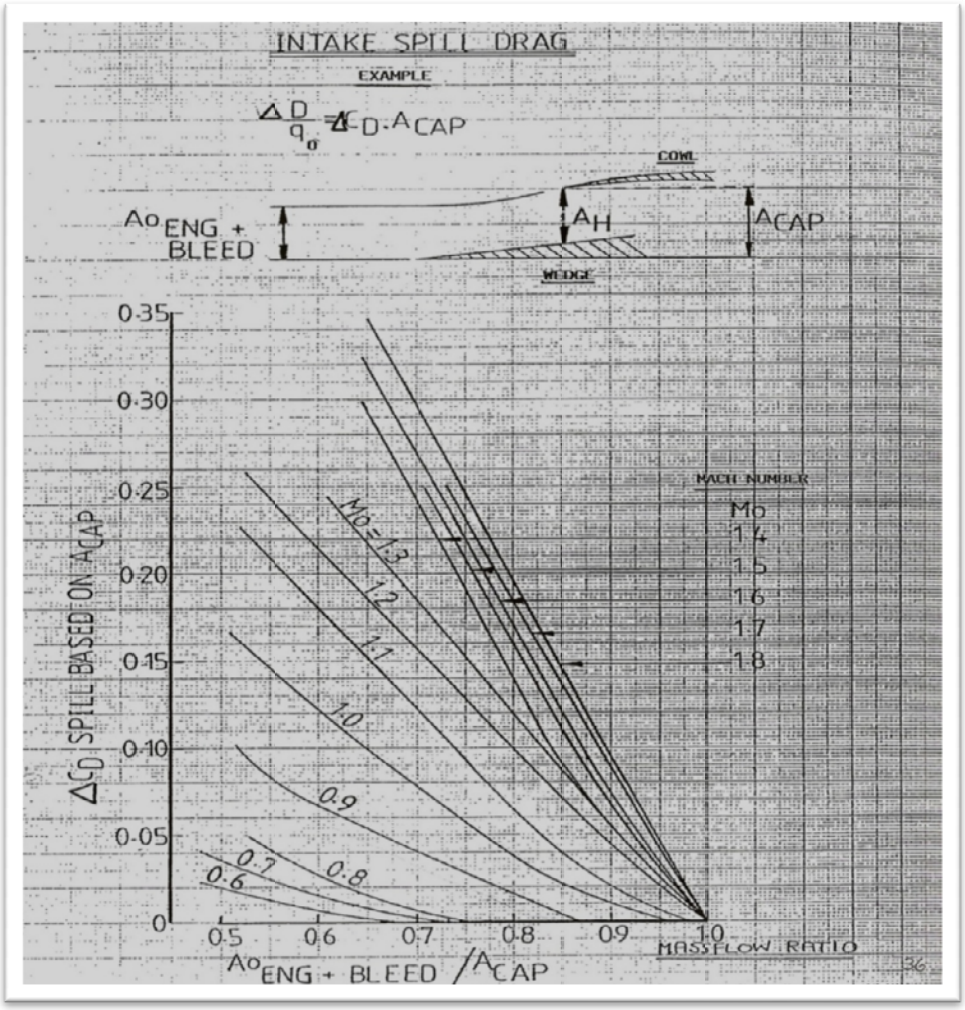

Figure 2-6: Spillage drag coefficient calculation [6]

This chart is for a subsonic flight for a specific configuration of the inlet and as it is apparent the decrease of the mass flow ratio and the increase of the Mach number leads to an increase in spillage drag.

2.4 Uninstalled and Installed Net Thrust

The 'uninstalled net thrust' is the manufacturer's engine thrust which is estimated based on:

- assumed inlet pressure recovery ,
- manufacturer's nozzle
- calculations without distortion effects.

The 'installed net thrust' is the thrust that is available after the installation of the engine in the aircraft. The uninstalled net thrust is equal to installed net thrust plus the installation losses. The installation losses come from the:

- actual nozzle performance,
- actual pressure recovery,
- power "off-take",
- intake flow distortion and
- engine bleed.

The installed net thrust can be expressed from the following equation [6] :

$$F_{N,installed} = F_{N,uninstalled} - \Delta F_{N,bleed} - \Delta F_{N,pot} - \Delta F_{N,dist} - \Delta F_{N,ni} \qquad (2.9)$$

where the term $\Delta F_{N,bleed}$ is the thrust loss from the air bleed that is used e.g. for the cockpit air-conditioning,

the term $\Delta F_{N,pot}$ is the thrust loss from the power extraction that is used e.g. for electrical generation,

the term $\Delta F_{N,dist}$ is the thrust loss from the effects of intake flow distortion and finally the term $\Delta F_{N,ni}$ is the thrust loss from the actual pressure recovery.

2.5 Flow Distortion

Initially and traditionally, the flow distortion at entry of the engine has been described [5] based on the variation of the total pressure across the face of the engine. Nevertheless, serious exceptions have arisen during the development of the propulsion systems, where performance and stability problems were noticed. The basic source of these problems was the failure [5] to understand the nature of the intake flow field and the sensitivity of the engine to it. Generally, the maldistribution of flow is described from the variation of the total pressure across the engine face and more specifically at the aerodynamic interface plane [5] between the intake and the engine. In propulsion systems a better understanding of this phenomenon is necessary because the compatibility problems can be characterized in great extend by the total-pressure distortion.

2.5.1 Sources and Descriptors of Distortion

As it is apparent from the Figure 2-7, basic reasons that can cause total-pressure distortion [5] are the following:

a) flow separation which is the result of the interaction between the compression surface boundary layer and the intake shock,
b) spillage of the aircraft,
c) ingestion of aircraft vortices,

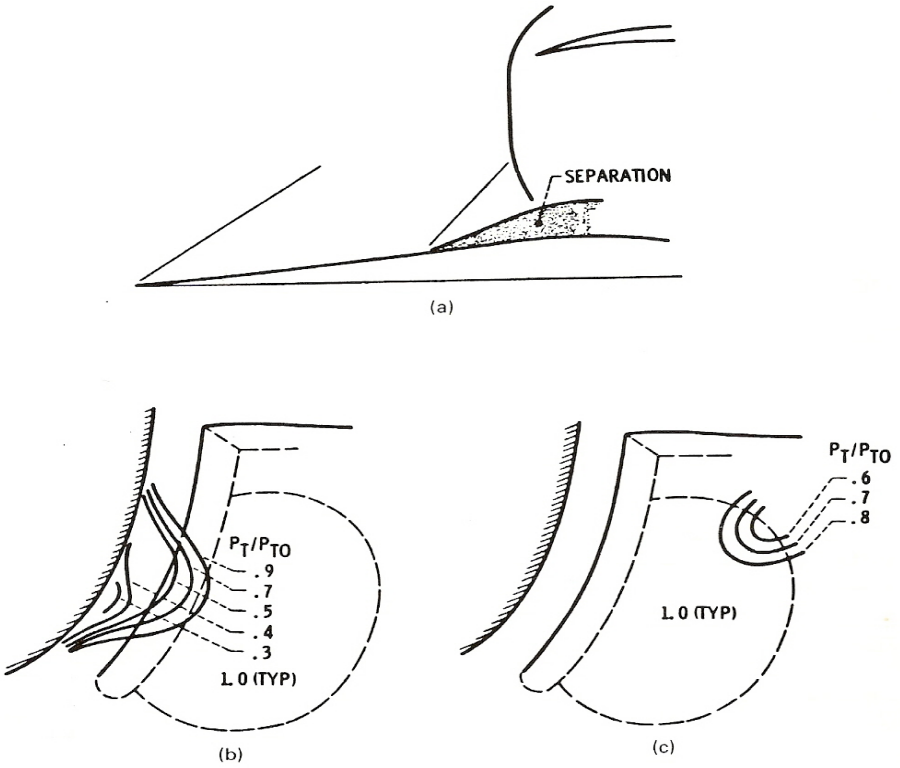

Figure 2-7: Sources of distortion [5]

Nevertheless, there are secondary reasons that can also cause total-pressure distortion and some of them are the ingestion of vortices that were formed from the interaction between the ground and the intake, the ingestion of hot-gas that comes from missiles exhausts or thrust-reverser operations and the local flow curvature due to proximity of bends in the intake.

The general way to visualize the intake distortion is the total-pressure contours at the aerodynamic interface plane as it is illustrated in the Figure 2-8.

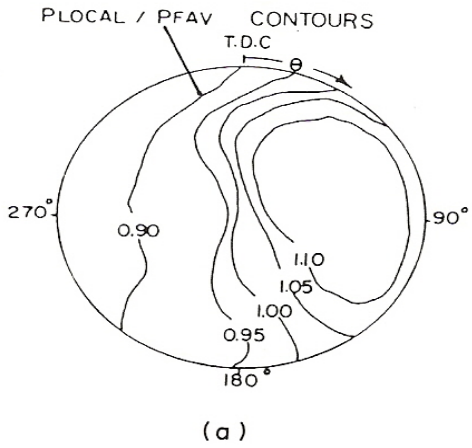

Figure 2-8: Distortion pattern [5]

This descriptor is useful [5] because can relate the total-pressure defect regions to problem sources in the intake flow. However, it cannot give information about the effect of the distortion on the engine because is an 'upstream looking'. Current technique for the measurement of the total-pressure distortion at the aerodynamic interface plane is the use 40-48 total-pressure probes in full-scale instrumentation array and the further analysis of the data by using specific parameters.

Apart from the distortion patterns there are also and other distortion descriptors that are in use. Such descriptors are the [5]:

- Root mean square total pressure
- Distortion elements
- Distortion (screaming) parameters
- Critical-sector angle.

The distortion is affected from the angle of the spoiled sector and as indicated in the Figure 2-9, distortions with a large circumferential extend have a more pronounced effect on compressor performance.

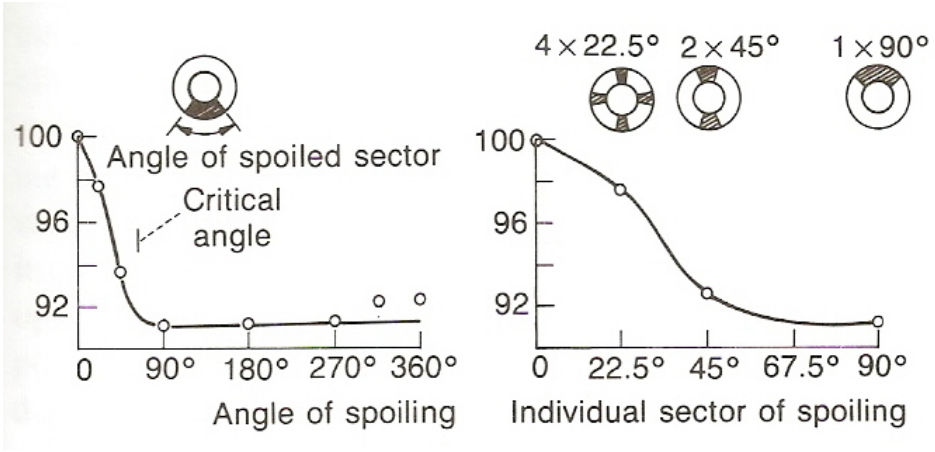

Figure 2-9: Angle's of spoiling effect in the performance of the compressor [21]

For the assessment of the distortion was defined a coefficient [21] which average the low stagnation pressure over the worst arc of the circumference with the extend of the arc being the angle at which it is judged that the plateau in Figure 2-9 is reached. This distortion parameter is $DC_{(\theta crit)}$ where θ_{crit} is the circumferential angle at which the full effect of distortion is felt. The θ_{crit} very often has been taken to be 60^o and in this case the DC_{60} parameter is defined by

$$DC_{60}=\frac{average\ inlet\ stagnation\ pressur-average\ inlet\ stagnation\ pressure\ over\ liwest\ \ 60°}{average\ inlet\ dynamic\ pressure} \quad (2.10)$$

For contract guarantee purposes [21] a DC_{60} of 0.5 would be typical but many engine compressors can tolerate a value of 1.0 or more.

2.5.2 Engine Performance

The effects of the distortion on the engine performance are directly connected with the effects of the distortion on the performance of the compressor. As it is known the basic tool in the assessment of the compressor stability is the compressor map where the

total-pressure ratio (R) is plotted with the non-dimensional air mass flow for different non-dimensional speeds.

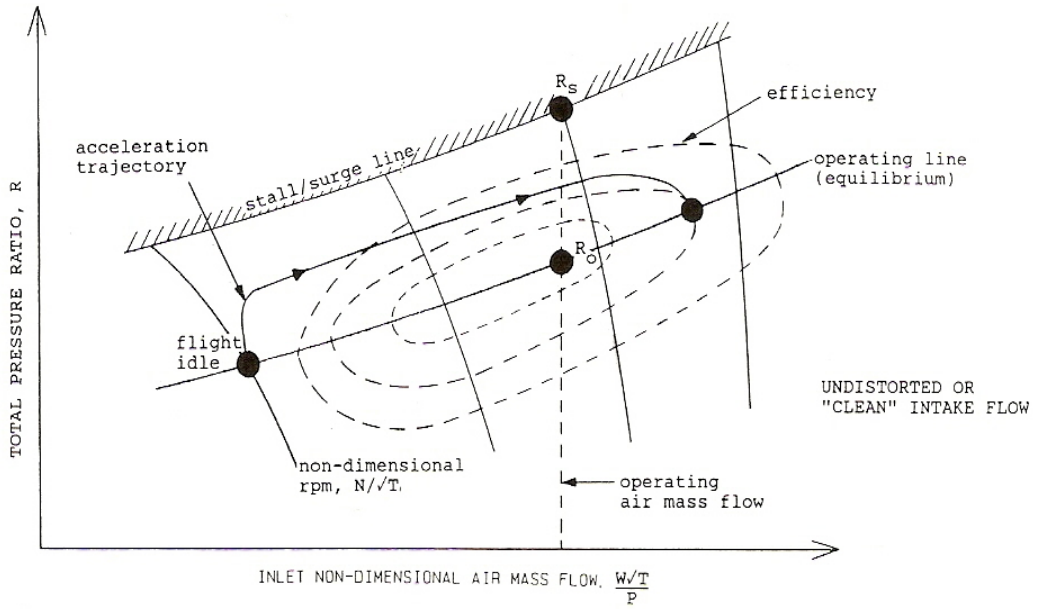

Figure 2-10: Compressor map [5]

The main effects [5] of the total-pressure distortion on the compressor performance are the loss of the airflow capacity for a specific non-dimensional speed and the loss of efficiency. These effects reduce the engine output and simultaneously affect and other parameters such as the fuel consumption and the general performance of a military aircraft.

Moreover, as it is obvious from the Figure 2-11, the total-pressure distortion can cause a loss of compressor surge pressure ratio, fact that can leads to compressor surge if the operating line (e.g. power off take) reaches the distortion surge line. Furthermore, the new surge line distortion influence directly the performance of the engine because the transient operating line that correspond to the maximum acceleration cannot be the same with the initial one due to the fact that the new distance between the steady operating line and the surge line (distortion) is smaller. This means that the acceleration capability of the engine is affected and consequently the engine cannot maintain the initial performance.

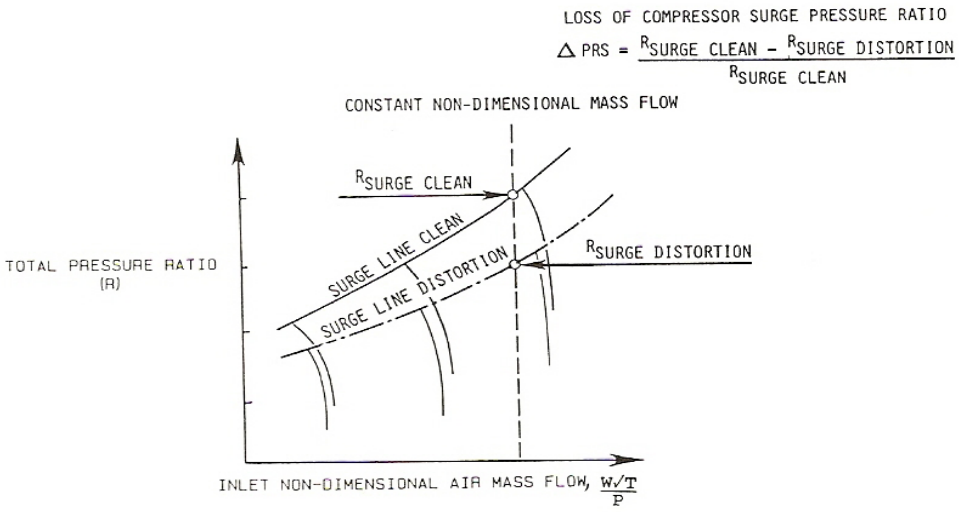

Figure 2-11: Surge pressure ratio loss [5]

2.6 Net Propulsive Force

The Net Propulsive Force (NPF), as it is illustrated in the Figure 2-12, is the actual available thrust and is equal to installed net thrust minus the drag contributions.

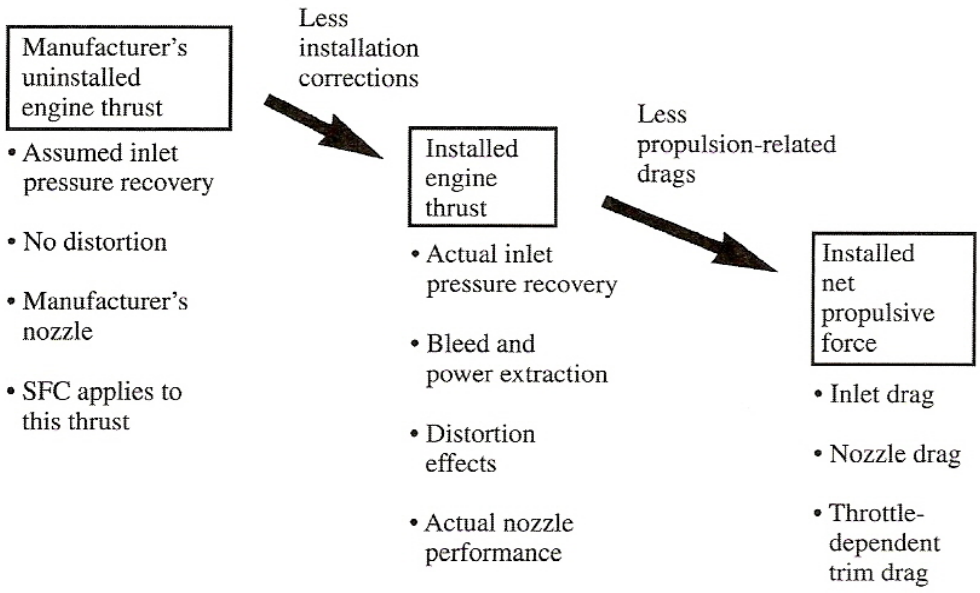

Figure 2-12: Net Propulsive Force [4]

The Net Propulsive Force [6] can be expressed from the following equation:

$$NPF = F_{N,\ installed} - \Delta Dspill - Dnac,ref - \Delta\Phi a \qquad (2.11)$$

where $F_{N,\ installed}$ is the installed net thrust, ΔDspill is the spillage drag , Dnac,ref is the nacelle reference drag and ΔΦa is the afterbody force. As it is known, in the highly-integrated aircraft the nacelle of the engine is the aircraft itself. Consequently [6] the nacelle reference drag (Dnac,ref) is carried on the airframe drag account and for this reason the equation (2.11) becomes:

$$NPF = F_{N,\ installed} - \Delta Dspill - \Delta\Phi a \qquad (2.12)$$

Additionally must be mentioned that there are also some other terms, such as the trim drag, which can be included in this definition. Nevertheless, it is preferred to include them in the engine performance account because these terms are associated with the powerplant.

2.7 Computational Fluid Dynamics (CFD)

The computational fluid dynamics integrates engineering (fluid dynamics), mathematics and computer science. It is a powerful tool that can be used in many engineering applications such as aerospace, automotive, biomedical, chemical etc. The main advantage of the CFD is that can provide an alternative cost-effective mean of simulation with visualized and detailed information.

The CFD based on the governing equations of fluid dynamics. The physical laws that are used are the mass conservation, the first law of thermodynamics and the Newton's second law. More specifically the governing equations [2] are the following:

- Continuity Equation
- Momentum Equation
- Energy Equation
- Equations for turbulent flow

The process that is required to solve the governing equations of fluid dynamics consists of two stages. The first stage [2] is the discretization stage where the partial differential equations and auxiliary conditions are converted into discrete algebraic equations and the second stage [2] is a process that is used for the solution of the algebraic equations with the implementation of numerical methods.

The discretization stage consist of the following techniques [2] :

- Finite-difference method

This is a method which describes the partial differential equations in terms of time and space and is based on Taylor series.

- Finite-volume method

This method uses Taylor series as the Finite-difference method with the difference that the variable distribution will be determined at the faces of the volume around the nodes.

- Finite element method

This method is similar to Finite-volume method with the difference that uses polynomial functions on local elements and with the combination of the entire element gives the final description of the domain.

- Spectral method

This method is similar to Finite-difference and Finite-element methods with the difference that for the replacement of the unknowns at the governing equations instead of local approximations uses global approximations by implementing truncated Fourier series or Chebyshev polynomials.

At the second stage, for the solution of the algebraic equations are used two numerical methods:

- Direct methods (Gaussian elimination)
- Iterative methods.

The final concern [2] is whether the approximate solution can be guaranteed to approach the exact solution of the problem. The CFD can achieve this by implementing the following criteria [2] :

- Consistency

Consistency establishes a relation between the algebraic equations and the initial partial differential equations. A solution is consistent the system of the algebraic equations tends towards to differential equations when the mesh size becomes smaller.

- Stability

Stability is the criterion which relates the exact solution of the differential equation with the result of the discretized equation and it concerns [2] the growth and decay of errors introduced during the computation.

- Convergence

As defined by Tu, Yeoh and Liu [2] 'Convergence of a numerical process can be stated as the solution of the system of algebraic equations approaching the true solution of the partial differential equations having the same initial and boundary conditions as the refined grid system.'

- Accuracy

The errors and the uncertainties in the calculations can affect the accuracy of the solution. A systematic reduction of the errors and the uncertainties leads to a credible solution.

2.7.1 CFD Analysis

The CFD analysis consists of three (3) elements:

- Pre-processor
- Solver
- Post-processor

Each element consists of few steps that are necessary for the setup of the problem, the solution and finally the result report and visualization. These specific steps are analytically tabulated in the following Figure.

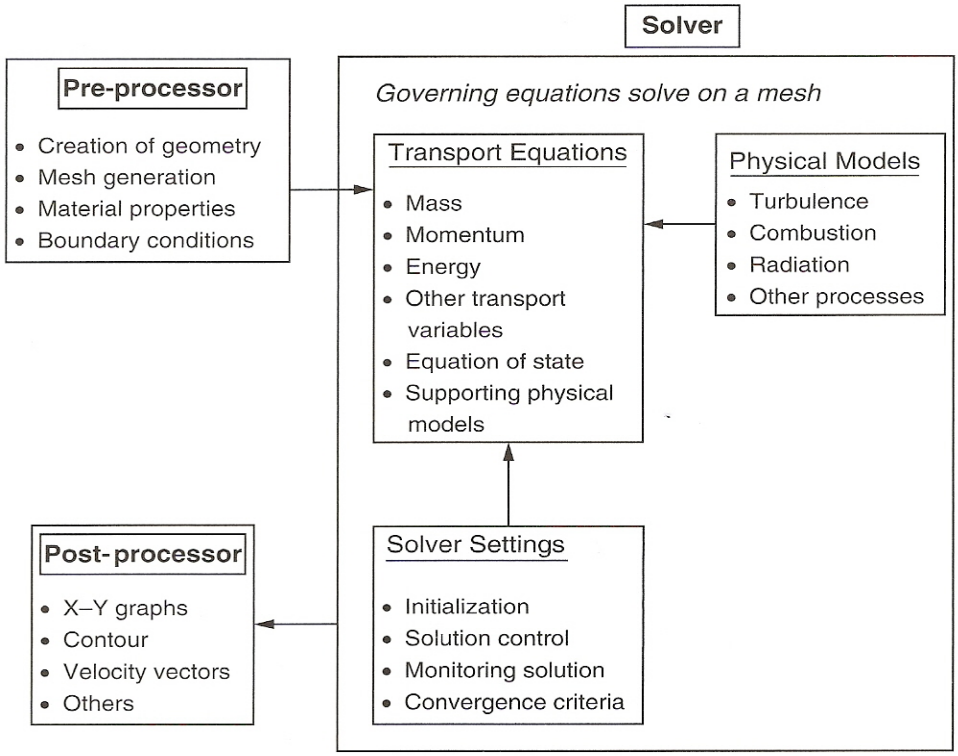

Figure 2-13: CFD analysis [2]

The most important part for a reasonable and credible simulation output is the pre-processor element. This element consists of the creation of the geometry, mesh generation, material properties and boundary conditions. All these steps are necessary for the model creation and possible mistake leads inevitably to insufficient results.

The building of a computer model involves a detailed geometry and a sufficient grid. Significant role plays the number of nodes that should be enough to compute the physical phenomena that take place in the computational domain. The types of mesh that can be used are the structured and unstructured grids. The basic factors for choosing the kind of grid are the ease of generation, the flexibility to conform to complex geometry and of course the memory requirement. The basic differences between this two kinds of grid are the computational cost, which for the unstructured grid is bigger

because the connectivity has to be stored explicitly, the number of cells because for the unstructured grid is demanded large number so as to reduce the aspect ratio of the cells and consequently the errors and the different effectiveness in the resolution of specific problems-cases e.g. wall boundary layers, complex geometry etc.

The last two steps in the pre-processor element, which are the materials properties and the boundary conditions, are also significant. Their definition is a very important step in a CFD study because must mimic the real physical representation of the fluid flow. Many times these two parameters are the cause of insufficient simulation results and for this reason a detailed and precise handling is demanded.

2.8 Gas Turbine Engine Performance Estimation

In the past years, major advances have been made in the ability to determine the performance of the aircraft during flight tests. These advances have been made possible bigger by the increased reliability of calculated and experimental engine performance information through the progress in [12] analytical approaches that characterize the performance of the jet engines, ground and flight test techniques, the basic instrumentation, data-acquisition and data-processing systems. The progress in the aircraft propulsion performance estimation is undeniable, but there are still problems that require further improvement of the computational methods so as to be more usable, reliable and cost effective in calculating overall engine performance.

The current methods that are used for the estimation of the gas turbine engine performance are the [12]:

- Analysis and calculation,
- Ground testing,
- Flight testing.

Through the further analysis of these three methods will be obvious that these methods are related each other and overlap in many areas.

2.8.1 Engine Performance Estimation by Analysis and Calculation

The engine performance estimation by Analysis and Calculation is based on analytical methods. Generally [12] in this estimation method the engine is regarded as a collection of components that conform to the definition of the stations used in the one-dimensional calculation of aerodynamic performance and the thermodynamic principles are used for the necessary calculations.

The key tool in analytical determination of engine performance is the computer simulation software. The function [12] of the simulation software is to satisfy gas mass, mechanical energy and momentum-conservation equations throughout the engine with result the establishment of a unique match of the engine components operating characteristics.

In this method is based the simulation tool that was developed in Cranfield University and is known as TURBOMATCH software [13]. This software simulates the design and off design performance of aero/industrial gas turbine engines and the basic characteristic is the satisfaction of the major thermodynamic principles of the working gas, such as the mass flow continuity and work compatibility.

The Turbomatch engine [13] model consists of several preprogrammed modular units called Bricks, which represent major engine components e.g. INTAKE, COMPRESSOR, BURNER, TURBINE and NOZZLE. The bricks are connected to each other with the use of station numbers as an interface.

The quantities that describe the gas state of a specified engine station number are known as station vectors. Each station vector consists of eight quantities. Turbomatch Brick Data with the inputs (inlet Station Vector, Brick data, Engine Vector data) and the outputs (outlet Station Vector, Engine Vector results) are illustrated in Figure 2-14.

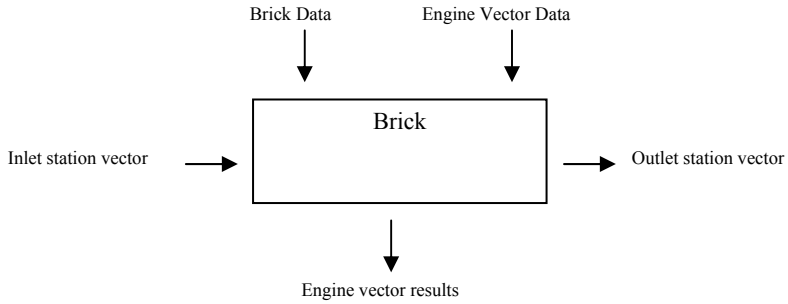

Figure 2-14: Turbomatch brick schematic [13]

2.8.2 Engine Performance Estimation by Ground Testing

The direct measurements of engine thrust performance for aircraft in flight is a quite difficult task. Performance [12] is instead deduced from the measurement of related engine parameters which are evaluated using measurements from ground-test facilities.

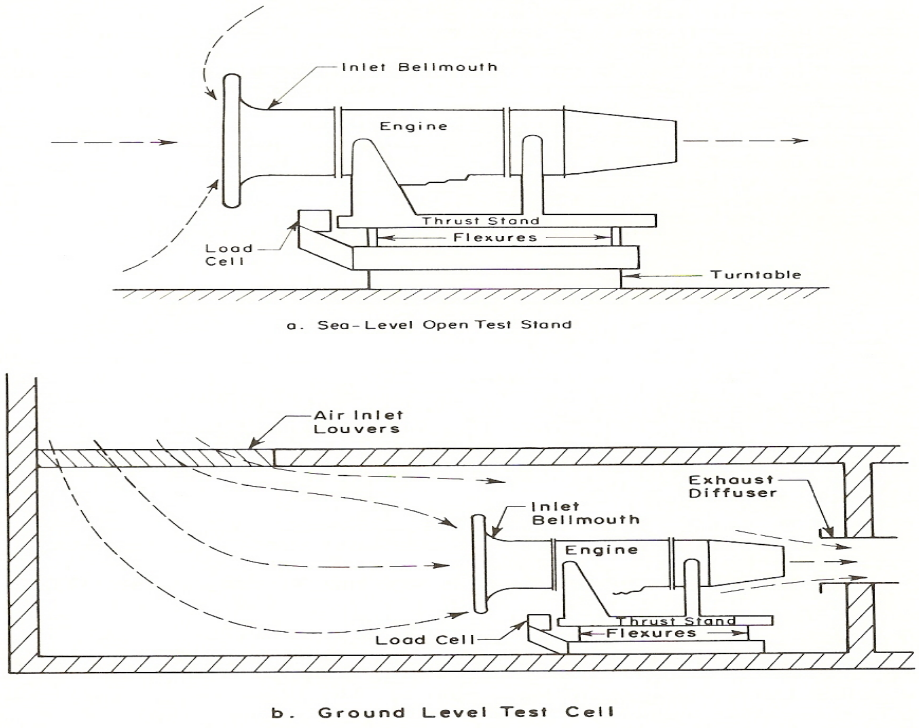

Figure 2-15: Direct-connect engine installation [12]

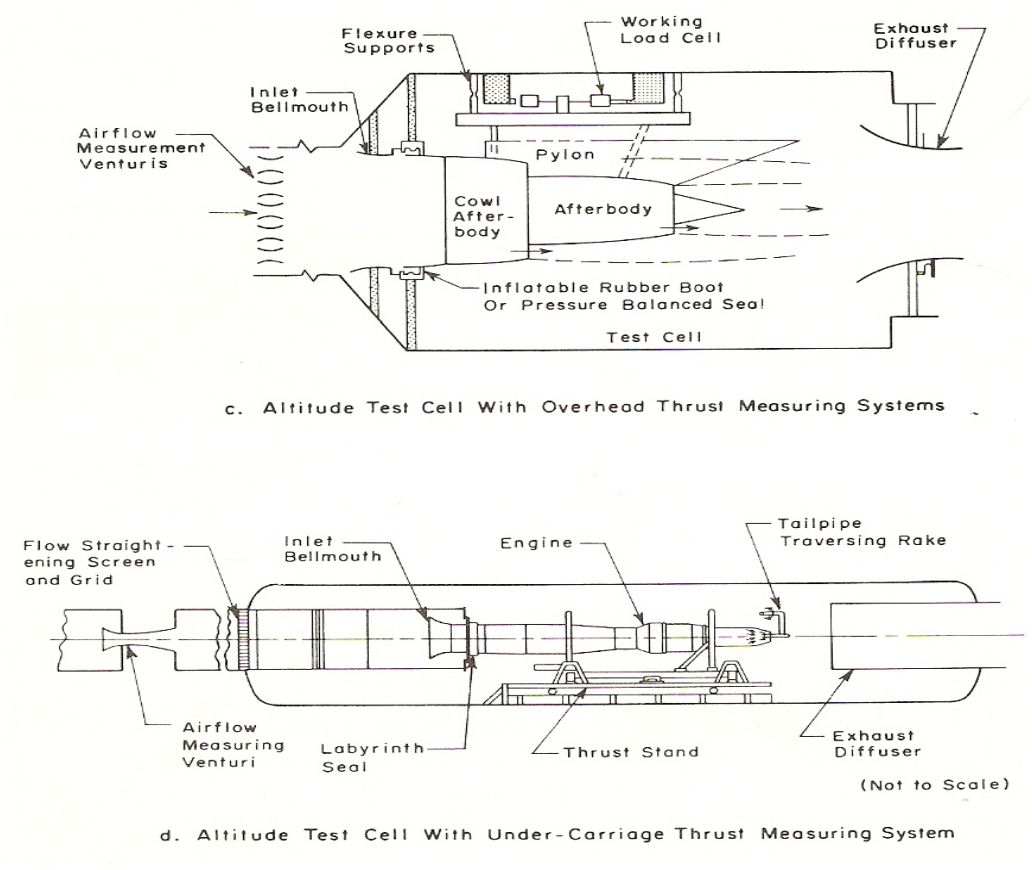

Figure 2-16: Direct-connect engine installation [12]

The direct-connect test configuration (Figures 2-15, 2-16) provides the best means of measuring the performance of jet engines. The name [12] of this configuration derives from the fact that the inlet is directly connected to a controlled-air supply system and the free-standing exhaust exits into a separately controlled environment.

The main factors that affect the engine performance measurement are the following[12] :

- Engine cycle
- Engine geometry
- Engine suspension system
- Operating environment
- Measurement uncertainty

The first three affect the mechanical options available for the test and the next two dictate the instrumentation available options and also have an influence on the mechanical options.

Additional factor that also affect the final outcome is the capability of the tester to accomplish the task. The tester must be capable of firstly making pretest measurement uncertainty estimates and relating the results to engine performance to ensure that an acceptable measurement system is selected and secondly identifying measurements errors.

For the measurement validation was developed a process that consists of the following steps [14] :

- Establishing a thrust measurement calibration hierarchy with traceability to the National Bureau of Standards,
- Quantifying and categorizing elemental measurement errors into precision and bias terms,
- Propagating the elemental errors to obtain measurement uncertainty values,
- Establishing an influence coefficient matrix to propagate element measurements uncertainties to a final in-flight thrust measurement uncertainty values.

The execution of this process is very difficult because is demanded a coordinated effort between the ground test personnel and the engine and airframe manufacturer.

2.8.3 Engine Performance Estimation by Flight Testing

Flight testing [12] is the process of evaluating performance of full scale airframe and propulsion system under actual environmental conditions. In a flight test can be included takeoff/landing tests, climb tests, cruise and turning performance evaluation.

Flight-test data include effects on engine operation as a result of the aircraft installation. The most predominant effects are the engine compressor bleed airflow, the pressure recovery and the inlet airflow distortion. As far as concern the airflow distortion [12] since the cruise performance testing is done at level, steady flight conditions, inlet flow distortion must be minimal.

However, in cases [12] where inlet flow distortion is more than several percent of the bulk average pressure value, it may be necessary to equip the flight engine with a full set of inlet pressure rakes. Engine performance adjustments can be estimated using the ground-test [15] distorted flow performance data. For purposes of analysis, various analytically defined distortion indices [16] are used to characterize the different types of flow distortion.

The methods that are used in flight engine tests for acquiring the data are quite different for those used for ground propulsion tests. The factors [12] that affect these methods are the space and weight limitations and the installation problems that prevent the use of extensive instrument packages. As a result the measurement uncertainties in flight are higher than those in propulsion ground-test facilities. The magnitude of the difference depends on [12] the in-flight performance prediction method and the instrument requirements associated with that method.

The methods that are used for the evaluation of the in-flight engine performance are the following [12] :

- Engine computer math model. This model is a very useful tool because it provides a capability for components evaluation and also can be used to adjust engine data for cycle changes. Additionally [12] , monitor the engine health and evaluate engine operational performance deterioration.

- Gas-path/ Nozzle methods. These methods use calibrated measurements of gas generator flow properties at various stations in the engine or station properties calculated from calibrated measurements made at other stations in the engine.

- Calibrated flight engines. The most accurate method of determining the in-flight engine performance is the direct calibration of the engine in a n altitude ground test facility.

2.9 Wind Tunnel Simulation

The fundamental complication [11] in the use of simulation to develop the performance model data is that the engine does not scale. Hence full scale engine testing is required to identify the engine performance. On the other hand there are rules that permit the aerodynamic scale. Scale model testing in the wind tunnel gives the aerodynamic performance and also characterize the aircraft/engine integration that include inlet drag exhaust jet effects, inlet pressure recovery and engine face distortion. Thus the performance modelling process is a combination of propulsion system that characterized by full scale simulations and the aerodynamics that characterized by scaled simulations. The separation [11] of engine and aerodynamic performance requires multiple sets of reference conditions. For the engine [11] the reference is the condition in the engine face and for the aerodynamics [11] are the wind tunnel free stream conditions and flow through aerodynamic model mass flow ratio and nozzle pressure ratio.

The aerodynamic model [11] usually is equipped with fixed inlet and nozzle geometry configuration. The flow through the inlet and nozzle has only one mass flow and nozzle pressure ratio per test condition. The inlet model [11] has real geometry and bleed but simplified or incomplete external fidelity and it is located far enough from the inlets so as not to affect the inlet flow. The jet effects model [11] includes an accurate aircraft aft geometry with engine nozzles.

In the wind tunnel simulations the inlet pressure recovery and distortion indices are based on weighted averages of pressure measurements. These measurements are made, with the use of rakes, at the aerodynamic interface plane (AIP) because is very difficult to be done at the engine face. The measurements produce maps [11] of total pressure at the AIP and the inlet recovery is characterized by various weighted averages of the total pressure [17] .

The separation of the engine and aerodynamic simulation introduces significant problems. Further difficulties [11] are caused by the:

- Compromise in the model geometry,
- Wind tunnel interference effects,

- Test facility limitations.

The compromise in the model geometry derive from the inability to include small features in the scales models (Figure 2-17), the alterations that are required for the model strength and the integration of instrumentation and finally from the requirement of the model support within the test facility.

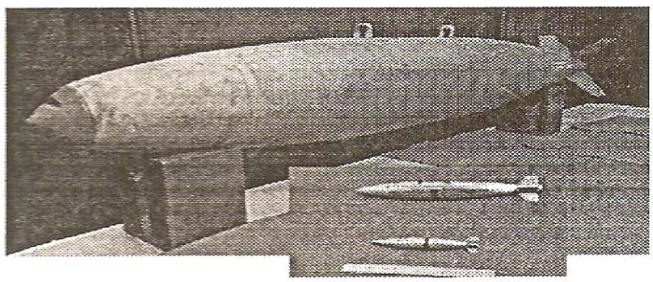

Figure 2-17: Geometric fidelity with decreasing model scale [11]

The wind tunnel interference effects come from the wind tunnel wall and the model support structure and are more predominate as the size of the model increases relative to the wind tunnel dimensions. Finally the test facility limitations derive from the inability to duplicate all the values from the key simulation parameters such as the Reynolds number (Figure 2-18).

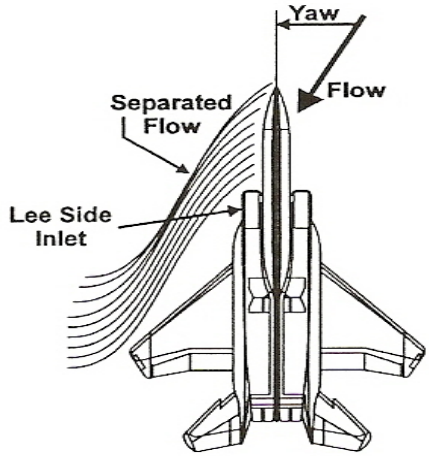

Figure 2-18: Yawed aircraft inlet flow field [11]

2.10 CFD Simulation

In the previous subchapters was described the way that the aircraft/engine integration is performed and also some of the areas in which the traditional experimentally based simulations are deficient were noted. In this chapter will be analyzed the contribution of the Computational Fluid Dynamics (CFD) in the final evaluation of gas turbine engine through the use of the aircraft performance characteristics and engine /airframe integration in particular.

CFD is a excellent diagnostic tool [11] because allow computed flow parameters to be presented in many combinations and to be seen from many view points. The CFD also permit [11] the determination of the origin disturbances [18] , instabilities and the location, extend and strength of flow structures [19] . CFD generated increments of interest to engine/airframe integration include the estimation of transonic wall interference. There is available demonstration [20] of agreement between measured and computed corrections to an aircraft configuration.

The calculation of the drag that is contributed from an external store, this is the reason that the CFD is used in this study, can be achieved through a specific procedure. The procedure consists of three steps. The first one made up from the grid generation,

the connectivity of the grid volume and the specification of the boundary conditions. The completion of the first step is feasible with the use of Gambit software. The following step is the integration with Fluent software, where all the necessary parameters such as turbulence model, scaling, operating conditions, under-relaxation factors, the convergence criteria etc are defined and the model is ready to run the simulation. The last step is the drag estimation through the CFD simulations.

Additionally, the calculation of inlet flow distortion can be achieved through the pressure maps which can be derived from the CFD using an appropriate turbulence model. The procedure is the same with the aforementioned one apart from the last step. The last step is the assessment of the distortion with the use of the DC_{60} parameter (subchapter 2.5.1). The DC_{60} parameter for the exit section at various iteration levels is evaluated with the use of the User Defined Function (UDF) provided by Fluent. The distortion coefficient [22] is calculated from the flow variables and it can be stored in an output file. The values of the parameter are useful for the further procedure that is required for the assessment of the distortion and the way that the distortion affects the final engine performance.

2.11 HERMES Software

The HERMES [23] software was developed in Cranfield University and is an integrated aircraft-engine performance tool for civil aircraft. As referred in the Dr Laskaridi P. PhD thesis [23] 'the model was built in a manner that allows for different aircraft to be modelled by altering appropriate input data such as aircraft data and geometric details , mission specifications as well as secondary power systems mass and off-take requirements.'

The model [23] is able to calculate aircraft performance data such as drag and lift coefficient, distance for take-off , the fuel usage, time elapsed and distance covered and finally to specify the maximum payload, take-off weight and the fuel load that is required for the accomplishment of the mission. A flowchart of calculations is presented in the following Figure.

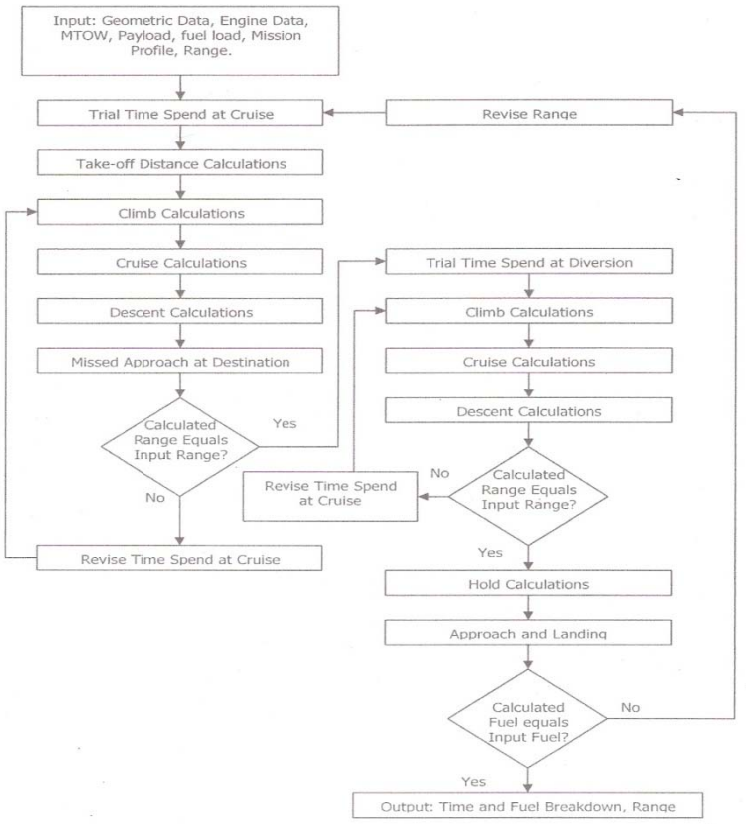

Figure 2-19: HERMES Flowchart of calculations [23]

This model refers to civil aircraft and takes into account the civil podded propulsion system which has short straight intake so that in climb, cruise and descent the loss of ram total pressure in the intake to be extremely small and the engine experiences very little as far as concern the flow distortion.

HERMES, through the mission analysis results and the gas turbine performance evaluation, give the opportunity for further engine studies such as the structural and thermal analysis, component sizing and geometry and of course life consumption.

However, HERMES, as part of TERA, cannot cover the whole range of the aircraft/engine integration (military and civil) because refers only to civil and takes into account the civil podded propulsion system. Consequently, an integrated aircraft-engine performance tool for military aircraft is needed for the completion of TERA. This is the motivation for the development of ARES.

Chapter 3 ARES Method and Possible Improvements

3.1 Introduction

As referred to the MSc thesis of the author, the propulsion systems of new military aircraft differ markedly from those of previous aircraft as a consequence of the much higher demanded requirements in terms of thrust, efficiency, reliability and ease of maintenance. At the same time, interactions between the airframe and the engine have become of even greater significance than previously. Engine performance, aircraft characteristics, and aircraft/engine integration are issues that directly affect the performance and operational capability of combat aircraft.

ARES is based on the development of a method for combat aircraft/engine integration and consists of the Combat Aircraft Model and the Engine Model. This method takes into account engine performance, aerodynamic characteristics of the aircraft, requirements of the mission (amount of demanded fuel, payload, altitude, flight speed etc) and the effects of the aircraft/engine integration (thrust losses, spillage drag, afterbody force etc.). The final output of ARES is the drag for the complete aircraft, spillage drag under different flight conditions, net propulsive force for any segment of a specific mission, uninstalled net thrust, consumed fuel and the final aircraft weight.

This method through the assessment of the final aircraft/engine performance makes feasible the decision of the aircraft/engine configuration which has the best performance, permits the use of a greater payload (missiles, bombs, etc.) and is also the most cost-effective and reliable solution that will increase the availability and survivability of the aircraft.

3.2 Combat Aircraft Model

The Combat Aircraft Model was developed with the use of Fortran 90/95. The model [9] based on the equation of motion can calculate the demanded Net Propulsive Force, which is the actual thrust of the engine, at any segment of a mission such as climb, acceleration, combination of climb and acceleration etc. It takes into account all

the parameters that affect the aircraft drag and thrust and during the simulation recalculate the values of those parameters so as the final output to be realistic and reliable.

For instance [9] the temperature and pressure are affected directly by changes of altitude. The pressure and temperature are related with density (ρ) through the equation of state p= ρRT. From this equation is derived that the increase of altitude causes a decrease of density because the pressure falls much more quickly than the temperature. The density is used for the calculation of the dynamic pressure q and consequently directly influences the value of the aircraft drag. Therefore the recalculation of density for even a slight change of altitude is necessary in order to avoid possible miscalculations. Additionally [9], the temperature is related to the speed of sound through the equation $\alpha = \sqrt{\gamma RT}$. Increase in altitude causes a decrease in the speed of sound because in the lower atmosphere the temperature falls. The speed of sound is used for the calculation of the flight velocity. Similarly to the density, the change of the speed of sound affects the calculation of drag and thrust. The programme [9] uses specific files that contain the values of density and temperature for different altitudes and then, by using the method of interpolation, calculates the new values for any change of altitude.

Moreover, during the development of the programme code, was taken into account the very important issue for the combat aircraft which is the inlet/engine integration. The inlet/engine integration affects directly the acceptable efficiency levels of the aircraft and also degrade the installed performance. Characteristics such as maximum Mach number, low-altitude penetration, manoeuvrability and acceleration can be influenced resulting in the reduction of the operational capability of the aircraft. A specific procedure [9] was developed which based on the intake design and sizing can calculate the spillage drag (ΔDspill).

The model with the use of the spillage drag, Net Propulsive Force and equation 2.12 can calculate the $F_{N,\ installed}$ and consequently from the equation 2.9 the $F_{N,uninstalled}$. The Aircraft Model uses the $F_{N,uninstalled}$ and searches all the data of the engine which were calculated with the use of the Turbomatch software. The engine data produced after a lot of simulations and recorded in software's specific file. Based on these data

and with the interpolation method, the turbine entry temperature (TET) and the uninstalled specific fuel consumption ($SFC_{uninstalled}$) that correspond at the $F_{N,uninstalled}$ can be calculated.

Afterwards, the amount of fuel that was consumed at each segment of the mission is calculated with the use of the following equation:

$$\text{Amount of Fuel consumed} = F_{N,uninstalled} \times SFC_{uninstalled} \times \text{Time} \qquad (3.1)$$

The recalculation of the new aircraft weight is now possible, because it is the initial weight W minus the amount of fuel consumed. Simultaneously, the programme depending on the mission takes into account the new values of specific parameter e.g. the new aircraft weight, the new altitude, the new velocity etc and calculates the new demanded thrust. The same procedure as the one described before takes place so as to calculate the new amount of fuel consumed. This procedure is iterated until the end of the mission. The data from each segment of the mission are recorded in specific files so as to be used for other calculations or further study.

3.3 Engine Model

An example of an engine model that was created for ARES is the MT-200 which is illustrated in figures 3-1 and is similar to EJ-200. The EJ -200 [12] is a fully modular, low Bypass Ratio (BPR), augmented military turbofan engine and was designed to power aircraft for flight with Mach number up to 2. It uses a two spool configuration and was developed for the propulsion of the Eurofighter 2000.

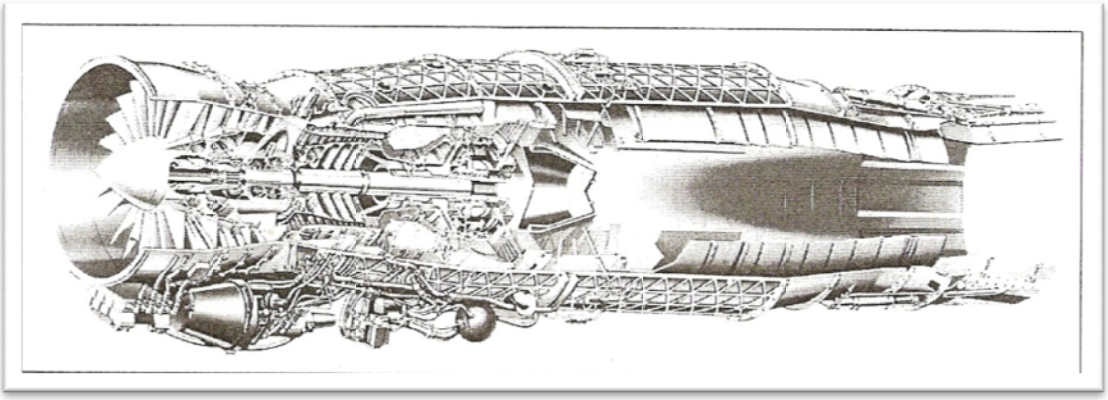

Figure 3-1: Cutaway drawing of EJ-200 [12]

The model was assembled using Pythia software and consists of 17 bricks. Station 21 corresponds to the exit of bleed air from the High Pressure Compressor, which enters again in the mixer prior to the High Pressure Turbine for blade cooling. Station 22 corresponds to the exit of bleed air from the High Pressure Compressor, which enters again in the mixer prior to the Low Pressure Turbine for blade cooling. Finally, station 23 corresponds to the exit of bleed air from the High Pressure Compressor for aircraft use e.g. air conditioning.

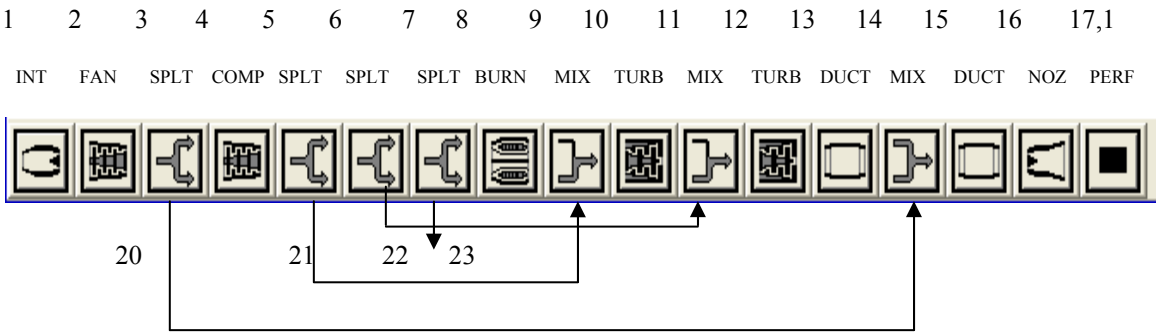

Figure 3-2: MT-200 engine model scheme in Pythia

The performance simulations are carried out with the use of TURBOMATCH and PYTHIA softwares. Cranfield University has developed TURBOMATCH software [2] a basic characteristic of which is satisfaction of the major thermodynamic principles of the working gas, such as the mass flow continuity and work compatibility. This software simulates the design and off design performance of aero/industrial gas turbine engines. The design point of the engine was in take-off sea level static condition and the simulation was carried out with the Turbine Entry Temperature (TET) as the handle of the model. Many of the parameters that were used for this engine model were gathered from the literature survey, while others which were not available or not exactly defined, were based on default values of the software or were appropriately guessed.

The most important input data that were used for the simulation of the engine are summarised in Table 3-1.

INPUT DATA	MT-200
Total Mass Flow (Kgr/sec)	77
Bypass Ratio (BPR)	0.4
Overall Pressure Ratio (OPR)	26
Fan Pressure Ratio (FPR)	4.2
High Pressure Compressor (HPC) Pressure Ratio (PR)	6.2
Low Pressure Compressor (LPC) isentropic efficiency	0.86
High Pressure Compressor (HPC) isentropic efficiency	0.85
High Pressure Turbine (HPT) isentropic efficiency	0.87
Low Pressure Turbine (LPT) isentropic efficiency	0.87
TET (K)	1820

Table 3-1: Simulation Input Data

The design point performance of the engine led to output data that were similar to the data obtained from the detailed literature survey. In Table 3-2 are tabulated the most important of these data.

OUTPUT DATA	MT-200	EJ-200
Thrust Maximum Dry (N)	60049	60000
Specific Fuel Consumption (SFC) Maximum Dry (mg/N sec)	22.47	21-23
Thrust Maximum Afterburner (N)	88828	90000
Specific Fuel Consumption (SFC) Maximum Afterburner (mg/N sec)	46.54	47-49

Table 3-2: Simulation Output Data

Such a model is very useful for the engine evaluation because it gives a lot of information about the performance. More specific the range of the Turbine Entry Temperature, the Uninstalled Specific Fuel Consumption and the Uninstalled Thrust of the engine for different altitudes and Mach Numbers, the amount of consumed fuel, the Exhaust Gas Temperature etc can be derived from the engine simulations. Additionally, with the use of the model can be calculated the thrust losses $\Delta F_{N,bleed}$, $\Delta F_{N,pot}$,and $\Delta F_{N,ni}$.. The calculation of these losses is very significant because the losses are demanded for the calculation of the Installed Thrust and consequently of the Net Propulsive Force.

The upper outputs can lead to very important conclusions. Firstly, the information of the TET range enables the user to evaluate the durability of the engine, due to the fact that the turbine entry temperature affects the turbine's life limit and consequently to realise if the engine is a reliable solution that will increase the availability of the aircraft. Secondly, the exhaust gas temperature affects directly the survivability, susceptibility and vulnerability of the aircraft because of the fact that many of the new, "clever" missiles detect and follow the aircraft based on its exhaust gas temperature. Lower exhaust gas temperature means higher possibility for the aircraft to survive from probable missile attack.

3.4 Performance Calculations

In the present sub-section there is a part of ARES performance calculations (Msc Thesis) that is based on the use of three different engines models which are similar to EJ-200, M88-2 and Redesigned M53-P2 and were developed with the use of Pythia software.

The aircraft (F-16)/engine performance is tested and evaluated, taking into account the thrust losses due to the engine installation and drag contribution. The same procedure was accomplished for the three engines and for a specific part of an aircraft mission, which includes the following segments:

- Climb in 15 seconds, from 16000 ft to 17000 ft with constant Mach number 0.6,
- Aircraft acceleration in 30 seconds, from Mach number 0.6 to 0.7 at constant altitude 17000 ft,
- Climb from 17000 ft to 18000 ft with aircraft acceleration from Mach number 0.7 to 0.88 in 125 seconds, and
- Flight of 600 seconds (10 minutes) at constant altitude 18000 ft with constant Mach number 0.88.

The aircraft weight is 10772 Kg and the aerodynamic characteristics of the F-16 are:

Aspect Ratio (AR) = 3

Wing Area (S) = 300 ft^2

Wing span (b) = 30 ft

The results that were derived from the whole procedure are summarised in Table 3-1.

	MT-200	**MT88-2**	**Redesigned Engine**
TET (K) Range	1476 - 1679	1534 - 1748	1381 - 1611
SFC (mg/Nsec)	26.7 - 30.7	26.1 - 30.4	27.1 - 30.8
Fuel Burn (Kg) per second	0.58 - 0.88	0.57 - 0.9	0.59 - 0.92
Final Aircraft Weight (Kg)	10225	10221	10219

Table 3-3: Performance Calculations

The spillage drag was calculated for different Mach numbers and altitudes and then, with the use of the interpolation method, the spillage drag for every combination of altitude, Mach number and time was estimated. Table 3-4 lists the calculated values of spillage drag (detailed calculations for MT 200 are included in Appendix B).

ALTITUDE (m):	4870					
Mach Number	0.6	0.65	0.7	0.75	0.8	0.88
MT200 : Spillage drag (N)	0	0	0	0	67.8	615.6
MT88-2 : Spillage drag (N)	0	0	0	52.3	178.3	767.3
Redesigned engine : Spillage drag (N)	0	0	0	0	75.6	594.9
ALTITUDE (m):	5000					
Mach Number	0.6	0.65	0.7	0.75	0.8	0.88
MT200 : Spillage drag (N)	0	0	0	0	66.7	605
MT88-2 : Spillage drag (N)	0	0	0	34.2	155.8	730.5
Redesigned engine : Spillage drag (N)	0	0	0	0	49.6	584.6
ALTITUDE (m):	5250					
Mach Number	0.6	0.65	0.7	0.75	0.8	0.88
MT200 : Spillage drag (N)	0	0	0	0	43	546
MT88-2 : Spillage drag (N)	0	0	0	16.6	113	661
Redesigned engine : Spillage drag (N)	0	0	0	0	48	493
ALTITUDE (m):	5500					
Mach Number	0.6	0.65	0.7	0.75	0.8	0.88
MT200 : Spillage drag (N)	0	0	0	0	41.6	490.2
MT88-2 : Spillage drag (N)	0	0	0	16	91	639
Redesigned engine : Spillage drag (N)	0	0	0	0	23.2	476.5

Table 3-4: Spillage drag for various Mach numbers and altitudes

At low Mach numbers the spillage drag is zero due to the fact the ΔCD is zero. As the Mach number increases and the MFR decreases, the ΔCD is different to zero and consequently the spillage drag is also different to zero. Furthermore, it is obvious that for the MT88-2 the spillage drag appears from Mach number 0.75 in contrast to the other two engines where it appears at Mach number 0.8. This happens because in the case of aircraft/ MT88-2 integration the MFR at Mach number 0.75 is lower than the MFR for the other two cases.

Moreover, from the spillage drag calculations was derived the conclusion that the amount of apparent spillage drag during the aircraft/redesigned engine integration is the lowest in comparison with the other two cases. This is a very important result, because it leads to the conclusion that the use of the redesigned engine causes the minimum decrease (in terms of the spillage drag) of the engine thrust.

As is obvious from the final calculations, all the engines had the demanded performance so as to fulfil the requirements of this part of the mission. The MT-200 had the lowest fuel consumption, following by the MT88-2 and the redesigned engine. The amount of fuel that was consumed was 547 Kg, 551 Kg and 553 Kg respectively.

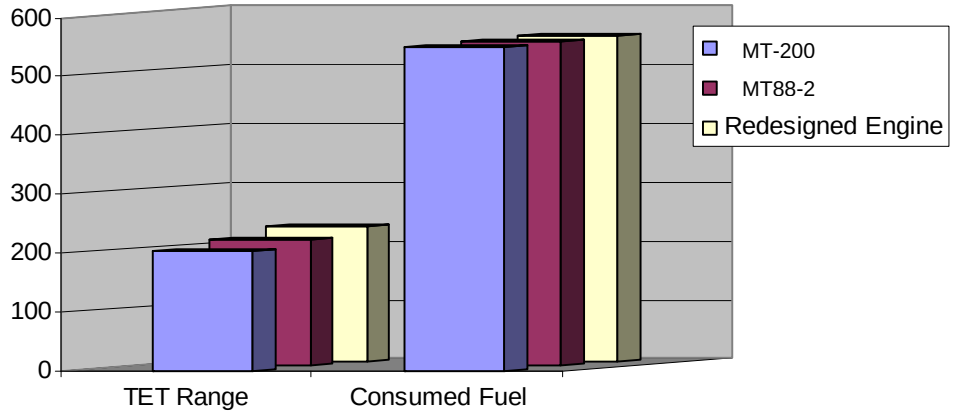

Figure 3-3: Results from the Performance Calculations

Based on the calculated results, is derived the conclusion that the performance of the MT-200 is better than the performance of both the MT88-2 and the redesigned engine. As is obvious from figures 3-4 and 3-5, apart from the fact that it consumes

0.9% (average percentage) less fuel than the other two engines, it also has 9.4% (average percentage) lower TET and 2.6% (average percentage) lower SFC range.

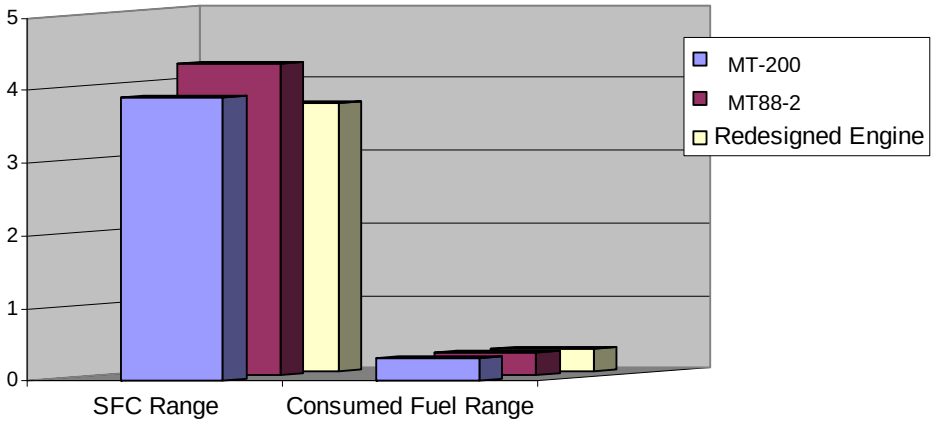

Figure 3-4: Results from the Performance Calculations

The combination aircraft/MT-200 for this specific mission has the best performance, permits the use of more payload (missiles, bombs, etc) and is also the most cost-effective and reliable solution that will increase the availability of the aircraft.

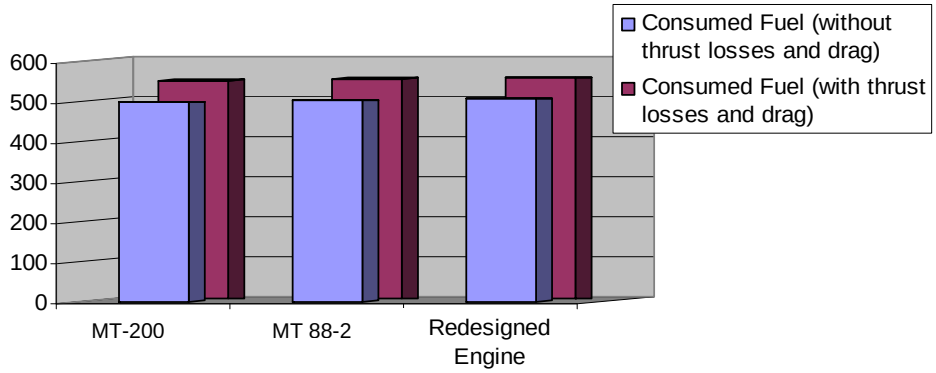

Figure 3-5: Comparison of the amount of the consumed fuel

The evaluation of the aircraft/engine performance, by taking into consideration the thrust losses and drag contribution, led to results that are presumable. The contribution of the spillage drag and the thrust losses had as a result the increase of the uninstalled net thrust $F_{N,uninstalled}$ by approximately 7.5% (average percentage) and

consequently the increase of the consumed fuel by approximately 8.4% (average percentage).

3.5 Possible Improvements

As it is referred in the previous chapters, the final outputs that can be derived from ARES are based on calculations that depend on the aerodynamic characteristics of the aircraft, the effects of the aircraft/engine integration (thrust losses, spillage drag, afterbody force etc.) and the results of the engine performance simulations. Further development of the software is feasible and can be focus in two specific fields that affect firstly the engine performance and secondly the aerodynamic characteristics of the aircraft.

A far as concern the first part (engine performance) the possible improvement refers to the effects of the flow distortion. As it is mentioned in the previous chapters the effects of the flow distortion on the engine performance are directly connected with the effects of the distortion on the performance of the compressor. The main effects [5] of the total-pressure distortion on the compressor performance are the loss of the airflow capacity for a specific non-dimensional speed and the loss of efficiency. A very important step for ARES's improvement is the development of a process which will be able to connect the effects of the flow distortion with the engine performance.

A far as concern the second part (aerodynamic characteristics of the aircraft) the possible improvement refers to the external configuration of the aircraft. ARES calculate the drag and the demanded thrust based on the fact that the combat aircraft is clean. A possible use of external tanks, bombs, missiles, pylons or combinations of them change the external configuration of the aircraft and consequently affects directly the aircraft drag and the demanded thrust. The steps that can be followed so as to be incorporated in the software the influence of the external loads in aircraft drag is the following:

- The creation of the external load's geometry with the use of an appropriate software (Gambit)

- The creation of the F-16's wing geometry
- The creation of different models that will cover all the possible combinations of the aircraft wing and external loads
- CFD simulations for different altitudes, velocities and angle of attacks
- The calculation of the drag
- Modification of the ARES code so as to integrate the external load's drag contribution.

Additionally, as possible improvement can be considered the incorporation of a code module (FORTRAN) in ARES method, which will be able to deal with specific segments of a flight mission which are the Take off and Landing.

The objective of this study is to cover the second part of the possible improvements and also to create the aircraft model so as to be feasible the creation of a data base of aircraft flight conditions (altitude, speed, AOA) tied together with the resulted flow distortion in the engine face.

The embodiment of all the previous improvements in ARES model will lead to the creation of a complete integrated aircraft-engine performance tool for combat aircraft which through the mission analysis results and the gas turbine performance evaluation, will give the opportunity firstly for further engine studies such as the structural and thermal analysis, component sizing and geometry, life consumption and secondly for the study and evaluation of specific military missions.

Chapter 4 Aircraft Model CFD Study

4.1 Introduction

The objective of this study is to develop a procedure so as to be feasible for a researcher to illustrate, for different operating conditions (altitude, Mach number, angle of attack etc), the fluid path in the vicinity of the combat aircraft (especially in the intake and nozzle area) and to receive information about the main parameters (pressure, velocity, temperature etc) in the area of the engine face.

From a computational fluid dynamic point of view, the flow under analysis is significantly complex because is viscous, fully turbulent and three dimensional. All these reasons lead to increased computational power and resources and additionally to increased geometry meshing difficulties.

The general procedure that will be used in this case is illustrated at the Figure 4-1.

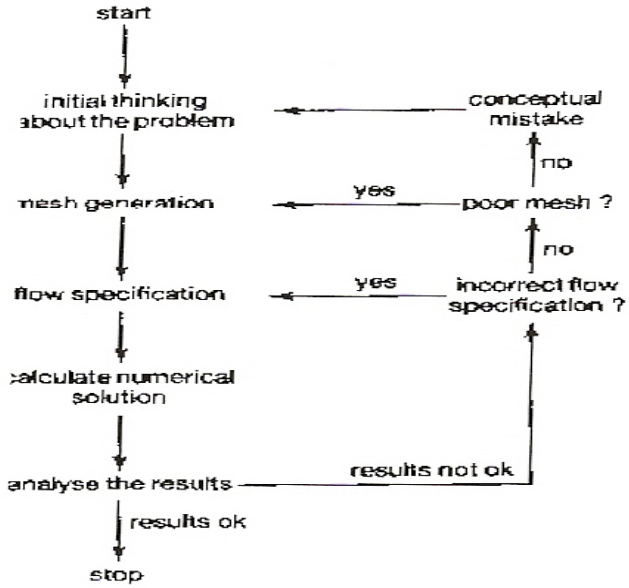

Figure 4-1: "The analysis process" according to Shaw [1]

The steps that must be followed are, firstly the creation of the aircraft geometry and the computational domain, secondly the meshing and thirdly the simulation of the case with specific boundary conditions. As it is apparent from the previous Figure, the basic reasons that can lead to insufficient results are:

- a conceptual mistake,
- a poor meshing,
- an incorrect flow specification.

The correct geometry and the reasonable computational domain are the basic parameters for a sufficient simulation output. The quality and the density of the mesh play also a vital role in the final results and for this reason a researcher have to check whether the results are meshing dependent or not. The final but also very important parameter that must be checked is the flow specification and more specifically the boundary conditions. In the present study this step is quite complicated and difficult due to the fact that the decision of the boundary conditions is affected directly from the different operating conditions (altitude, Mach number, angle of attack etc) that are demanded for the completion of a military mission.

4.2 Geometry and Meshing (Gambit)

Since the geometrical data of a combat aircraft are confidential, it is very difficult for a researcher to find out detailed information about the exact shape and geometry of a specific combat aircraft. For this reason, in this study was used a diagram (Figure 4-2) which refers to the F-16's geometry but without any detailed information. Apparently, the combat aircraft model that was created is similar to F-16 and by no means the exact F-16.

In this specific case the software that was used for the creation of the aircraft model is Gambit. Although the Gambit software has some limited CAD options, the use of Gambit's standard procedure for creating 3D objects can lead to a very reliable and

detailed model. Having the coordinates of the vertices it is feasible to create a surface and then generate a volume.

From the diagram that is illustrated at the following Figure, were extracted the

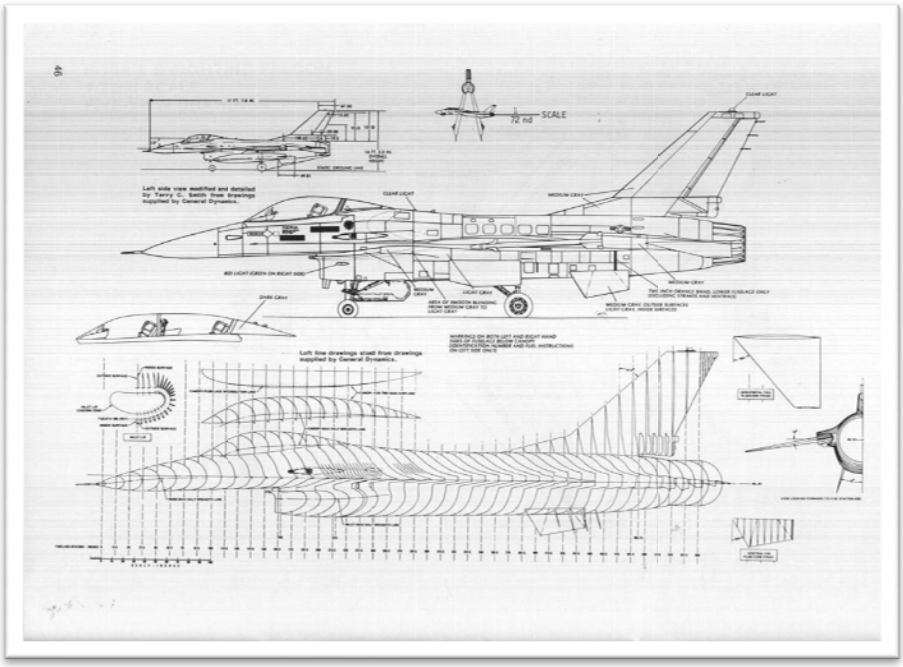

Figure 4-2: Source of Military Aircraft's Geometric Data [37]

coordinates for over a thousand vertices, then were imported to the Gambit software and continuously the surfaces and the volumes were created. The whole procedure was very difficult, because the geometry of the aircraft requires the application of splines and curved surfaces which need to be done very carefully so as to avoid incomplete closed volumes that lead to leakages during the simulation.

The aircraft model that was created consists of the fuselage, the intake and a small part of the aircraft's wings. This approximation is acceptable due to the fact that the main objective in this specific case is the study of the aircraft-engine integration and the influence of the airframe/intake in the engine thrust. The model is available in the following figures.

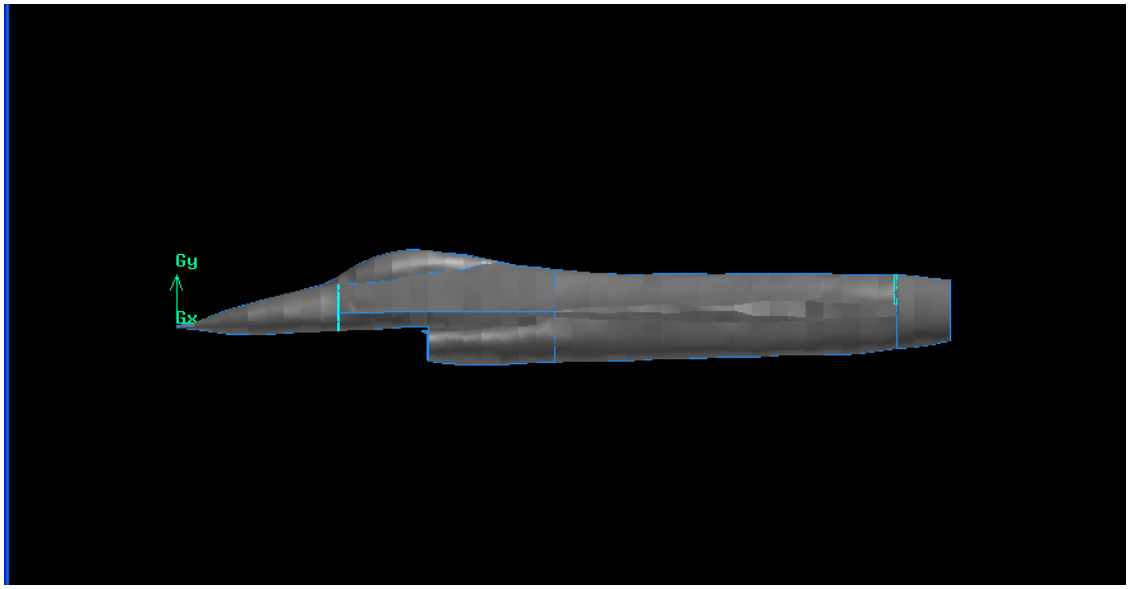

Figure 4-3: Aircraft model

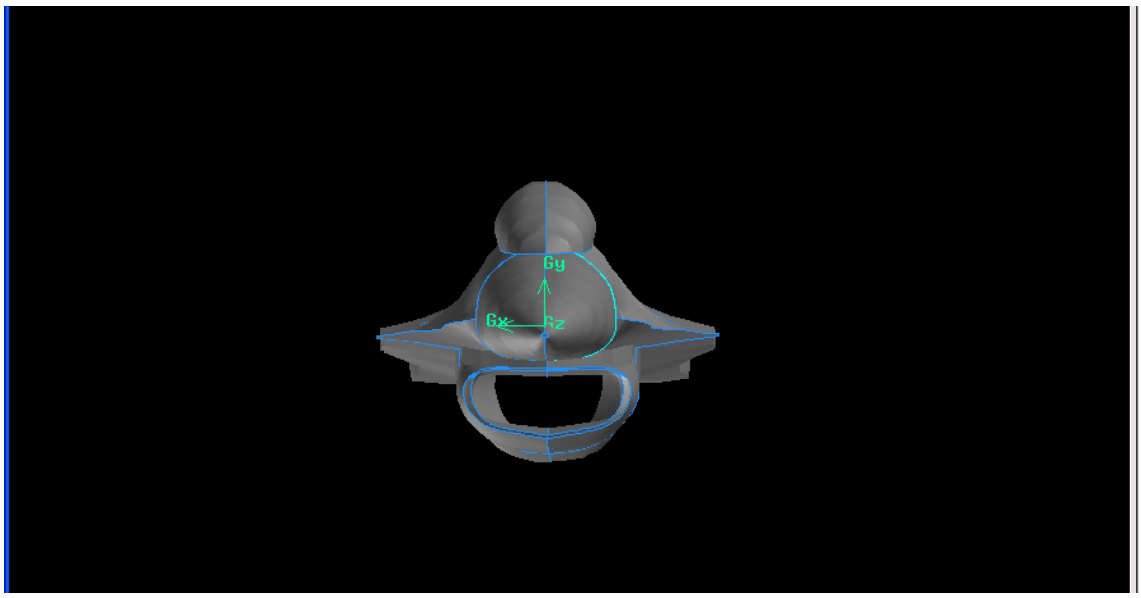

Figure 4-4: Front part of the Aircraft model

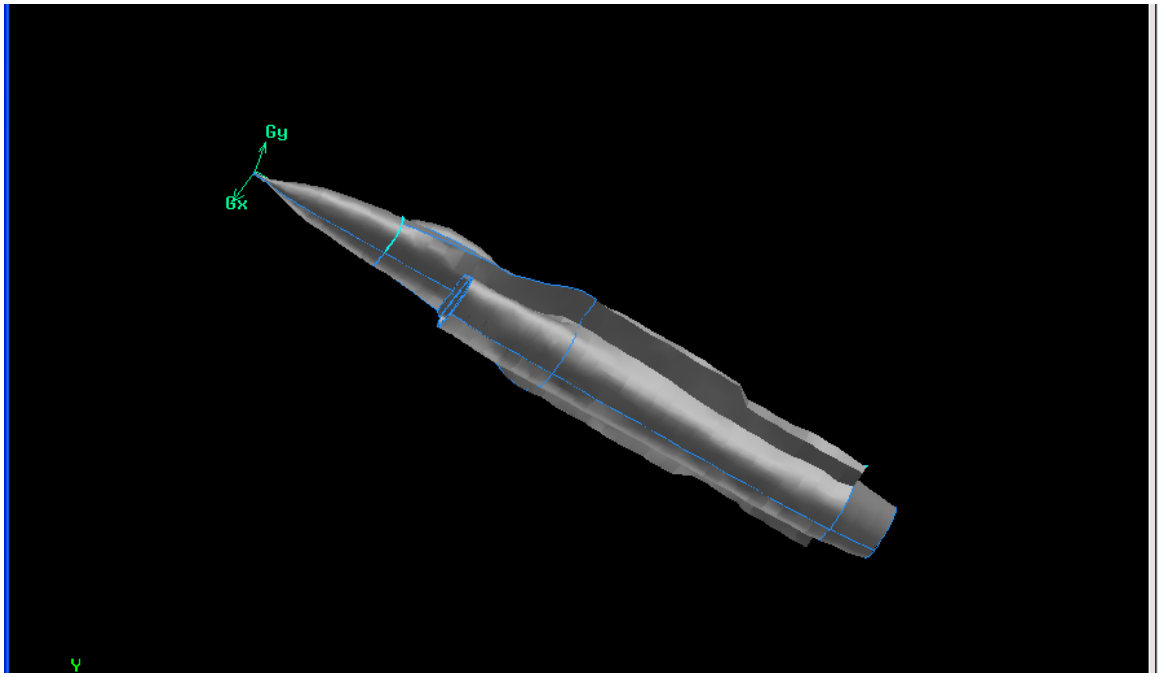

Figure 4-5: Lower part of the Aircraft model

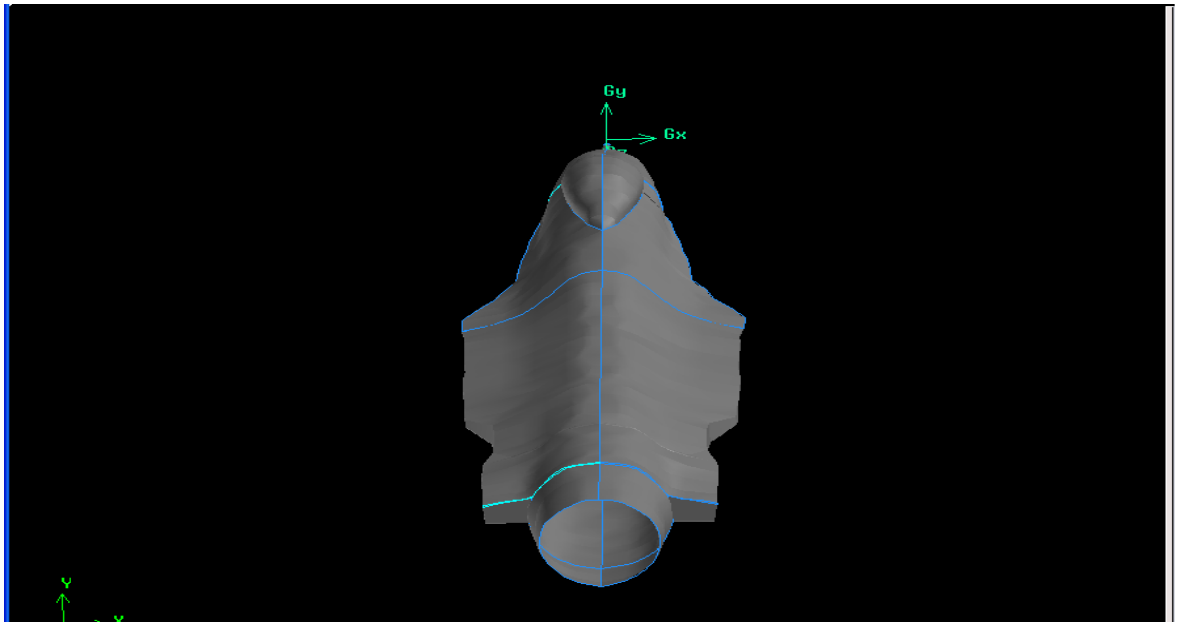

Figure 4-6: Upper part of the Aircraft model

One of the most important steps in the grid generation is the computational domain. The shape and size of the domain is a compromise of two parameters. These two parameters are firstly the impact of the aircraft on the free stream and secondly the

computational load. Based on them was created a computational domain (Figure 4-7) with five volumes and the aircraft in the middle. As it is apparent from the Figure, the final domain has cavities in the form of the half aircraft and intake. These two cavities were created after the subtraction of the aircraft and intake volumes from the outer volume.

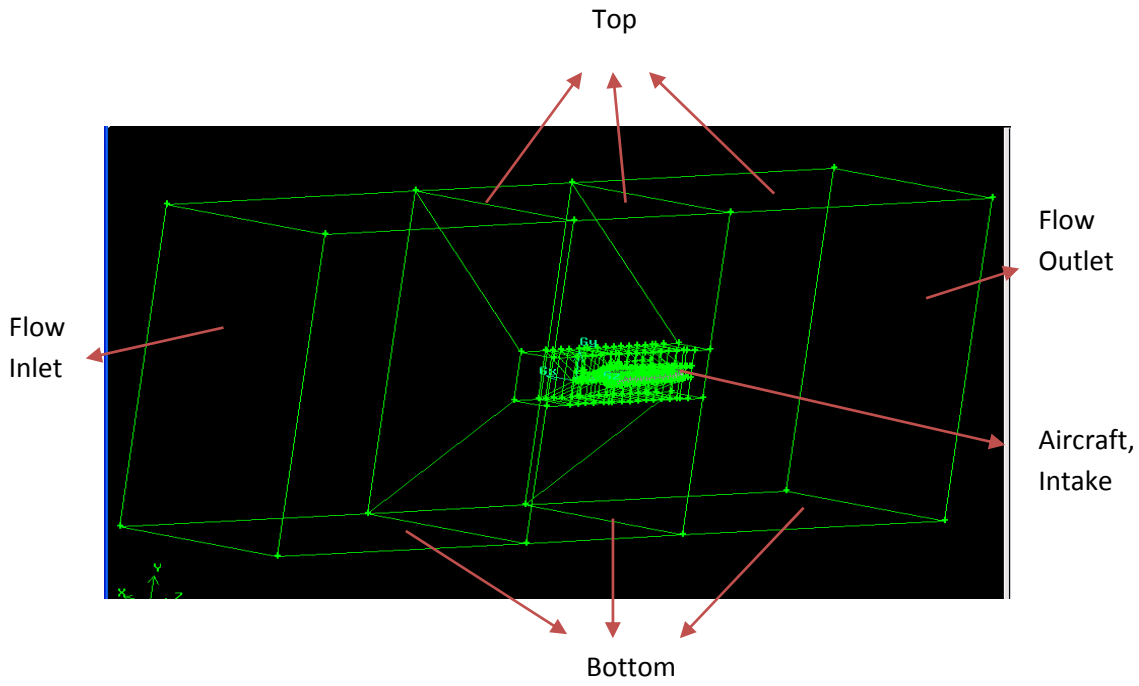

Figure 4-7: Computational domain (without meshing)

The next step after the creation of the aircraft geometry is the meshing. This process is very significant for the simulation output and simultaneously the most time consuming procedure in the whole study. The creation of a good mesh demands the investment of time because in many cases is necessary the changing or the optimization of the initial grid so as the final meshing to be finer and with the right density. The density of the mesh depends on the area that is applied, the accuracy that is demanded in the study of each case and finally the necessity to keep the computational load low.

In the present study the density is higher in the aircraft's surface and in the areas around that, so as to achieve a detailed display of the flow path in the vicinity of the aircraft, and additionally in the entrance and inside the intake, so as to succeed an

accurate simulation output and simultaneously an acceptable study of the phenomena that take place in the intake. These specific areas are illustrated in the following Figures.

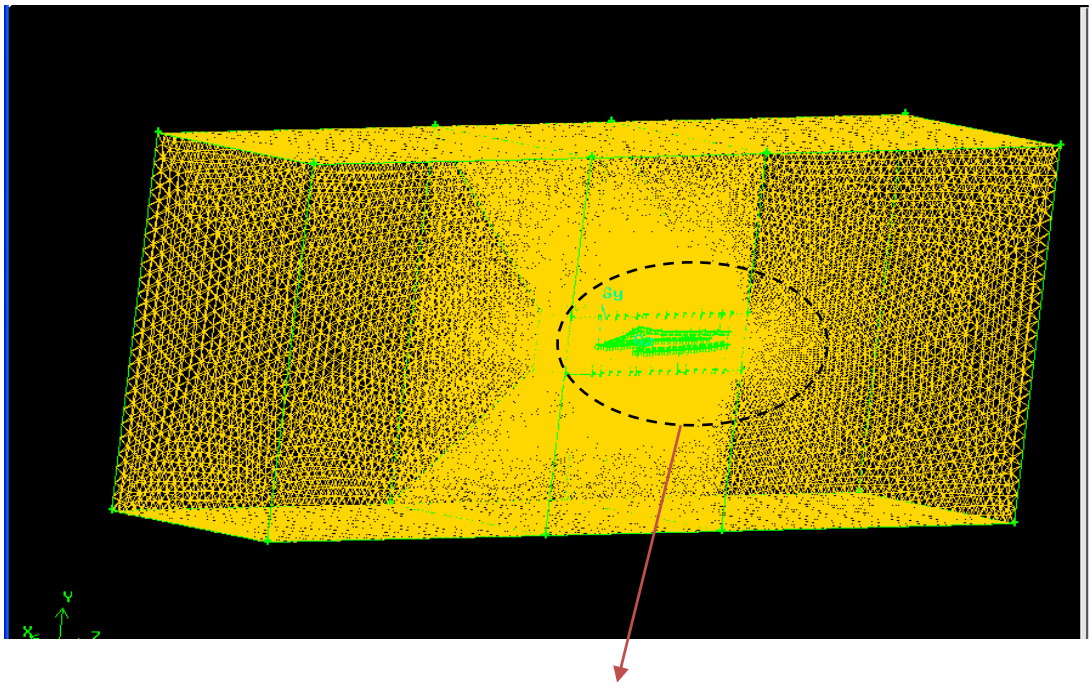

Figure 4-8: Computational domain (with meshing)

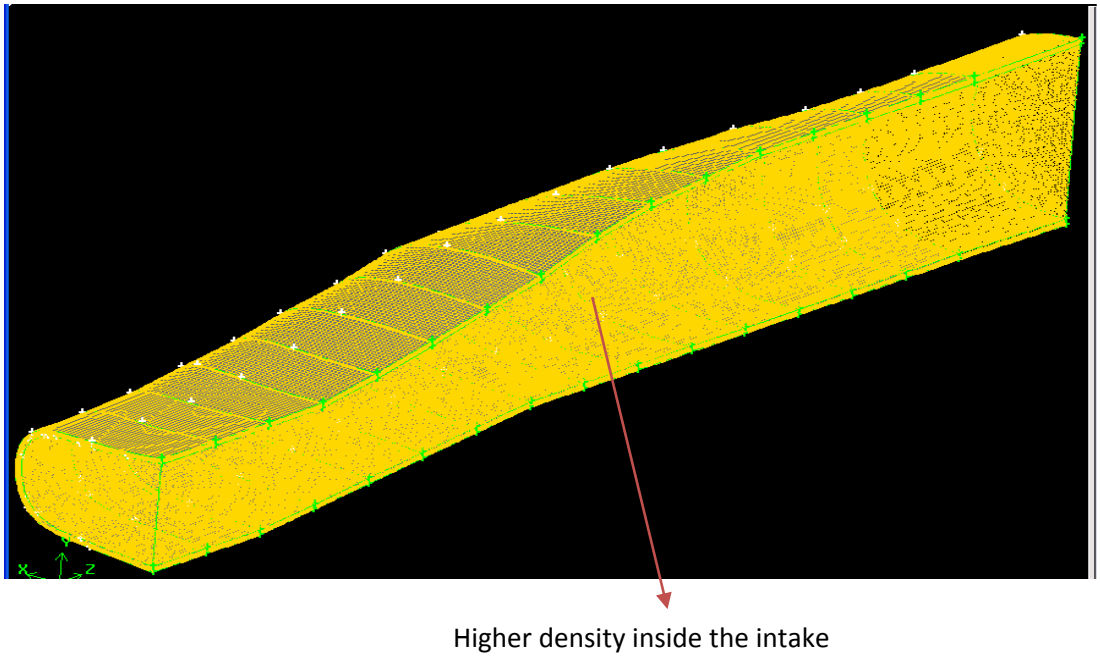

Figure 4-9: Intake of the aircraft

The procedure which is used for meshing is the same with the one that is applied in creating the aircraft geometry. Firstly a specific number of nodes (in compliance with the demanded density of the mesh) are located in every edge, secondly the software create the mesh of each face (surface) and finally the mesh of each volume and consequently the 3D grid. The final mesh must be fine without skewed elements or negative volumes so as the final output to be reasonable and reliable.

In the present study the number of the nodes that were used was almost four (4) millions and the number of the cells that finally were created in the interior of the mesh was almost sixteen (16) millions. In the Figure 4-10 is illustrated the mesh of the aircraft and the intake. As it is apparent from the same Figure, the area around the aircraft was divided into sixteen (16) volumes. This procedure is preferred when the geometry is complex with lots of curved surfaces. The smaller volumes give the opportunity of a better and finer meshing because the faces are smaller, the partial geometry is less complicated and finally is much easier a possible re-meshing.

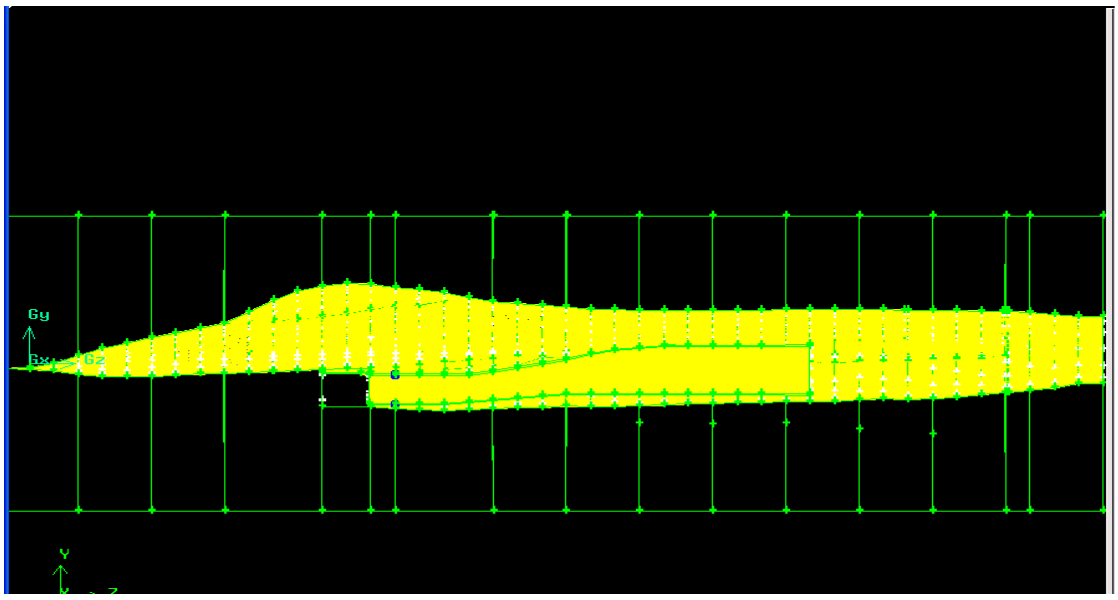

Figure 4-10: Mesh of the aircraft

As mentioned before, the density of the mesh plays vital role in the final result and computational load. In this study, as it is illustrated in the Figure 4-11, the mesh density is not constant throughout the whole domain and it is obvious that the mesh is

getting coarser away from the surface of the aircraft. This outcome is feasible when distance ratios and different numbers of nodes are applied on the edges of the outer volumes.

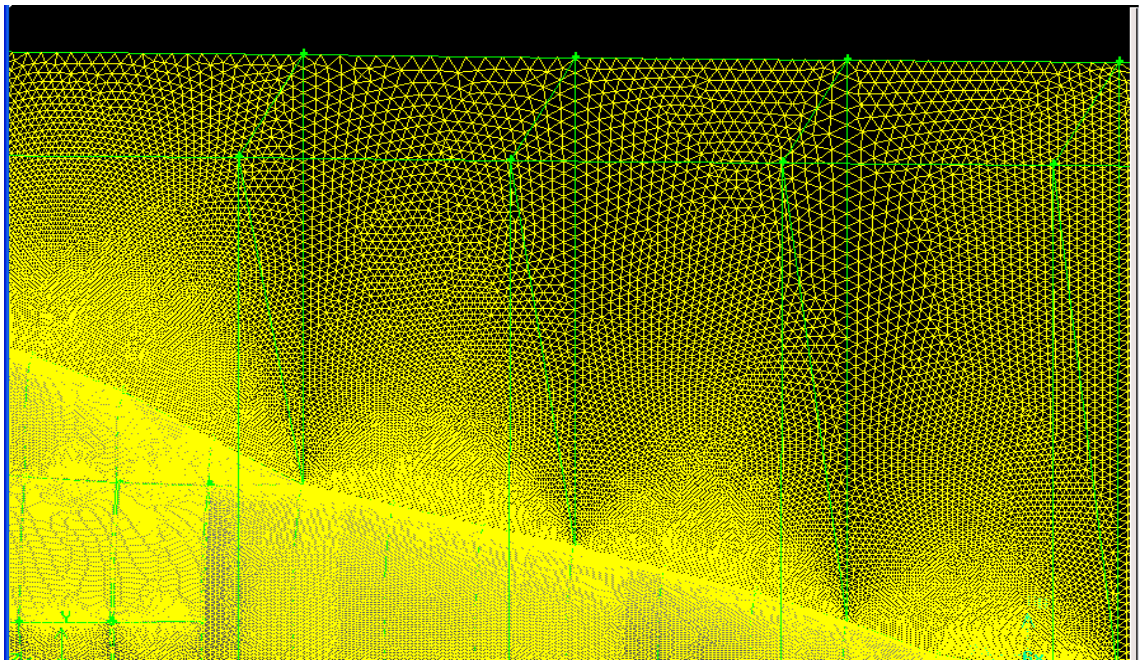

Figure 4-11: Mesh around the aircraft

Due to the fact that one of the main objectives of this study is to find out the values of some parameters such as pressure, velocity, temperature etc in the area of the engine face for different operating conditions, it was inevitable the creation of a more detailed and thicker meshing in the area inside the intake. As is illustrated in the Figure 4-12 in model was created a boundary layer on the internal surface of the intake. The advantages of the boundary layer are firstly the fact that there is a fine near wall grid so as to achieve a better study of the phenomena near the wall and secondly a more accurate simulation output. The disadvantages are the slow convergence due to elongated cells and the high storage requirements.

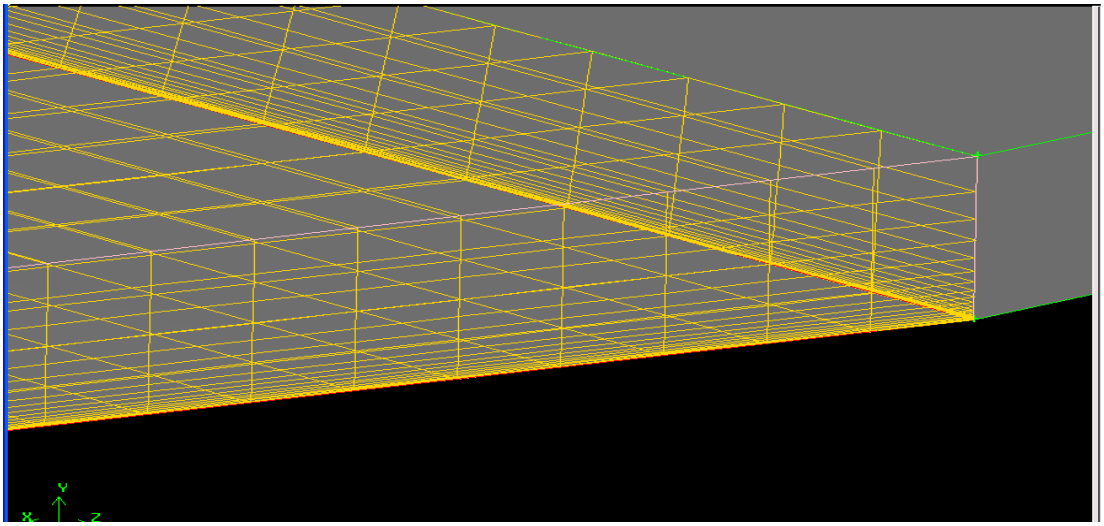

Figure 4-12: Boundary layer inside the intake

The creation of the boundary layer based on initial estimations (Figure 4-13) and more specifically used for the parameter "a" (first row) the value of 0.0002, for the growth factor ($\frac{b}{a}$) the value of 1.3, for the depth (D) the value of 0.0743 and finally created eighteen (18) rows. As it is logical and understandable, after the study of the first simulations results maybe will be necessary the reconstruction of the boundary layer for better results.

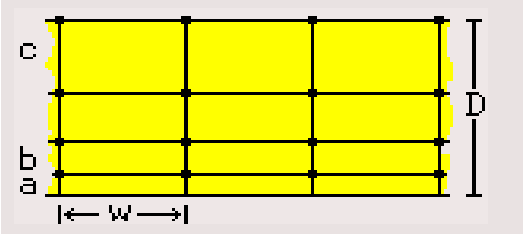

Figure 4-13: Characteristics of the Boundary layer

4.3 Specification of the Boundary Conditions

The definition of the boundary conditions is a very significant step in a CFD study because must mimic the real physical representation of the fluid flow. Initially [2] suitable fluid flow boundary conditions are required in the Flow Inlet and Flow Outlet (Figure 4-7) so as to accommodate the fluid behavior entering and leaving the flow domain.

In the present study the Flow Inlet, Flow Outlet, Top, Bottom (Figure 4-7) and the side opposite the aircraft were defined as pressure far-field [2] due to the fact that they are open boundaries and additionally far enough away from region of the aircraft.

The surface of the aircraft and intake can be considered as internal [2] "obstacles" within the computational domain so were defined as "walls".

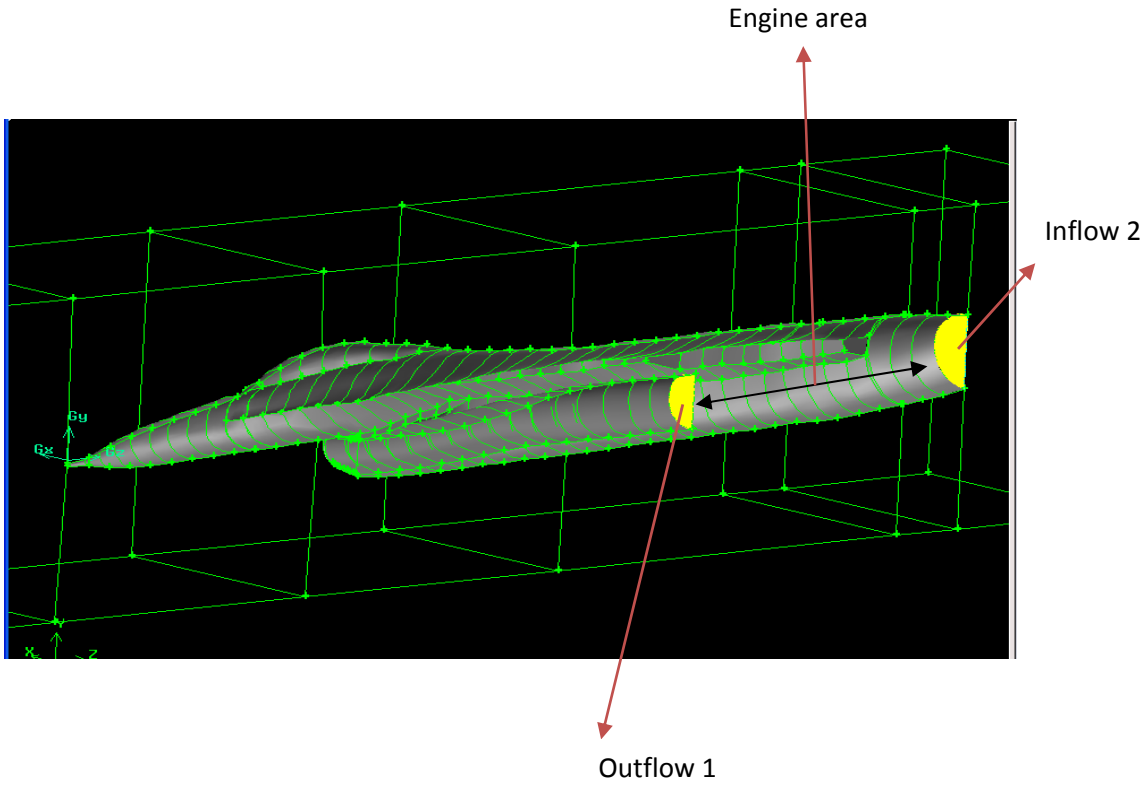

Figure 4-14: Boundary Conditions

As it is apparent from the Figure 4-14 inside the aircraft and after the intake there is the engine area. In this specific area it is necessary to be allocated [2] sink and source of mass at the boundaries, so as to ensure the correct mass flow into and out of the solution zone. The "outflow 1" was defined as a "pressure outlet" where a target mass flow was set and the "inflow 2" was defined as "mass flow inlet". At this point must be mentioned that because of the fact that only half of the intake is simulated, the value of the mass flow that is used in the simulation is the half of the mass flow that is calculated in TURBOMATCH software.

4.4 Numerical Solution

The next step after the creation of the aircraft model geometry, meshing and the definition of the boundary conditions is the numerical solution with the use of a CFD solver. The solution procedure [2] that usually is used can be described by the chart that is presented in the Figure 4-15.

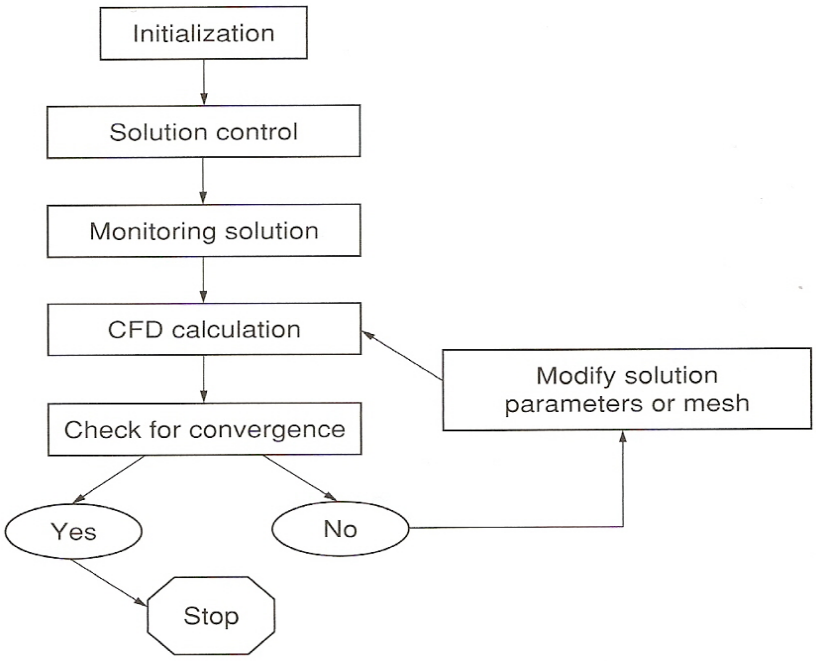

Figure 4-15: Solution Procedure [2]

The previous procedure can be followed so as to be obtained the finally simulation results. The accomplishment of the necessary software (FLUENT) settings is ready and more specifically, after the model was scaled, the material was defined as air ideal gas (compressible), the energy equation was enabled (since there are flows with different temperature mixing), the operating and boundary conditions were set for a flight with Mach number 0.5 in altitude 5000 m, an initial adjustment was made for the under-relaxation factors and the convergence criteria and finally was used the solution procedure SIMPLE with the First-Order Upwind interpolation scheme as a start. In the present study because of the turbulent flow, is demanded the use of a turbulent model.

The turbulent models that can be used are the k-ε and the k-ω. The comparison of the results will show which turbulent model is more accurate and appropriate for this specific case. After the decision of the turbulent model the interpolation scheme that will be used is the Second –Order Upwind for more detailed and reliable simulation outcomes.

4.5 Future Work

The interaction between the airframe and the engine alters significantly the performance of the uninstalled Gas Turbine engine. The airflow has to go through the air intake and as a result additional losses are induced, degrading thus the output of the engine.

The aircraft model, which is described in the present chapter, can be used as the basic tool for a future study which will focus mainly on the effect that a distorted air flow will have on the performance of the engine. More specifically, through the fluent simulations can be obtained a database of aircraft flight conditions (altitude, speed, attitude) that are connected directly with the resulted flow distortion in the engine face. The model is capable to simulate different flight conditions coupled with different angle of attack of the aircraft. Furthermore the produced database gives to a future researcher the main information so as to find out how the flow distortion affects the compressor function and consequently to develop a method to estimate the final change of the engine performance.

Due to the fact that the case has a huge number of cells (sixteen millions), the computational load will be big and consequently the time that will be needed for the completion will be quite big too. It is obvious that the whole procedure is time consuming and apparently, any changes in the settings will lead to new simulations and simultaneously in further delays.

Chapter 5 External Tank CFD Study

5.1 Introduction

The objective of this study is to create a procedure which can be used for the calculation of the additional drag that an external load (external tanks, bombs, missiles, pods) contribute in the flight of a combat aircraft. This procedure contains the creation of a external load CFD model which through the simulations will give as output the additional drag that this load produce in all operating conditions (altitude, Mach number, angle of attack etc) of a combat aircraft.

The information that can be received from this study are valuable because can help in the evaluation of the engine performance and simultaneously to make apparent if a specific aircraft- engine system is capable to accomplish the demanded operating requirements. More specifically in this chapter are analysed the basic steps for the calculation of the drag that is contributed from the use of an external fuel tank.

From a computational fluid dynamic point of view, the flow under analysis is significantly complex because is viscous, fully turbulent and three dimensional. All these reasons lead to increased computational power and resources and additionally to increased geometry meshing difficulties.

5.2 Geometry and Meshing (Gambit)

As mentioned in Chapter 4 (4.2) the geometrical data of a combat aircraft are confidential and it is very difficult for a researcher to find out detailed information about the exact shape and geometry of the wing of a combat aircraft and also of a specific external tank. For this reason, in this study for the creation of the demanded models, were used a diagram (Figure 5-1) which refers to the wing of the F-16, but without any detailed information, and a plastic F-16 model. The two models that were created are similar to F-16's (wing and external tank) and by no means exactly the real.

In this specific case the software that was used for the creation of the models is again Gambit. Having the coordinates of the vertices it is feasible to create a surface and then generate a volume.

The procedure that was followed is the same with the one that was used for the creation of the aircraft model. More specifically from the diagram that is illustrated at the following Figure, were extracted the

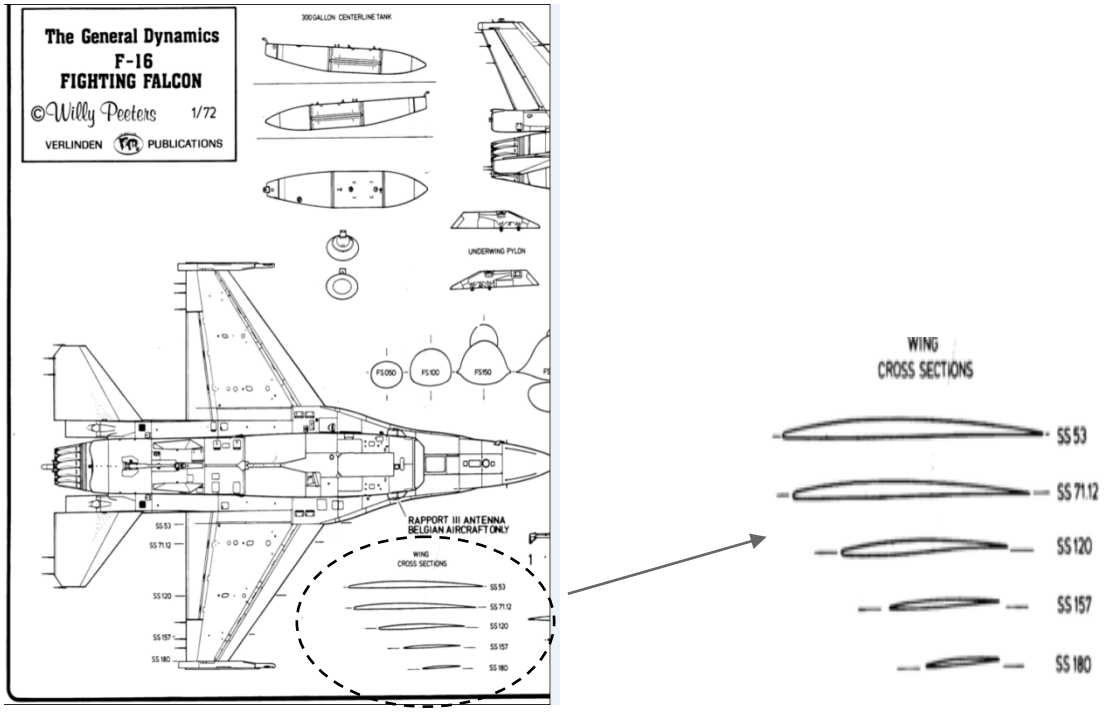

Figure 5-1: Source of F-16's Wing Geometric Data [38]

coordinates for two hundred vertices, then were imported to the Gambit software and continuously were created the surfaces and the volumes. The procedure was very difficult, because the geometry of the aircraft wing requires the application of curved surfaces which need to be done very carefully so as to avoid incomplete closed volumes that lead to leakages during the simulation. The model is available in the following figures.

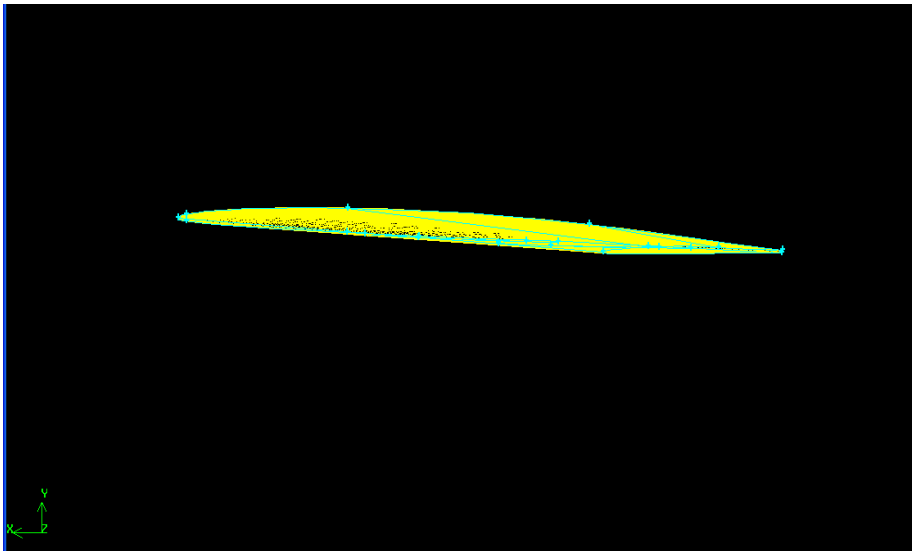

Figure 5-2: Wing model

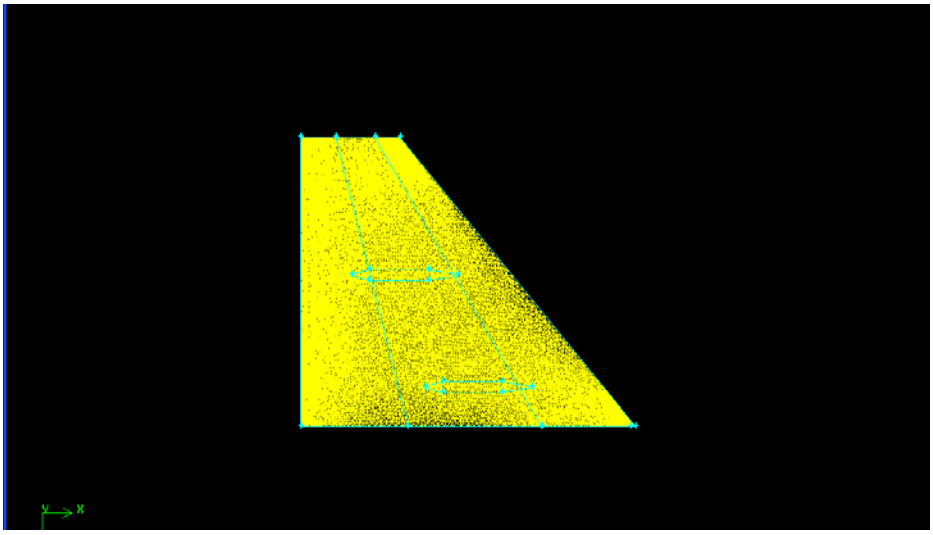

Figure 5-3: Wing model

Additionally, for further accuracy as far as concern the wing model and for the creation of the external tank model was used a plastic F-16 model with full external configuration (bombs, external tanks, pylons etc). From this model were used the aircraft wing and one of the external tanks. These two parts were cut in strips so as to be feasible the extraction of specific vertices and afterwards the calculation of the coordinates of each vertex. Through this procedure and with the use of AutoCAD, were extracted the coordinates of over three hundred vertices, then were imported to the Gambit software and continuously were created the surfaces and the volumes. The external tank model is available in the following figures.

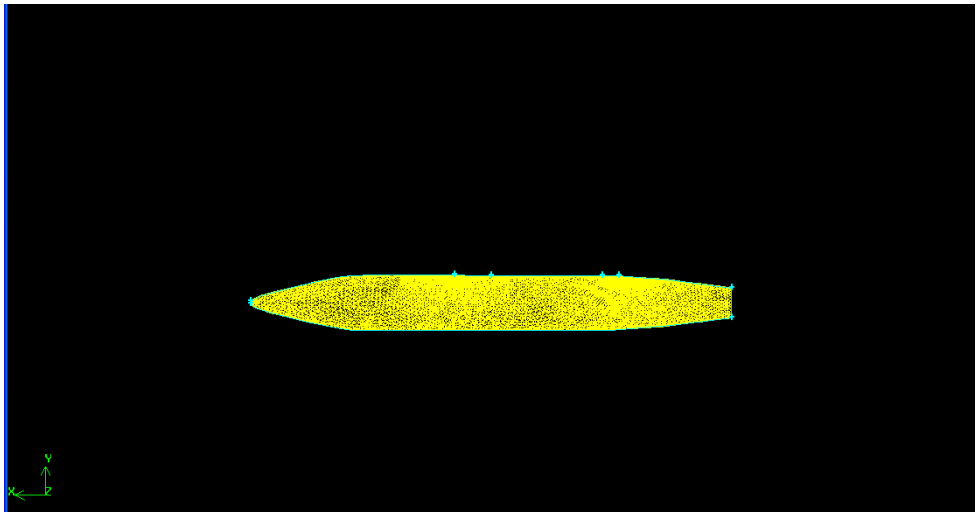

Figure 5-4: External tank model

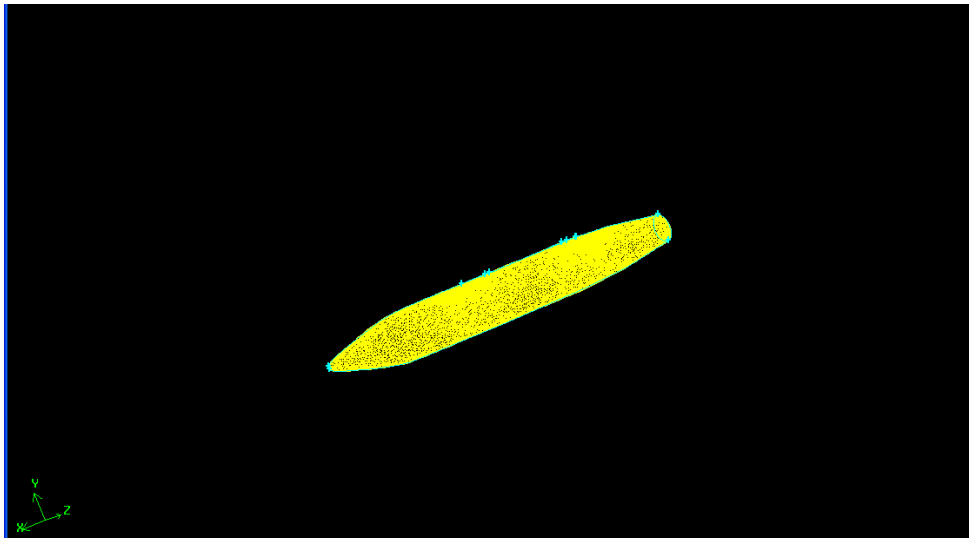

Figure 5-5: External tank model

In this part of the study the main goal was the calculation of the external tank's drag for different operating conditions (altitude, Mach number, angle of attack etc). For this reason it was necessary the combination of the two models (wing and external tank) so as to take into account the interaction between the wing and the tank. The missing part for this connection was the pylon. For the pylon, the only available source of information was the plastic F-16 model. The procedure that was followed was the same that was used for the creation of the external tank model. Although this procedure was much more difficult and time consuming than the previous one, because of the small size of the pylon from the plastic model, the final output was satisfactory. The final model is available in the following figures.

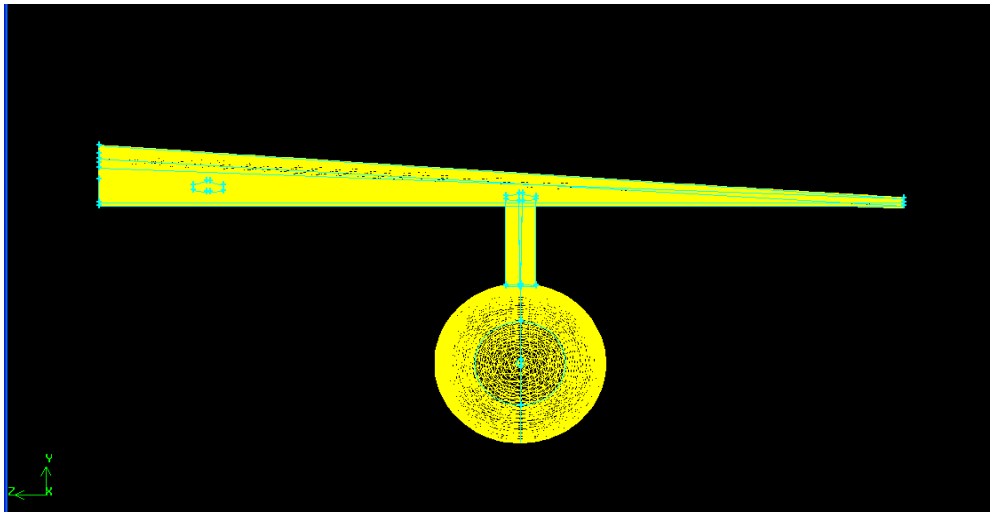

Figure 5-6: Wing, External tank and pylon model

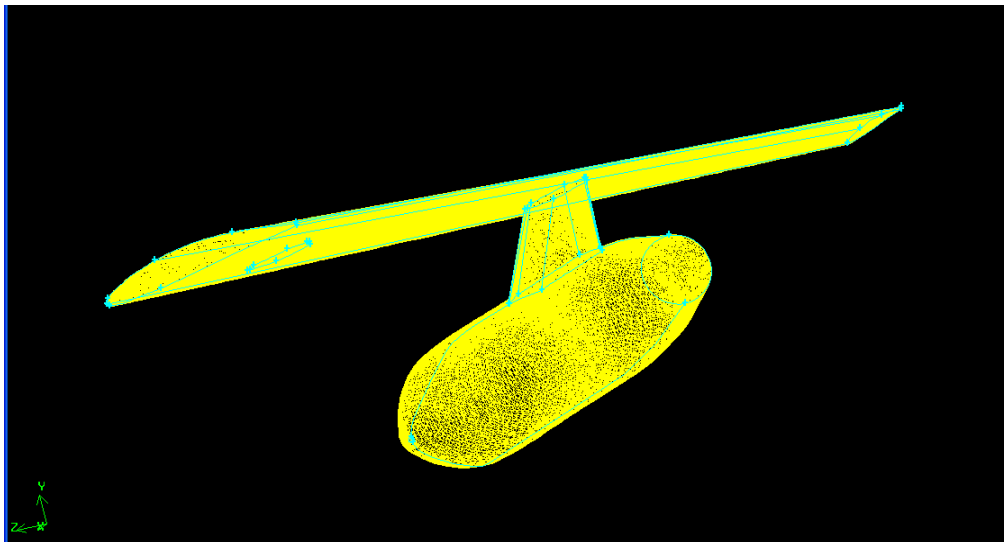

Figure 5-7: Wing, External tank and pylon model

In the grid generation vital role plays the computational domain, which depends on the impact of the wing-tank on the free stream and the computational load. The computational domain that was created is (Figure 5-8, 5-9) a half cylinder shape and both the wing and external tank in the middle. This specific computational domain was adapted because was proved from the aircraft model simulations that this specific shape is better in meshing and also reduces the computational load.

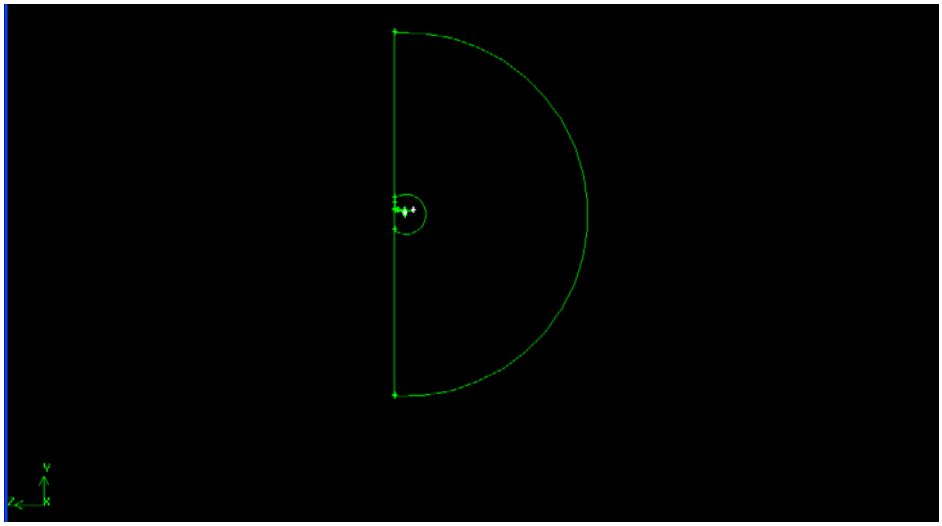

Figure 5-8: Computational domain

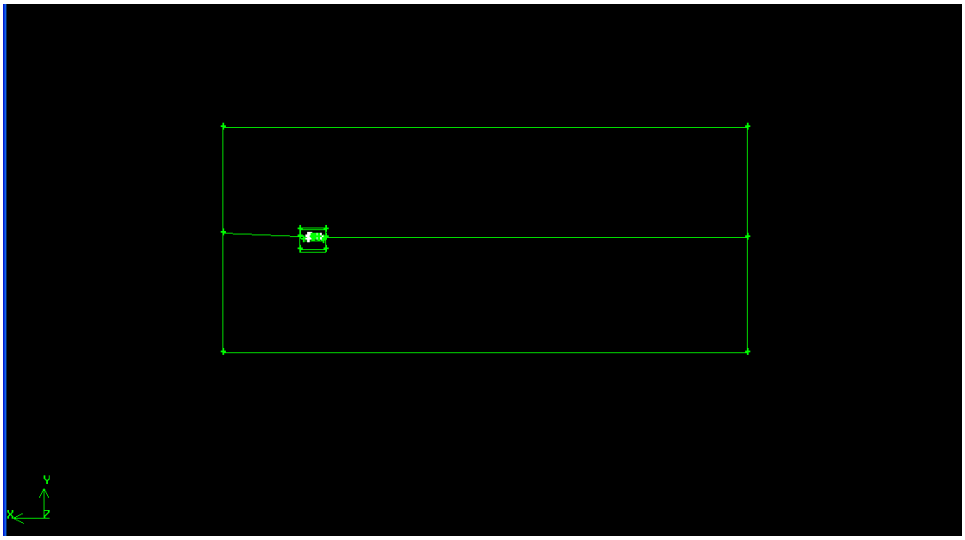

Figure 5-9: Computational domain

The final domain has cavities in the form of the wing and external tank. These cavities were created after the subtraction of the wing, external tank and pylon volumes from the outer volume (Figure 5-10, 5-11, 5-12).

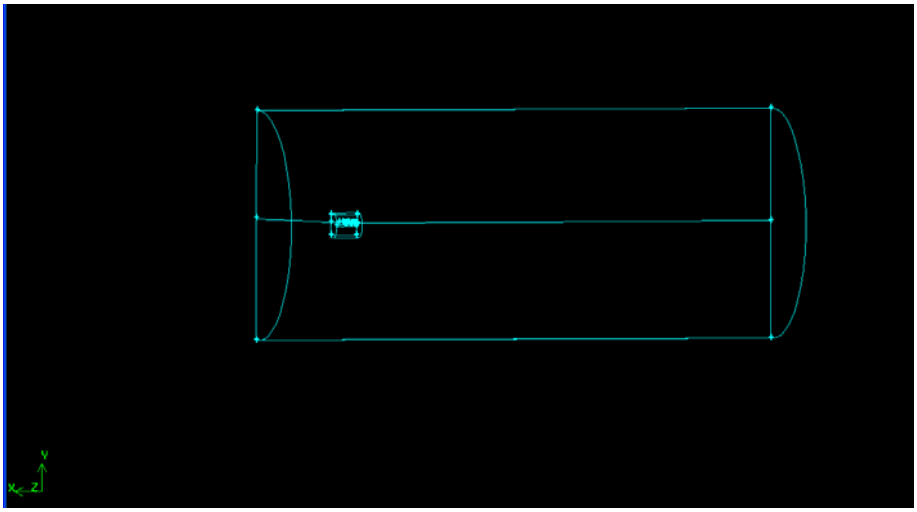

Figure 5-10: Outer volume

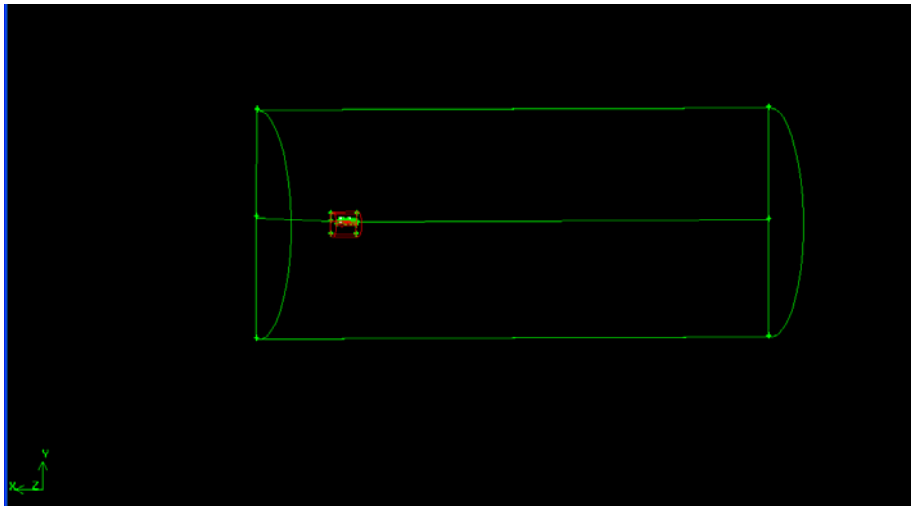

Figure 5-11: Wing, external tank and pylon volumes

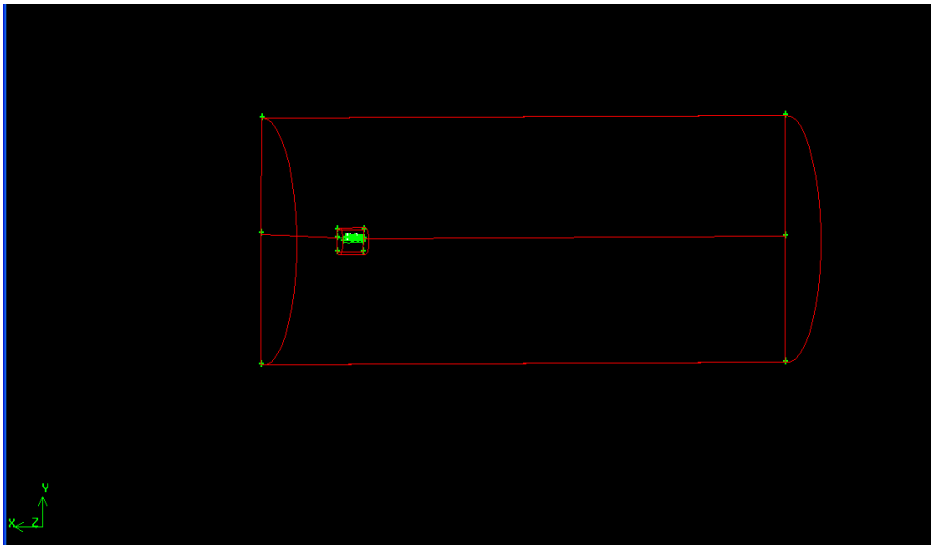

Figure 5-12: Final volume

The next step is the creation of the mesh. This process as referred in the previous chapter is very significant for the simulation output and simultaneously the most time consuming procedure in the whole study. In the present study the density is higher in the wing's and tank's surfaces areas, so as to achieve a detailed display of the flow path, an accurate simulation output and simultaneously an acceptable study of the phenomena that take place in these areas. For better results was used a second domain with half cylinder shape around the model so as in this area the meshing to be finer and without problems. This procedure is more effective because is much easier to mesh the model in a smaller domain and then to connect this domain with the larger one exactly as demanded. These specific areas are illustrated in the following Figures.

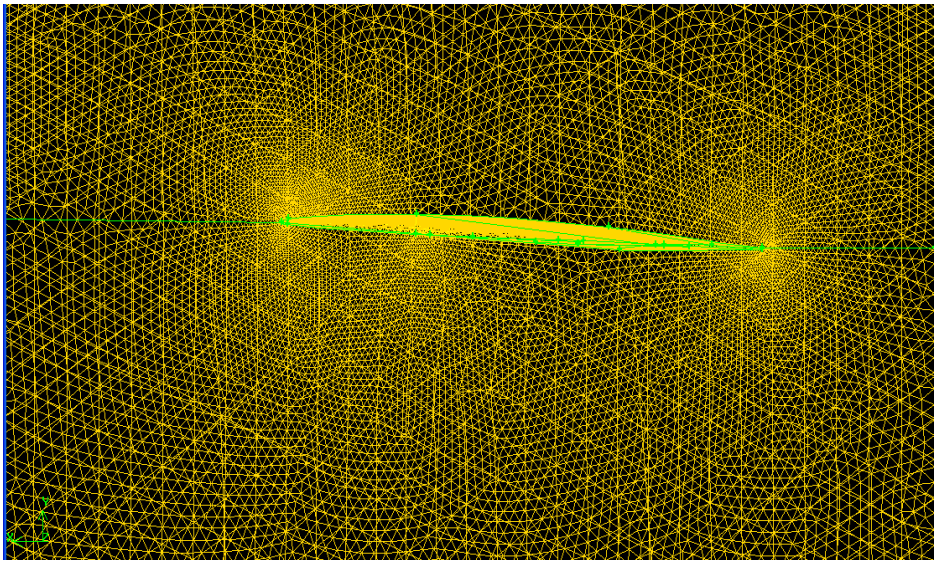

Figure 5-13: Meshing around the wing

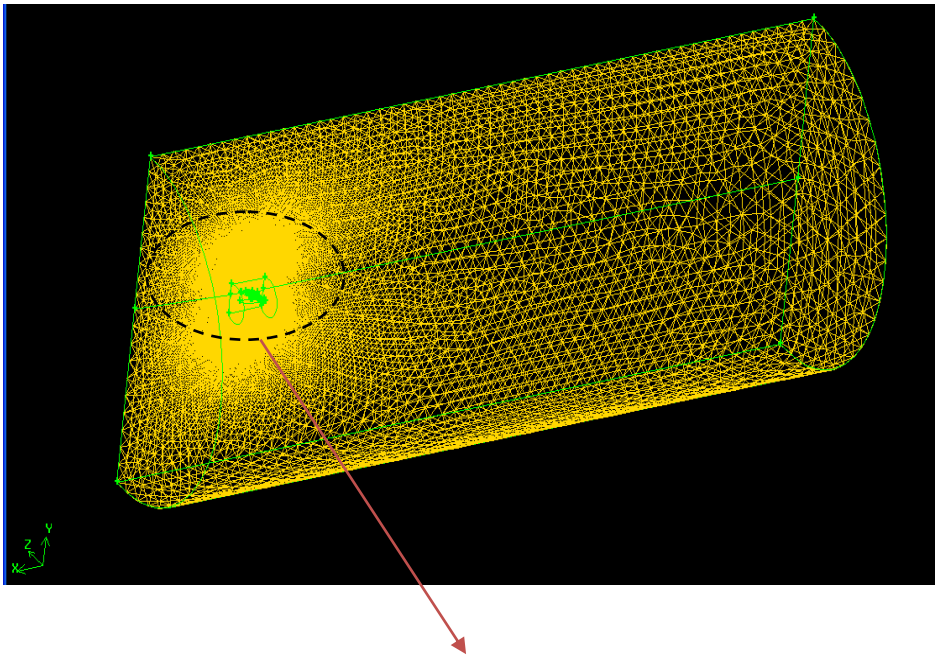

Figure 5-14: Computational domain (with meshing)

The procedure which is used for meshing is the same with the one that is applied in creating the aircraft geometry. Firstly a specific number of nodes (in compliance with

the demanded density of the mesh) are located in every edge, secondly the software created the mesh of each face (surface) and finally the mesh of each volume and consequently the 3D grid.

In the present study the number of the nodes that were used was almost 200k and the number of the cells that finally were created in the interior of the mesh was almost 800k. In the Figure 5-15 is illustrated the mesh of the final model.

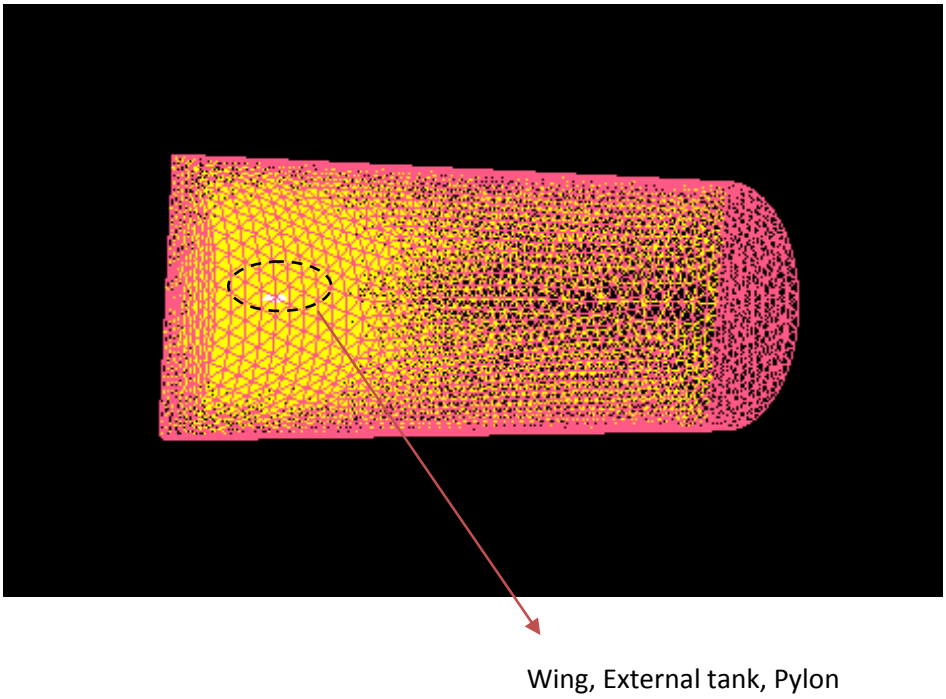

Figure 5-15: Mesh of the final model

The density of the mesh plays vital role in the final result and computational load. As is illustrated in the Figure 5-16, the mesh density is not constant throughout the whole domain and is getting coarser away from the surface of the wing - tank.

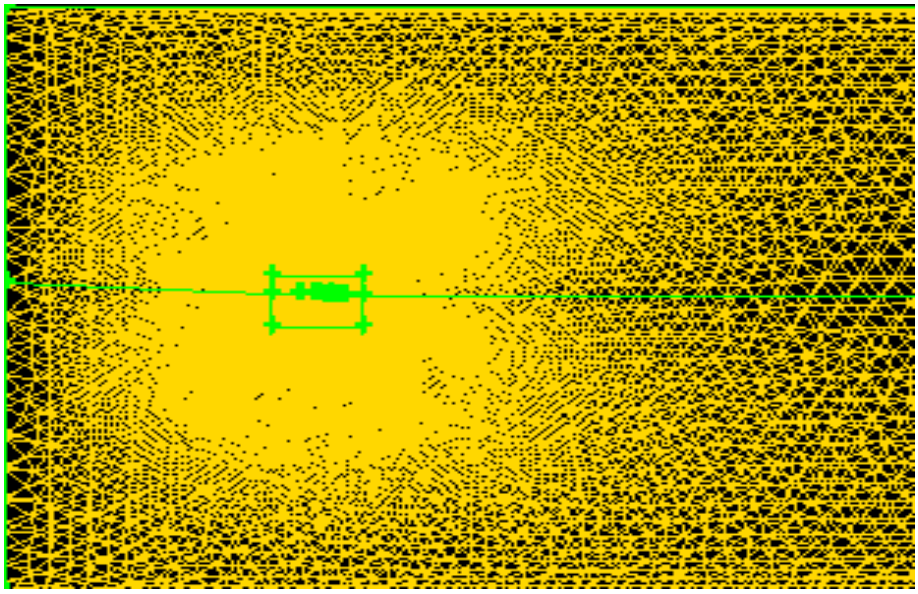

Figure 5-16: Mesh of the final model

Additionally, in the present study is necessary the calculation of the tank -drag for different angle of attacks. This specific necessity was covered with the creation of models in different angles. Such a model is illustrated in the following Figure in which the model is in eight (8^{o}) degrees angle.

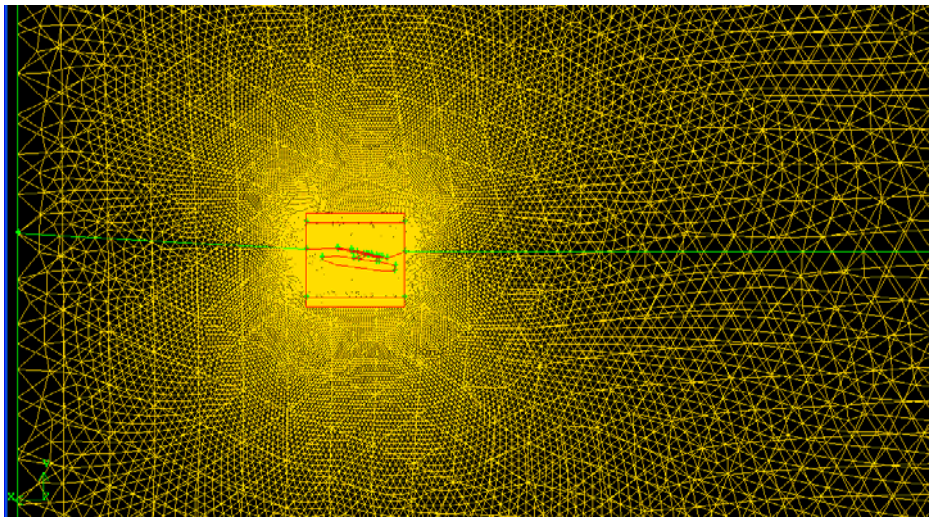

Figure 5-17: Model in eight (8) degrees angle

5.3 Specification of the Boundary Conditions

The first demand for the definition of the boundary conditions is the choice of suitable fluid flow boundary conditions. This choice is very significant because affect the way that fluid entering and leaving the flow domain (Figure 5-18).

In the present study the Flow Inlet, Flow Outlet and the surface of the cylinder opposite the wing- tank-pylon model (red color in Figure 5-18) were defined as pressure far-field [2] due to the fact that they are open boundaries and additionally far enough away from region of the wing- tank-pylon.

The surface of the wing, tank and pylon can be considered as internal [2] "obstacles" within the computational domain so were defined as "walls" (white color in Figure 5-18). Finally the yellow surface in Figure 5-18 was defined as "symmetry" so as the conditions to be the same in the other half part of the cylinder that is missing.

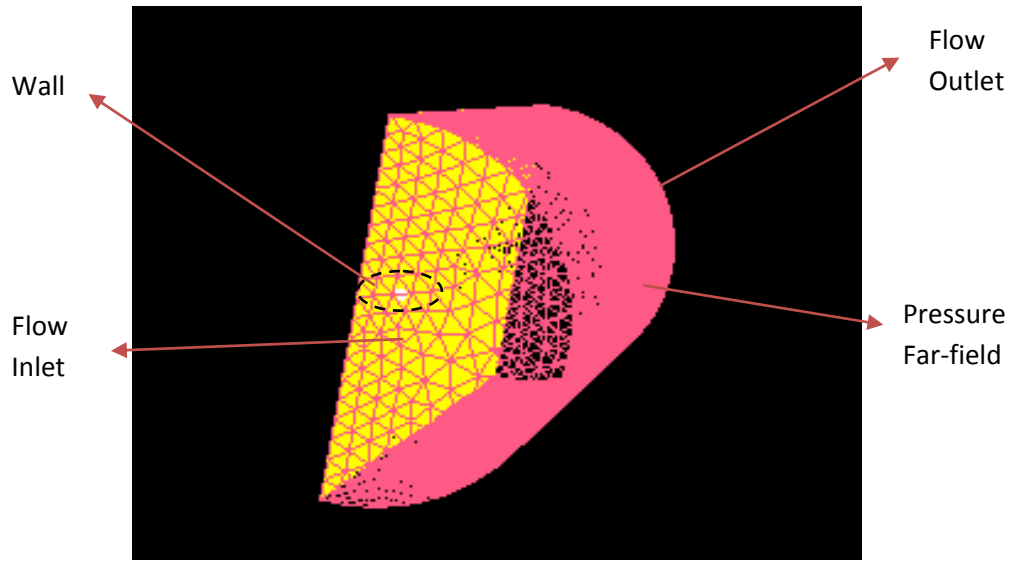

Figure 5-18: Boundary Conditions

5.4 Numerical Solution

The solution procedure [2] that usually is used can be described by the chart that is presented in Chapter 4, Figure 4-15. The CFD solver is the basic tool for the numerical solution of study.

The previous procedure was followed in the present study and after the accomplishment of the necessary software (FLUENT) settings, the finally simulation results that were obtained were satisfactory. More specifically, after the model was scaled, the material was defined as air ideal gas (compressible), the energy equation was enabled (since there are flows with different temperature mixing) and adjustments were made for the under-relaxation factors and the convergence criteria. In the present study the use of a turbulent model is demanded because of the turbulent flow. The turbulent model that was used was the k-ε. The comparison of the results between the k-ε and k-ω show that the k-ε turbulent model was more appropriate for this specific case. The interpolation scheme that was used was the Second –Order Upwind for more detailed and reliable simulation outcomes.

Due to the fact that the case has a quite big number of cells (800k), the computational load is also quite big and consequently the time that is needed for a simulation completion is big too. Indicatively is referred that the demanded time for ten thousand (10000) iterations is almost a week.

In this specific case is necessary the calculation of the tank drag for different angle of attacks. The range of a loaded F-16 AOA varies between 0^0 and 15^0. Three simulations (0^0, 8^0 and 15^0) were performed in order to cover the whole range of the F-16 AOA. Additionally a range of altitude between 0 and 25k feet (5000 ft, 10000 ft, 15000 ft, 20000 ft and 25000 ft) and a range of velocity between 0 and 1 Mach Number (0.4M, 0.6M and 1M) were covered. For each AOA were run fifteen (15) simulations and for the completion of the case were demanded forty five simulations. In the followings Figures are illustrated some of the final simulations outputs.

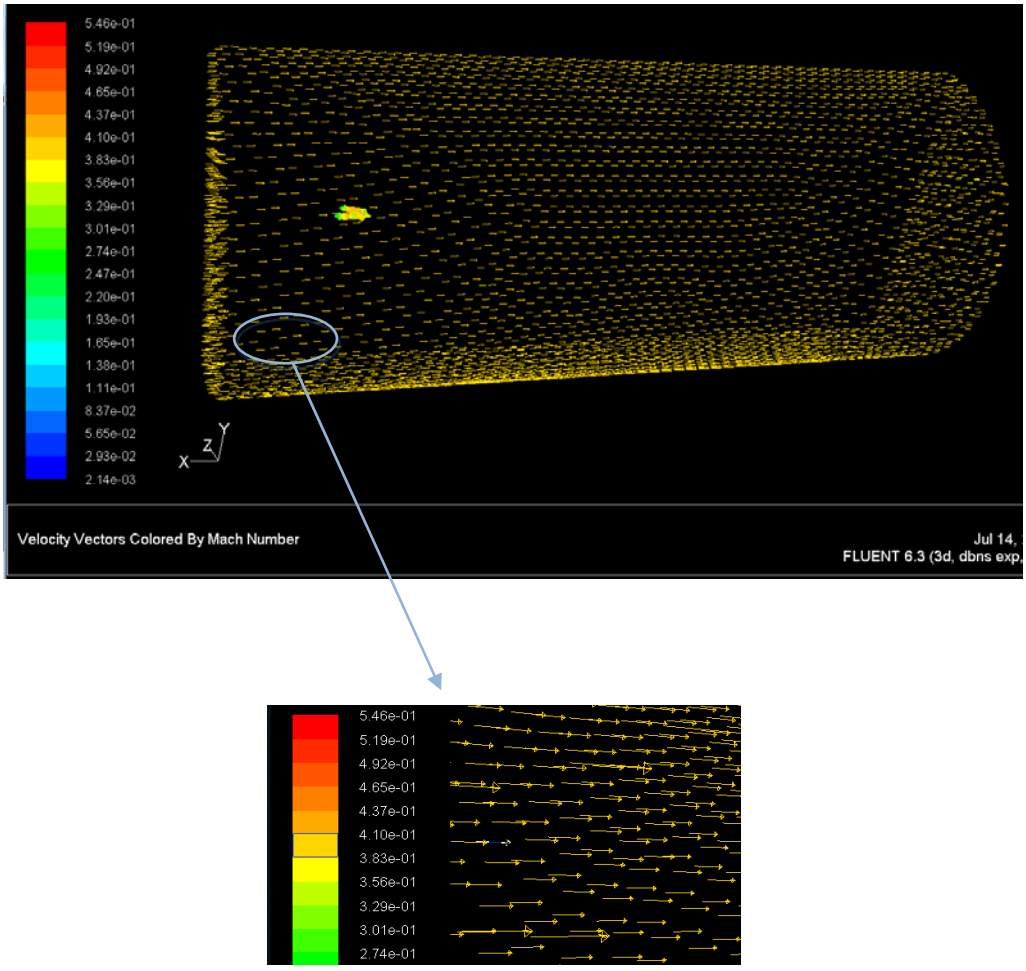

Figure 5-19: Velocity vectors display in 5000ft and 0.4M

In the Figure 5-19 are displayed the velocity vectors (5000ft and 0.4M) in the computational domain and in the wing- pylon- tank model. It is apparent how the flow comes from the Flow Inlet, goes around the model and finally abandons the computational domain through the Flow Outlet.

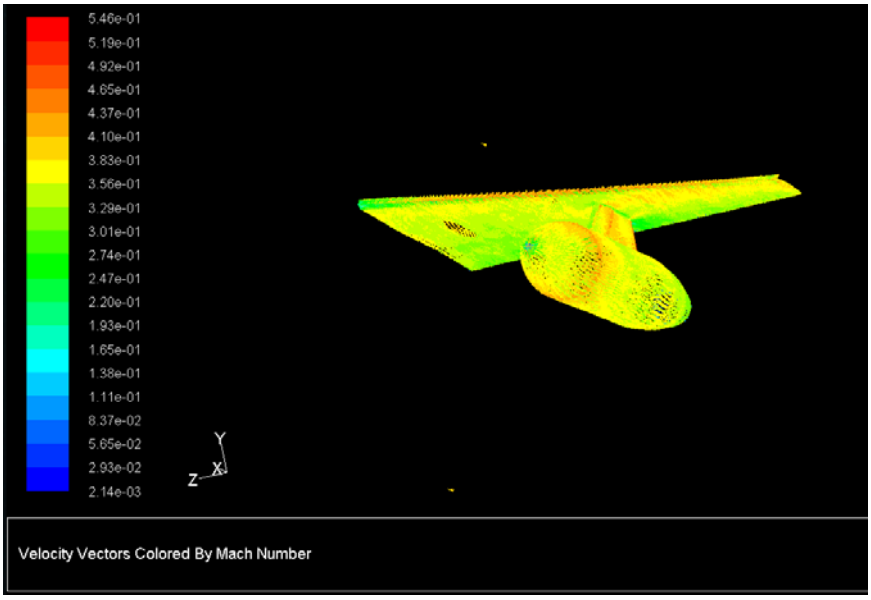

Figure 5-20: Velocity vectors display in 5000ft and 0.4M

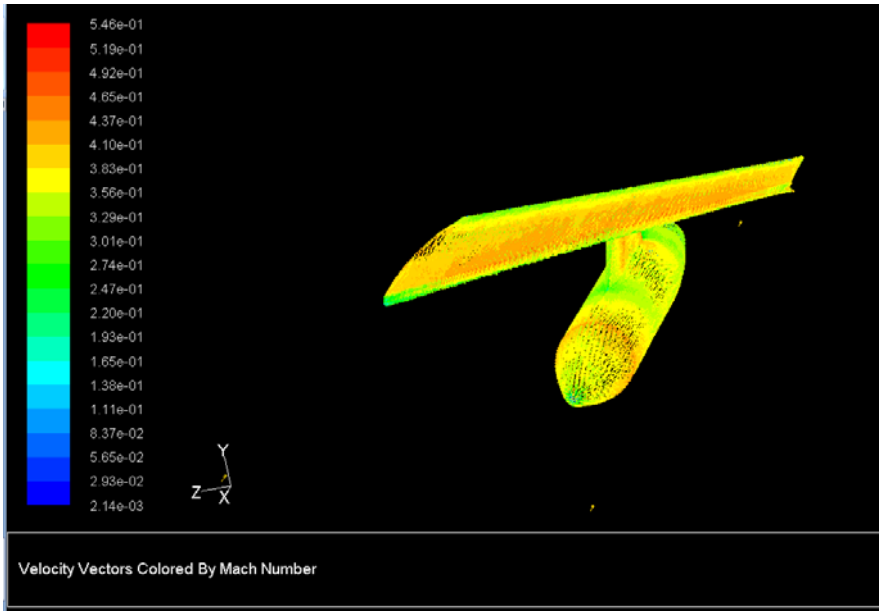

Figure 5-21: Velocity vectors display in 5000ft and 0.4M

In the Figure 5-20 and 5-21 are displayed the velocity vectors (5000ft and 0.4M) on the surface of the model and is obvious the difference in the velocity between the upper and the lower part of the wing.

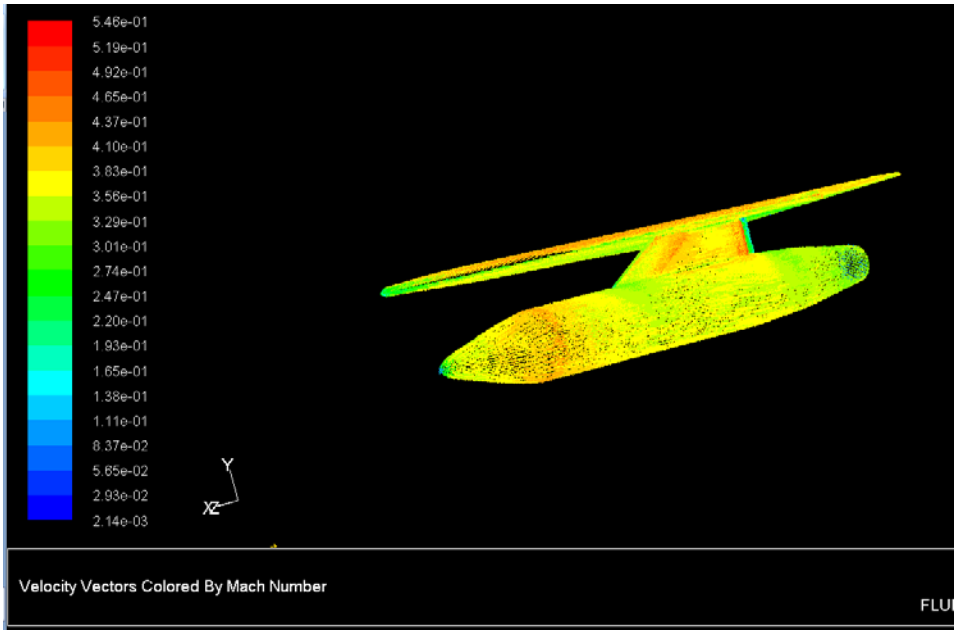

Figure 5-22: Velocity vectors display in 5000ft and 0.4M

In the Figure 5-22 also is displayed the velocity vectors on the surface of the model, where the velocity in the nose of the tank and in the leading edge are zero then there is an acceleration and then a reduction as the flow approach the back part of the tank. All these information are logical and act as an indication that the simulation results are logical and reliable.

For the convergence of each simulation were demanded 20000- 45000 iterations. A tactic that was used so as to be sure about the final simulation outcomes was the monitoring of the value of parameters such as the lift coefficient (C_L) and the drag coefficient (C_D) of the tank. As it is illustrated in the following Figures there was a change in the values of these parameters (up and down) and after lots of iterations the value was constant. This was an indication that the simulation is near to converge and also that in this point the results are logical and correct.

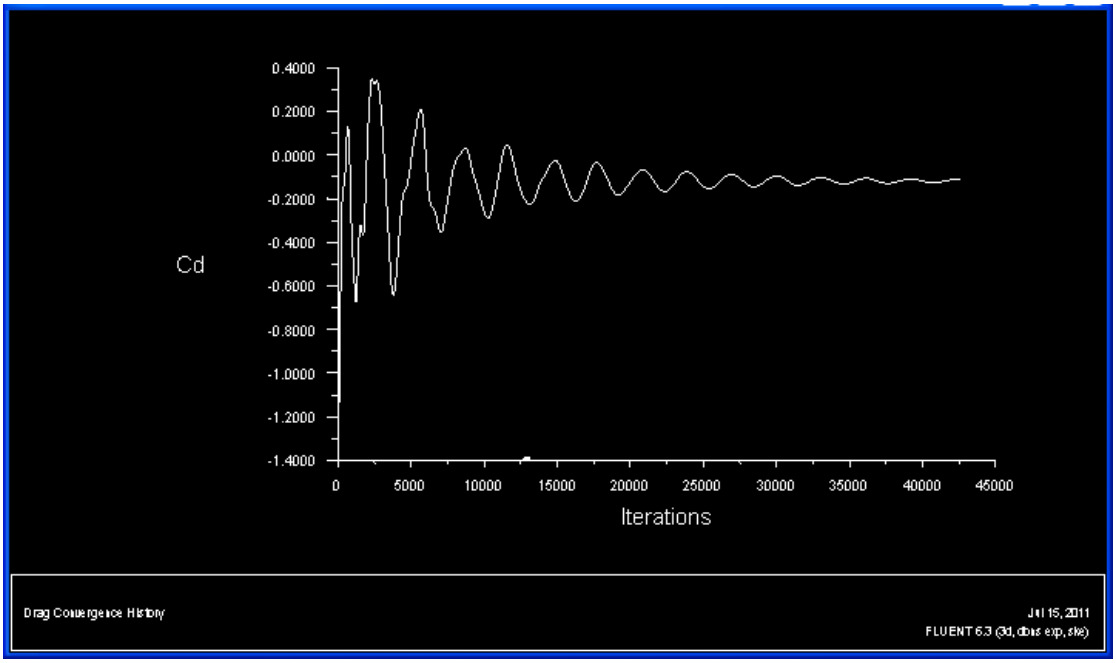

Figure 5-23: Tank Drag Coefficient

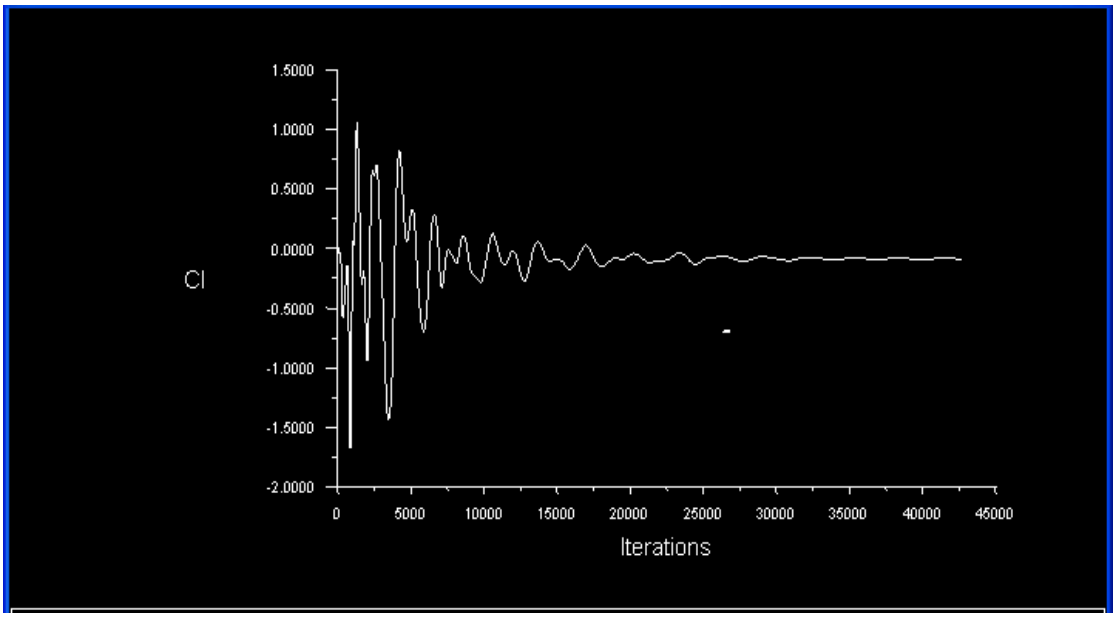

Figure 5-24: Tank Lift Coefficient

5.5 Simulation Results

The basic issue of this study is that due to the fact that the CFD simulations are time consuming, the calculations of the tank's drag refer to specific altitudes (5000ft, 10000ft, 15000ft and 20000ft), specific Mach numbers (0.4M, 0.6M, 1M) and specific AOA (0^0, 8^0, 15^0 degrees). The available points for plotting are three and for this reason the curves of the final results are not so detailed as probably would be with more points. Nevertheless the curves of basic quantities and forces such as drag are similar to generic variation of these parameters with Mach number.

In Figure 5-25 is illustrated the drag of the external tank versus Mach number at 5000 ft altitude and for 0^0 AOA. Generally, the drag, as the velocity increases, initially decreasing, reaching a minimum value, and then increasing as velocity further increases. In Figure 5-25 the curve is quite different because is based only on three Mach numbers (0.4, 0.6 and 1).

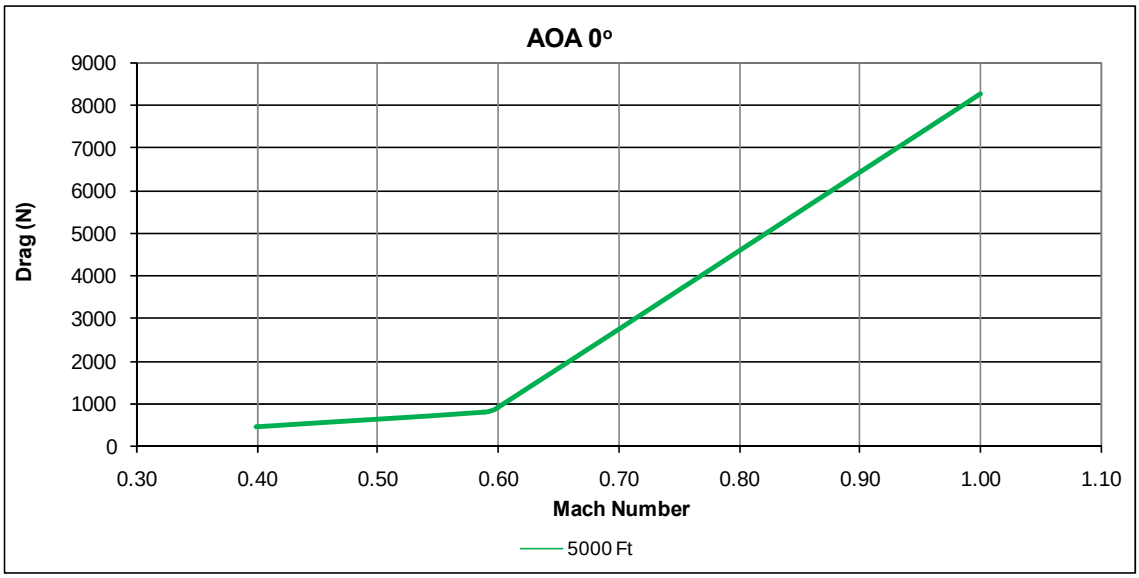

Figure 5-25: Drag vs. Mach number

The drag can be expressed from the following equation

$$D = \frac{1}{2} p_\infty V_\infty^2 S C_D \qquad (5.1)$$

The C_D can be expressed as

$$C_D = C_{D,0} + K C_L^2 \qquad (5.2)$$

So, from the equations (5.1) and (5.2) is derived

$$D = \frac{1}{2} p_\infty V_\infty^2 S C_{D,0} + \frac{1}{2} p_\infty V_\infty^2 SK C_L^2 \qquad (5.3)$$

At low velocity the total drag is dominated [32] by the drag due to lift. Due to the fact that the C_L decreases rapidly as the velocity increases, the drag due to lift, since it is proportional to the square of C_L , rapidly decreases in spite of the dynamic pressure $\frac{1}{2} p_\infty V_\infty^2$ is increasing. This is the reason that the drag curve decreases as the Mach number increases. At high velocity the total drag is dominated [32] by the zero lift drag. The velocity at which the drag is minimum is the velocity where the increasing zero lift drag [32] compensates for the decreasing drag due to lift. Finally at higher velocity the increase of zero lift drag causes the increase [32] of the drag.

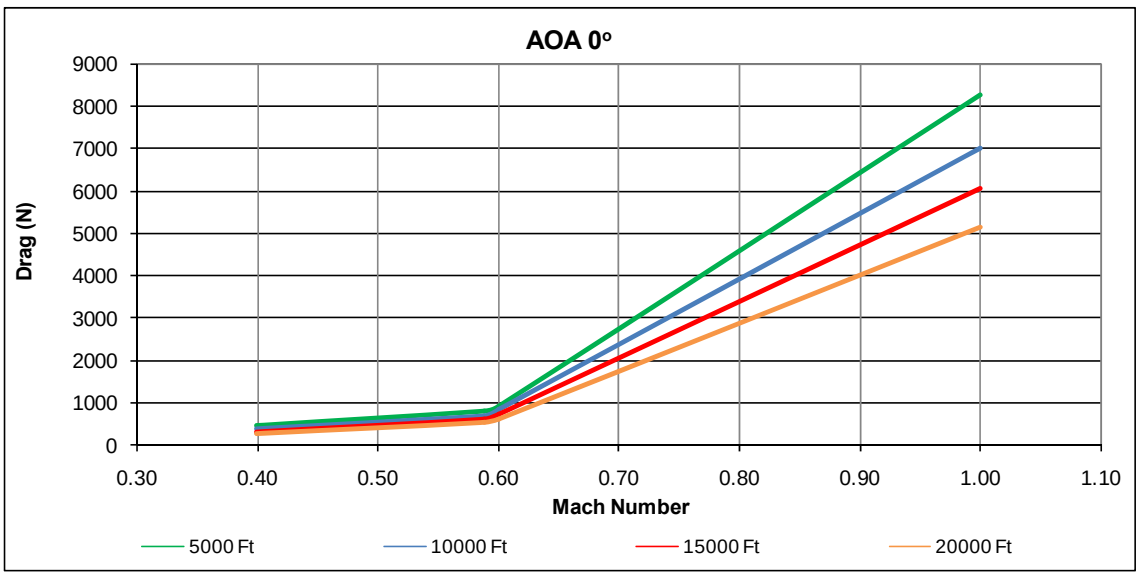

Figure 5-26: Drag vs. Mach number for different Altitudes

In Figure 5-26 is illustrated the drag of the external tank versus Mach number at different altitudes (5000ft, 10000ft, 15000ft and 20000ft) and for 0^0 AOA . As it is apparent from the diagram the drag for specific Mach number but for different altitude has a lower value. From the equation of state (p= ρRT) is derived that the increase of altitude causes a decrease of density. Additionally, the temperature is related to the speed of sound through the equation $\alpha = \sqrt{\gamma RT}$. Increase in altitude causes a decrease in the speed of sound because in the lower atmosphere the temperature falls. Based on the way that the increase of altitude affect the density and the velocity and through the Equation 5.1 is explained the reduction of the drag with the increase of altitude for a specific Mach number.

For a chosen V_∞ the C_L can be calculated from the following equation

$$C_L = \frac{2W}{p_\infty V_\infty^2 S} \qquad (5.4)$$

From Equations (5.3) & (5.4) is derived the following Equation

$$D = \frac{1}{2} p_\infty V_\infty^2 S C_{D,0} + \frac{2KS}{V_\infty^2 p_\infty} \left(\frac{W}{S}\right)^2 \qquad (5.5)$$

or

$$V_\infty^2 = \frac{\frac{D}{S} \pm \sqrt{(D/S)^2 - 4 C_{D,o} K (\frac{W}{S})^2}}{p_\infty C_{D,o}} \qquad (5.6)$$

The term $\frac{D}{S}$ can be replaced with $\frac{D}{W}\frac{W}{S}$ then the Equation (5.6) can be

$$V_\infty^2 = \frac{(\frac{D}{w})(\frac{W}{S}) \pm \sqrt{(DW/WS)^2 - 4\,C_{D,o}\,K\,(\frac{W}{S})^2}}{p_\infty\,C_{D,o}} \qquad \text{or}$$

$$V_\infty = \left(\frac{(\frac{D}{w})(\frac{W}{S}) \pm (\frac{W}{S}))\sqrt{(D/S)^2 - 4\,C_{D,o}\,K}}{p_\infty\,C_{D,o}}\right)^{1/2} \qquad (5.7)$$

When the discriminant in Equation (5.7) equals zero the only one solution is obtained for V_∞ and this corresponds to the minimum drag. So

$$\left(\frac{D}{S}\right)^2_{min} - 4\,C_{D,0}\,K = 0 \quad \text{or}$$

$$\left(\frac{D}{S}\right)_{min} = \sqrt{4\,C_{D,0}\,K} \qquad (5.8)$$

From the Equation (5.8) is derived that the minimum drag is independent of altitude. Because of that, the minimum drag has the same value for different altitudes.

The final simulation results for 0^0 degrees AOA, specific altitudes (5000ft, 10000ft, 15000ft, 20000ft and 25000ft) and specific velocities (0.4M, 0.6M and 1M) are tabulated in the following Table.

ALTITUDE (ft):	5000 ft	ALTITUDE (ft):	10000 ft	ALTITUDE (ft):	15000 ft	ALTITUDE (ft):	20000 ft	ALTITUDE (ft):	25000 ft
Mach Number	**Drag (N)**	**Mach Number**	**Drag (N)**	**Mach Number**	**Drag (N)**	**Mach Number**	**Drag (N)**	**Mach Number**	**Drag (N)**
0.4	475	0.4	384	0.4	314	0.4	210	0.4	43
0.6	927	0.6	827	0.6	719	0.6	613	0.6	500
1	8261	1	7025	1	6072	1	5148	1	3983

Table 5-1: Drag calculations

As mentioned in the previous Chapter the range of a loaded F-16 AOA varies between 0^0 and 15^0. In order to cover the whole range of the F-16 AOA three simulations (0^0, 8^0 and 15^0) were performed. The altitudes and velocities that were used for these simulations were 5000ft and 25000ft and 0.4M, 0.6M and 1M respectively. The results are tabulated in the following table.

8° degrees			
ALTITUDE (ft):	5000 ft	**ALTITUDE (ft):**	25000
Mach Number	**Drag (N)**	**Mach Number**	**Drag (N)**
0,4	541	0,4	262
0,6	1126	0,6	533
1	9851	1	4645
15° degrees			
ALTITUDE (ft):	5000 ft	**ALTITUDE (ft):**	25000
Mach Number	**Drag (N)**	**Mach Number**	**Drag (N)**
0,4	642	0,4	320
0,6	1807	0,6	967
1	10589	1	5236

Table 5-2: Drag calculations

In Figure 5-27 is illustrated the drag of the external tank versus Mach number for the three AOA and for 5000ft altitude.

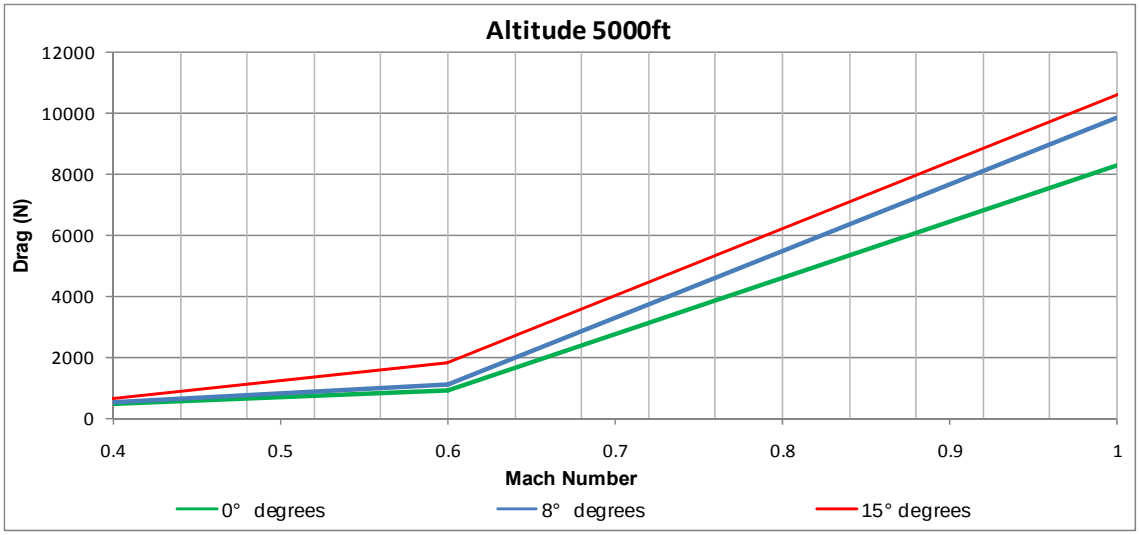

Figure 5-27: Drag vs. Mach number for different AOA

In general the magnitude of the drag [33] generated by an object depends on the shape and how it moves in the air. As an aerodynamic force [34], depends on the pressure variation of the air around the body and is proportional to the area of the object. Additionally, as the object moves through the air, air molecules stick to the surface of the object and this creates a layer of air near the surface (boundary layer [33, 35]) which changes the shape of the object. The flow reacts to the edge of the boundary layer just as it would to the physical surface of the object. The increase of AOA increases the reference (frontal) area and also increases the boundary layer thickness. As mentioned before, the increase of these two parameters (area and boundary layer) affect directly the drag and cause, as it is illustrated in Figure 5-27, increase of this force.

5.6 Verification of the Simulation Results

The major issue in this study is the verification of the simulation results. It is almost impossible for a researcher without test flights or experimental measurements, to know exactly the drag value of an external tank for specific flight conditions (altitude, Mach number, AOA, climb rate etc).

The use of advanced computational tools ensures the accuracy of the final output. The CFD packages incorporate computational techniques which accuracy has been

verified in various cases via extensive experimental and flight test data. The fact that the simulations that performed by CFD are reliable, allows the further use of their results in various applications.

Moreover, the definition of certain CFD parameters may also affect the simulation results. However, previous experience in similar cases and/or usage of typical parameter values for certain phenomena enhances the confidence for the validity of the extracted output data.

Furthermore, the use of the simulation results as input in ARES method for two specific missions (specific velocity and altitude), clean A/C and A/C loaded with two external tanks, revealed an increase in engine fuel flow (for the specific flight conditions) for the second case. The magnitude of that increase was similar to F-16's engine real data as estimated based on data that were gathered from literature review (private data). The aforementioned conclusion combined with the fact that the variation of the extracted quantities and forces, such as drag coefficient and drag, with velocity (Mach number) are similar to the generic curves prove the reliability of the simulation results.

5.7 Future Work

As mentioned in the previous subchapter, the objective of the CFD tank study, was the establishment of a procedure so as to be feasible the drag calculation contributed by an external load with the use of advanced computational tools. Advantages of using computational techniques are the ease of implementation and virtually no limitations to the fabrication as needed in ground tests and experiments.

Due to the fact that the CFD simulations are time consuming, the calculations of the tank's drag refer to specific altitudes, Mach numbers and AOA. This fact affects the accuracy of ARES results because the values that are needed for the calculations and are not available, are estimated with the interpolation method. It is apparent that if the available data cover more flight conditions (more combinations of Mach number, altitude and AOA), then firstly would be less necessary for ARES to estimate the

demanded values and secondly in case that a value estimation would be inevitable the interpolation method would be more accurate. For this reason, further performance of CFD simulations for the tank study can be considered as future work. This work will increase the available data, will cover more flight conditions and undoubtedly will improve the accuracy of ARES calculation.

Additionally, the development of CFD models for bombs, missiles, pods or for external tanks with different capacity and the performance of simulations, will lead to an updated data base with drag information for all the stores and stores loading combinations that a combat aircraft is capable of carrying.This work would be very important because will enable ARES to process all the flight missions either the aircraft is clean or carry external loads.

Chapter 6 Upgraded Version of ARES Method

6.1 Introduction

The ARES [23] method is an integrated aircraft-engine performance tool for combat aircraft. The initial model was built, by the author in the MSc study, in such a way that allows different combinations of combat aircraft/engine to be modelled by altering appropriate input data such as aircraft data and geometric details and mission specifications.

The present study will update the ARES method by integrating the influence of the aircraft external configuration in the aircraft/ engine performance. The external tanks affect the total drag of the aircraft, the engine thrust, the aircraft weight and consequently the final performance of the aircraft. The behaviour of the aircraft is completely different when there are changes in the external configuration of the aircraft.

The present work in combination with the complete future study, which will refer to the way that the performance of a fully integrated (buried) propulsion system is eroded by the loss of total pressure in the long and curved intake and by the effect of flow distortion on the engine in different operational conditions, will transform ARES in a innovated, powerful and very useful aircraft-engine performance tool. ARES, through the mission analysis results and the gas turbine performance evaluation, will give the opportunity for further engine studies such as the structural and thermal analysis, component sizing and geometry and life consumption.

6.2 ARES Modification

The modification of ARES method is the aim of this study. The model [23] is able to calculate aircraft and engine performance data such as drag and lift coefficient, spillage drag, installed and uninstalled net thrust, net propulsive force, the fuel

consumption, distance covered and finally to specify the maximum payload and the fuel load that is required for the accomplishment of a mission. The objective of the updated version is to include in the programme calculations the additional drag which is contributed by an external tank. This extra feature will enable the programme user to evaluate the final aircraft/engine performance for flight missions with external configuration.

During a mission simulation there are many slight changes in Mach number and altitude due to the fact that a flight mission may include different segments (climb, descend, accelerated flights, accelerated climb or descend, loiter, decelerated flights). This fact complicate the calculations because the available data refer to specific altitudes (5000 ft, 10000 ft, 15000 ft, 20000 ft and 25000 ft), velocities (0.4M, 0.6M and 1M) and AOA (0^0, 8^0, 15^0 degrees). For instance there are not data for an accelerated climb with velocity 0.42M at altitude 5015 ft. This problem was solved with the use of the linear interpolation and extrapolation methods. The accuracy of these methods is getting better as the amount of the input data increases.

The major issue in this process was the calculation of the drag force for simultaneous change of AOA, Mach number and altitude. This is the worst case because is needed a triple interpolation. The procedure that is followed by the programme for the drag calculation is the following:

- Isolation of the data that include the AOA of the aircraft

- Isolation of the data that include the Mach number and the altitude of the specific segment

- Calculation of the drag force for the specific Mach number and altitude but for two different AOA

- Final calculation of the drag force for specific AOA, Mach number and altitude

For example the drag force of the external tank when the aircraft flies with 10^o AOA, 0.65 M at 12500 ft is calculated as follows:

The programme isolates the data from 8^0 to 15^0 AOA that include the 10^o AOA of the aircraft. For the 8^0 AOA isolates the data from 0.6 M to 1 M that include the 0.65 M of the aircraft and the data from 5000 ft to 25000 ft that include the altitude of 12500 ft. With the interpolation method calculates the drag force for 8^0 AOA, 0.65 M and altitude 12500 ft. The same procedure is followed so as to calculate the drag force for 15^0 AOA, 0.65 M and 12500 ft altitude. Finally, again with interpolation method calculates the drag force for 10^0 AOA, 0.65 M and altitude 12500 ft.

10^0, 0.65M, 12500 ft ⟶ Drag Force?

FOR 8^0

0.6 M 5000 ft 1126 N

⇨ 0.6 M 12500 ft 904 N

0.6 M 25000 ft 533 N

⇨ 0.65 M 12500 ft 1778 N

1.0 5000 9851

⇨ 1.0 M 12500 ft 7899 N

1.0 25000 4645

FOR 25^0

0.6 M 5000 ft 1807 N

⇨ 0.6 M 12500 ft 1492 N

0.6 M 25000 ft 967 N

⇨ 0.65 M 12500 ft 2378 N

1.0 M 5000 ft 10589 N

⇨ 1.0 M 12500 ft 8582 N

1.0 M 25000 ft 5236 N

8^0 0.65 M 12500 ft 1778 N

⇨ For 10^0 0.65 M 12500 ft Drag force= 1849 **N**

25^0 0.65 M 12500 ft 2378 N

The accuracy of the calculated drag depends on the available data. If for example the altitude range 0- 25000 ft was covered with an altitude step of 1000 ft instead of 5000 ft then the accuracy of the final calculation would be better. The same would happen if the steps that were used to cover the ranges of Mach number and AOA were smaller.

The external configuration (one or two wing tanks) is declared in the file (txt) "AIRCRAFT CHARACTERISTICS". The software take into account the number of the external tanks so as to add in the total aircraft drag the correct amount of additional drag (e.g. double for configuration with two tanks). Detailed information for the final outputs are available in the file (txt) with the calculation results.

For the best study of the aircraft/engine performance and also for more accurate results, it was decided that all the calculations should take place every second. So, for example, if the duration of a mission is one hour, then the programme will calculate the new values of all parameters every second, i.e. 3600 times. Nevertheless, it is also possible the number of loops to be redefined and the calculations to take place for a period of time of less or more than a second. Additionally, a further modification is the creation of the files (txt) "missions" where can be specified the segments of the flight mission (climb, descend, accelerated flights, accelerated climb or descend, loiter, decelerated flights). This change enables ARES to know all the segments of the mission and to begin automatically the necessary calculations for each segment.

6.3 Mission Profile and External Configuration

The updated version of ARES method after the aforementioned modifications can integrate in the aircraft/engine performance calculations apart from the spillage drag

and the thrust losses due to the engine installation and a new feature that is the additional drag which is contributed from the external tank.

In order to evaluate the new feature of the updated version of ARES method, engine performance parameters for three different aircraft configurations (clean aircraft, one external wing tank and two external wing tanks) were computed. Aerodynamic characteristics of the F-16 and data for a jet engine MT-200 which is similar to EJ-200 were used. The engine parameters were computed for a specific part of aircraft flight path, including the following segments:

- 15 seconds climb, from 16000 to 17000 ft at Mach number 0.6 constant,
- 30 seconds acceleration from 0.6 to 0.7 Mach at constant altitude 17000 ft,
- 125 seconds combined climb to 18000 ft and acceleration to 0.88 Mach, and
- 600 seconds (10 minutes) flight at constant altitude 18000 ft and constant 0.88 Mach.

The aerodynamic characteristics of the aircraft that were used are:

Aspect Ratio (AR) = 3

Wing Area (S) = 300 ft^2

Wing span (b) = 30 ft

The aircraft weight depends on the external configuration. The used configurations are the following:

- Clean aircraft, aircraft weight =10772 Kg
- One external tank, aircraft weight =10953 Kg
- Two external tanks, aircraft weight =11134 Kg

The initial calculation was performed for clean aircraft (without any external loads), and the following were repeated by adding one external wing tank each time.

The asymmetry configuration (only one external wing tank) is noticed in a mission where weapons (bombs or missiles) were loaded on the other wing and released mid-flight. Proper balance of the aircraft demands the external wing tank to have a limited fuel quantity (almost empty) after the weapon release. For reasons of simplicity the external wing tanks were considered empty in both configurations involved. The weight of an empty external tank estimated at about 181 Kg (including a small amount of unusable fuel which remains in the tank).

6.4 Aircraft/Engine Performance Results

The results that were derived from the whole procedure are presented in detail in the Appendix C. Specifically there are detailed records about the Uninstalled Net Thrust, TET, Drag, Aircraft Weight and Fuel Consumption for each configuration and each segment of the fight path. Additionally, these records are illustrated in the following Figures.

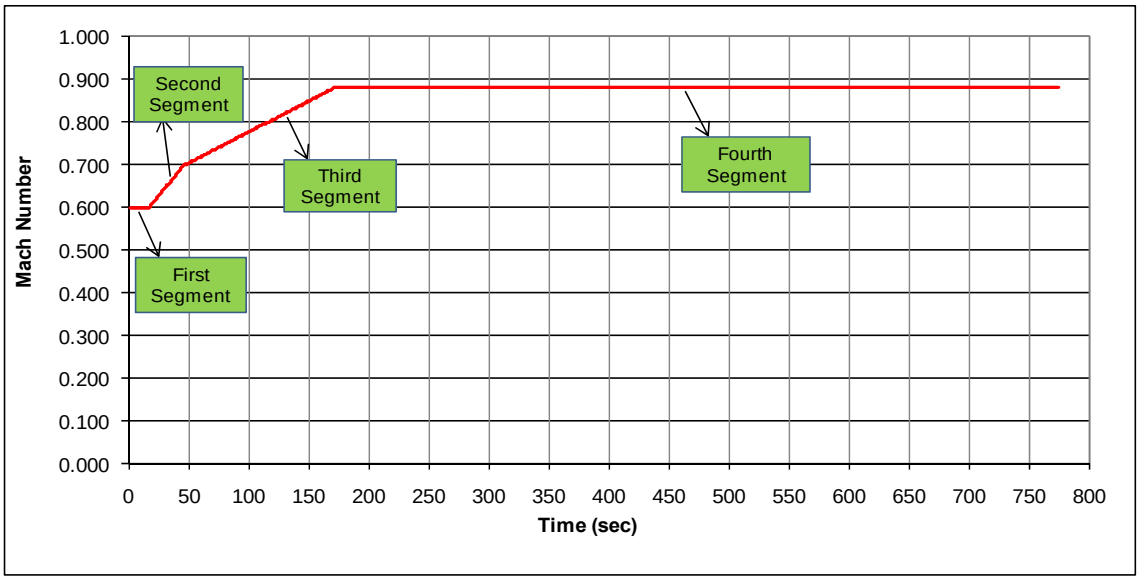

Figure 6-1: Mach number vs. Time

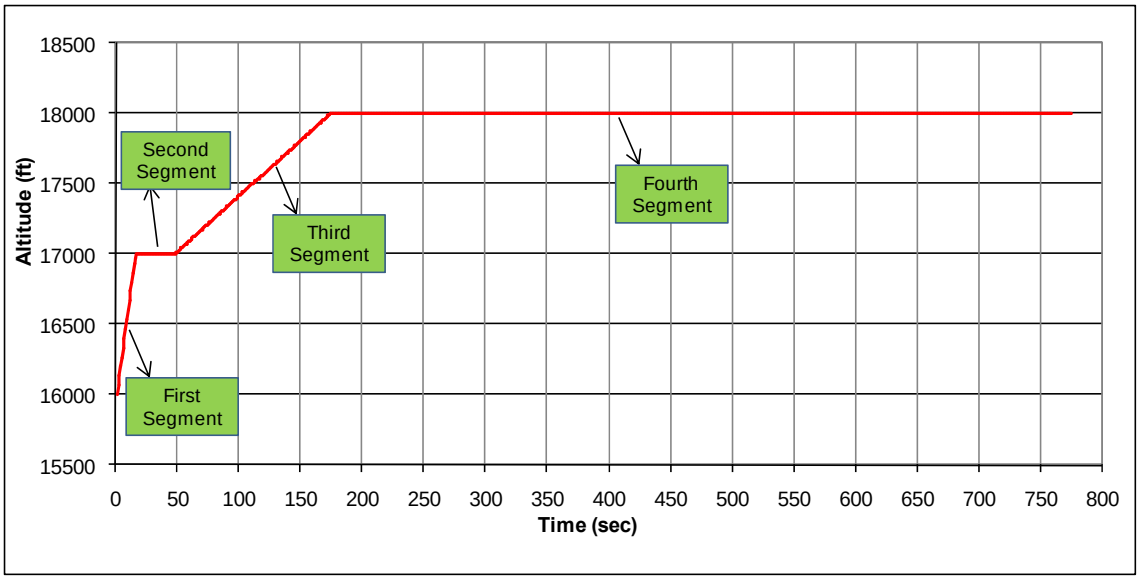

Figure 6-2: Altitude vs. Time

In Figures 6-1, 6-2 is illustrated the mission of the aircraft. At first 15 sec climb from 16000 ft to 17000 ft at constant 0.6M, at next 30 sec acceleration from 0.6 M to 0.7 M at constant altitude 17000 ft, at next 125 sec combined climb to 18000 ft and acceleration to 0.88 M and at the last 600 sec flight at constant altitude 18000 ft and constant 0.88 M.

In Figure 6-3 is depicted the variation of the drag with Mach number. The first and basic observation is that the addition of external wing tanks causes increase of the total drag. Moreover, the increase of the Mach number causes increase of the total drag of the aircraft. The large increase in the total drag at the higher Mach number is mainly due to the fact that there is an intense increase of the spillage drag and additional drag of the external tank at high velocity. The variation of the spillage drag and the drag of the tank with the Mach number is tabulated in Tables 3-4 and 5-1 respectively.

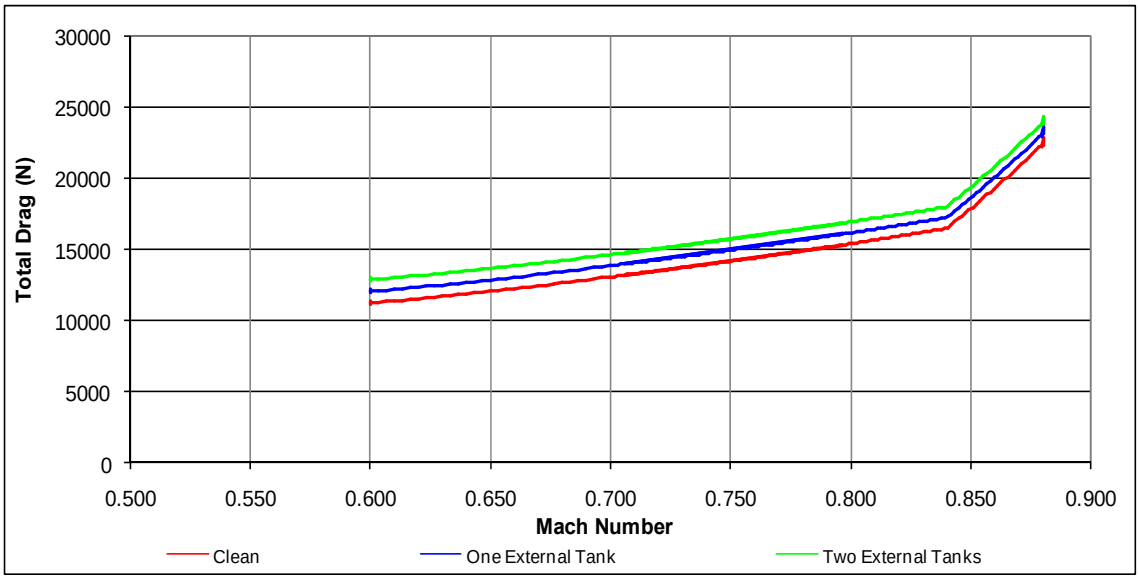

Figure 6-3: Drag force vs. Mach number

At 0.88 M is observed a minor decrease of the total drag (Figure 6-3). This can be justified because as is derived from the following equation the drag at constant altitude and constant velocity depends only on the aircraft weight (W).

$$D = \frac{1}{2} p_\infty V_\infty^2 S C_{D,0} + \frac{2KS}{V_\infty^2 p_\infty} \left(\frac{W}{S}\right)^2$$

As the aircraft flies, fuel is consumed and consequently the aircraft weight is reduced (Figures 6-9, 6-10, 6-11). The reduction of the aircraft weight causes the reduction of the total drag. Additionally at the first segment of the mission (climb with constant Mach number) is also observed a minor decrease of the total drag (Figure 6-4). This decrease is due to the fact that the increase of the altitude causes decrease of the density and also there is a reduction of the aircraft weight because of the consumed fuel. All the aforementioned observations are depicted clearly in the Figure 6-5 where represented the variation of the total drag with time (seconds).

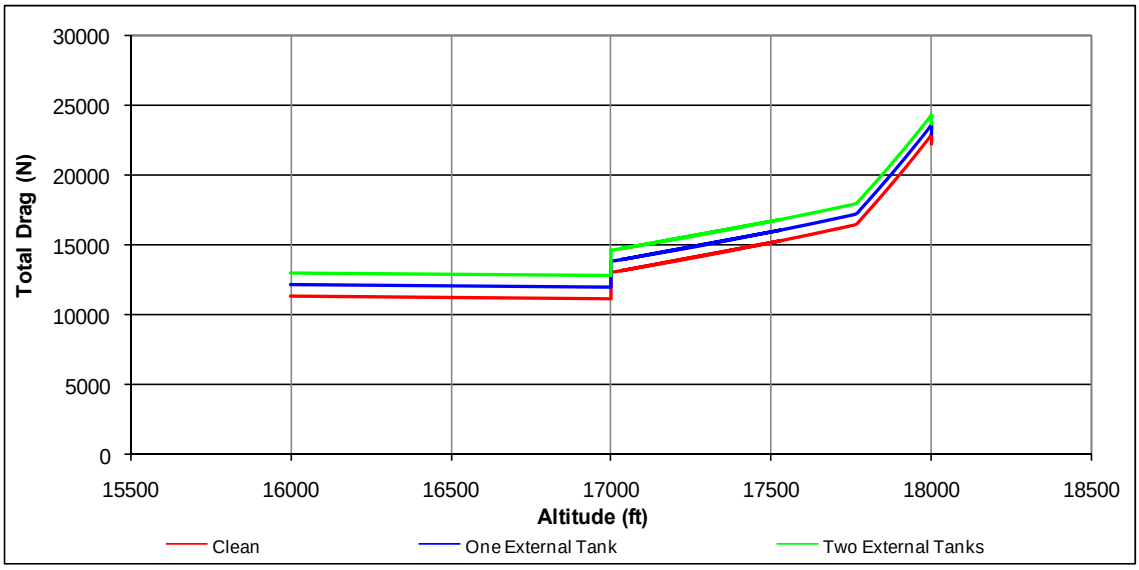

Figure 6-4: Drag force vs. Altitude

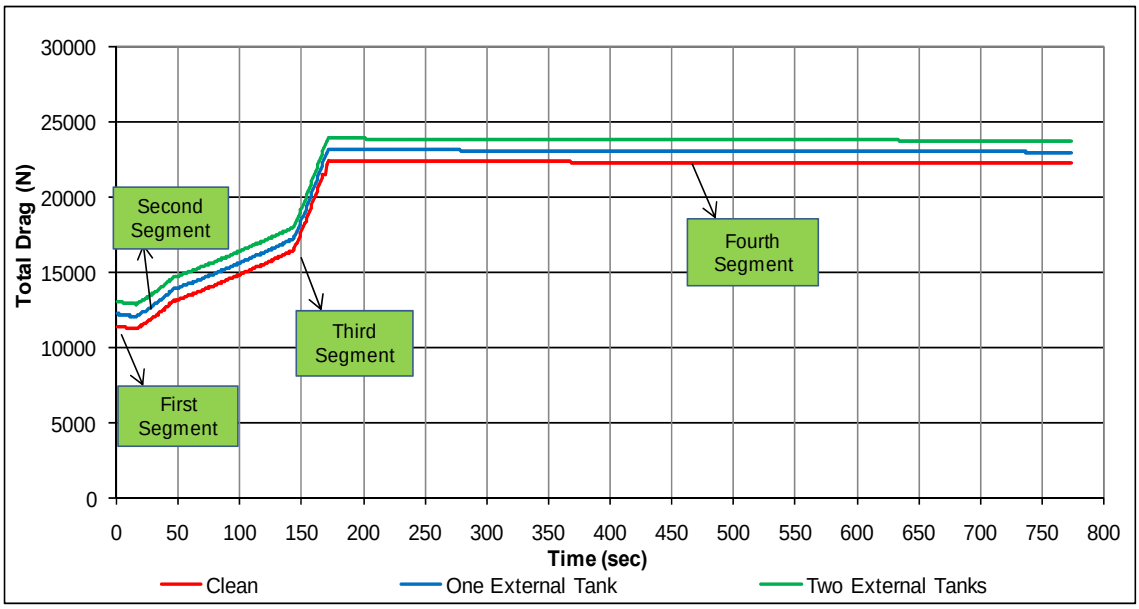

Figure 6-5: Total Drag force vs. Time

In the following three Figures (6-6, 6-7 and 6-8) is illustrated the variation of the Uninstalled net thrust with Time, Mach number and Altitude respectively.

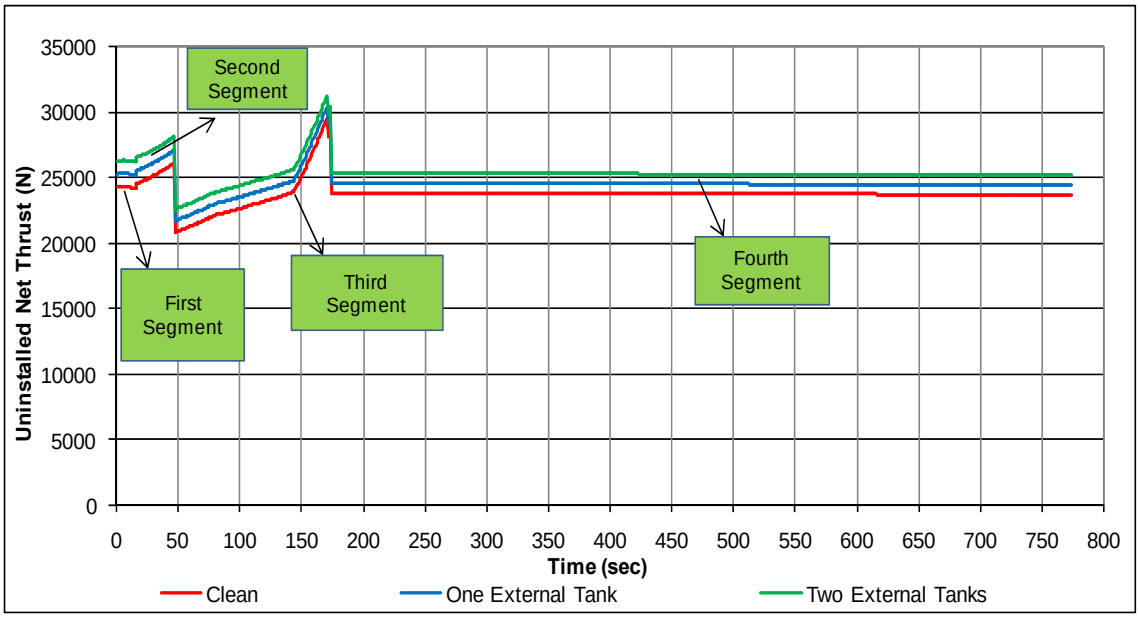

Figure 6-6: Uninstalled Net Thrust vs. Time

The demanded uninstalled net thrust is connected with the total drag of the aircraft. A comparison of the Figures 6-5 and 6-6 reveals that the variation of the thrust with time is proportional to the drag with time. At the first segment of the mission it is observed a decrease of the uninstalled net thrust, at the second and third segment the thrust increase and finally at the last segment there is a minor decrease.

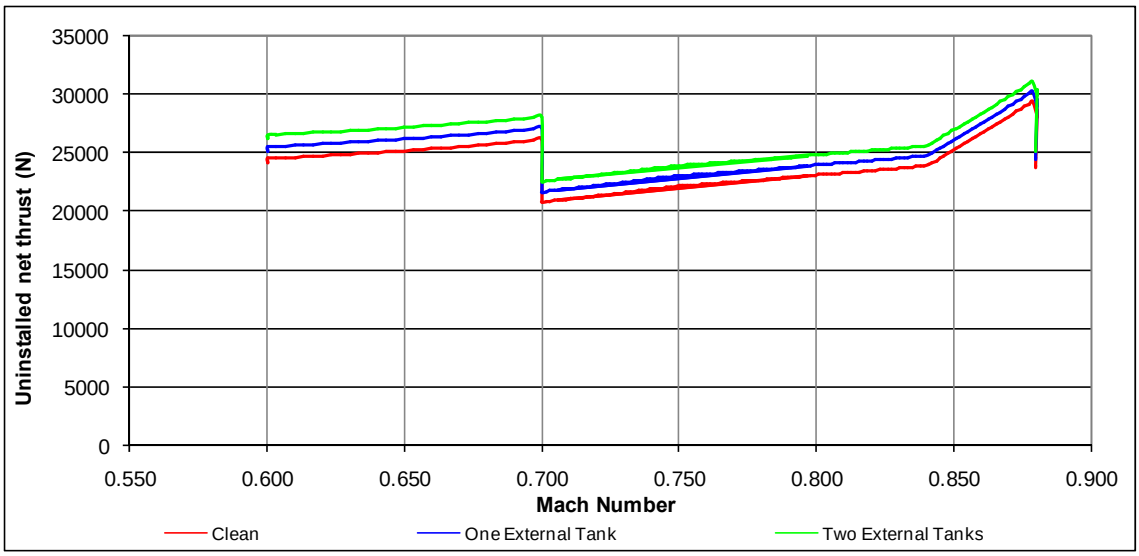

Figure 6-7: Uninstalled Net Thrust vs. Mach number

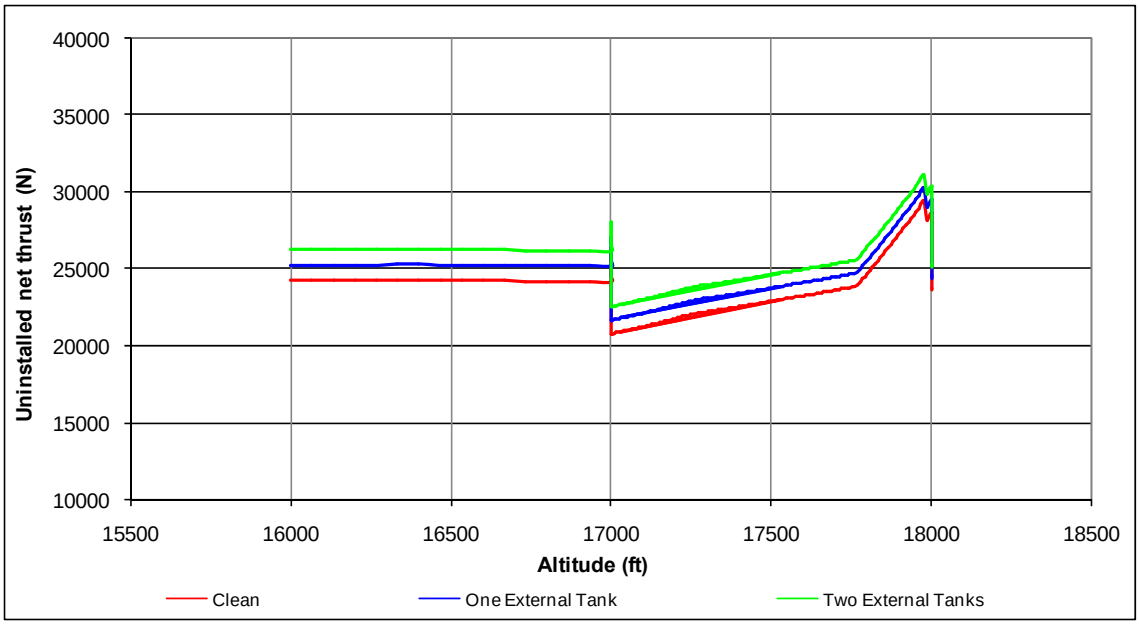

Figure 6-8: Uninstalled Net Thrust vs. Altitude

In Figure 6-6 is observed a steeply reduction in the value of the uninstalled net thrust in two points during the flight. The first one is between the second and third segment and the second one is between the third and fourth segment. These points are the transition points where a different demand of thrust is occur. Specifically, at the first point the demanded thrust is lower because at the begging of the second segment the acceleration rate is lower compared with the one at the end of the first segment. Then the combined demand of climb and acceleration, increase the thrust which at the end of the segment reaches the maximum value. At the second point there is also a change in the flight conditions. The flight requirement changes from a combined demand of acceleration and climb to a flight at constant altitude with constant Mach number. The required thrust for the new flight demand is lower and this fact causes the steep reduction that illustrated in Figure 6-6. Moreover, from the same Figure is confirmed the anticipated increase of the demanded uninstalled net thrust for the aircraft with external wing tanks.

In the following three Figures (6-9, 6-10 and 6-11) is illustrated the variation of the aircraft weight with Time, Altitude and Mach number respectively. The initial aircraft weight is different in each configuration because as mentioned before, was added in each instance, apart from the first, the weight of an extra empty wing tank. As

it was expected, is observed a reduction of the aircraft weight due to the fuel that is consumed for the completion of the mission.

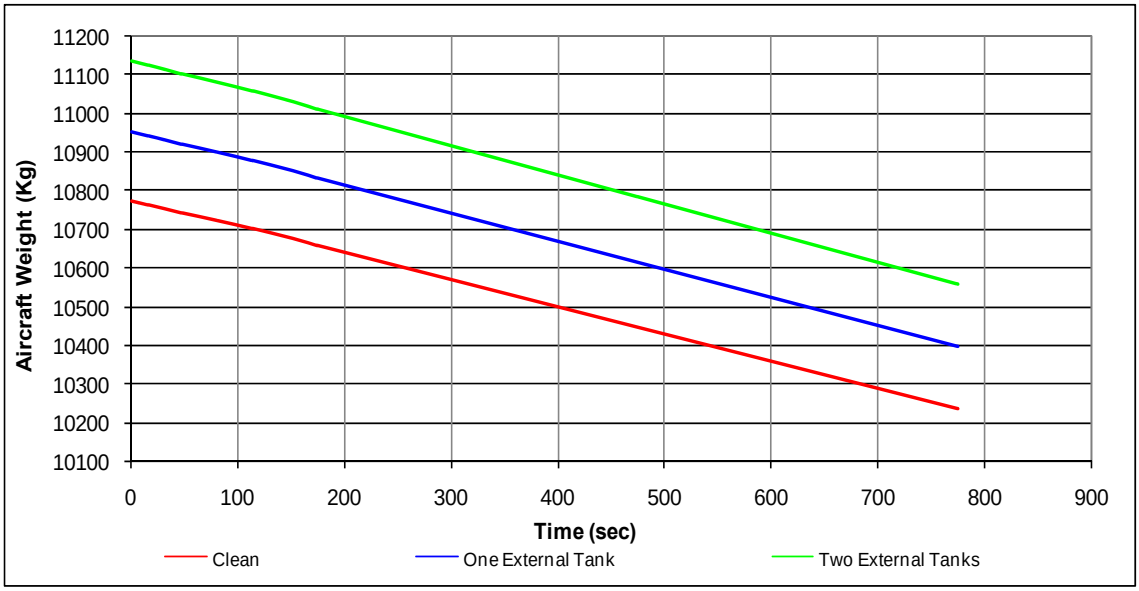

Figure 6-9: Aircraft weight vs. Time

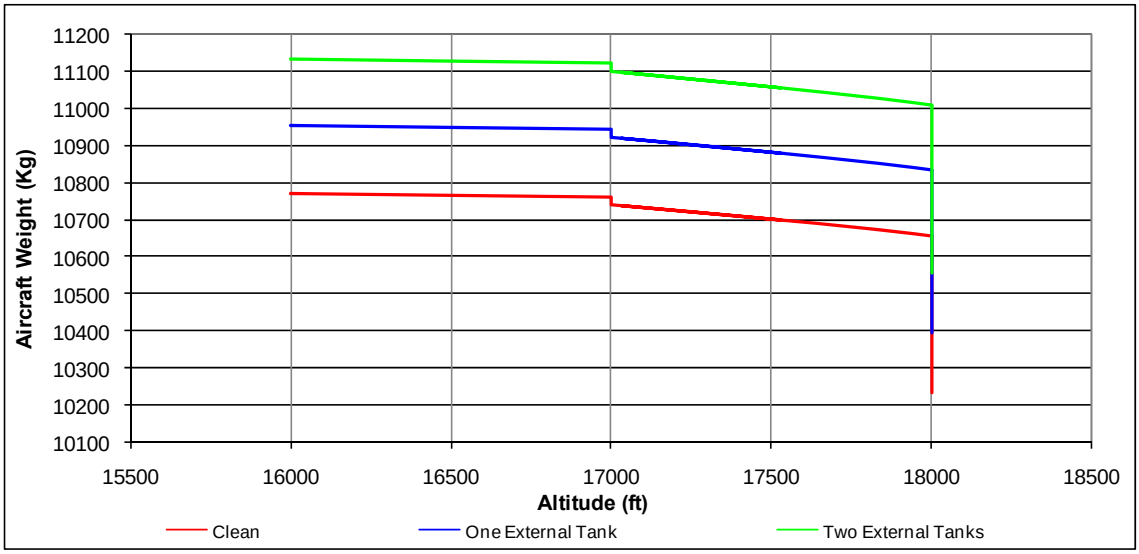

Figure 6-10: Aircraft weight vs. Altitude

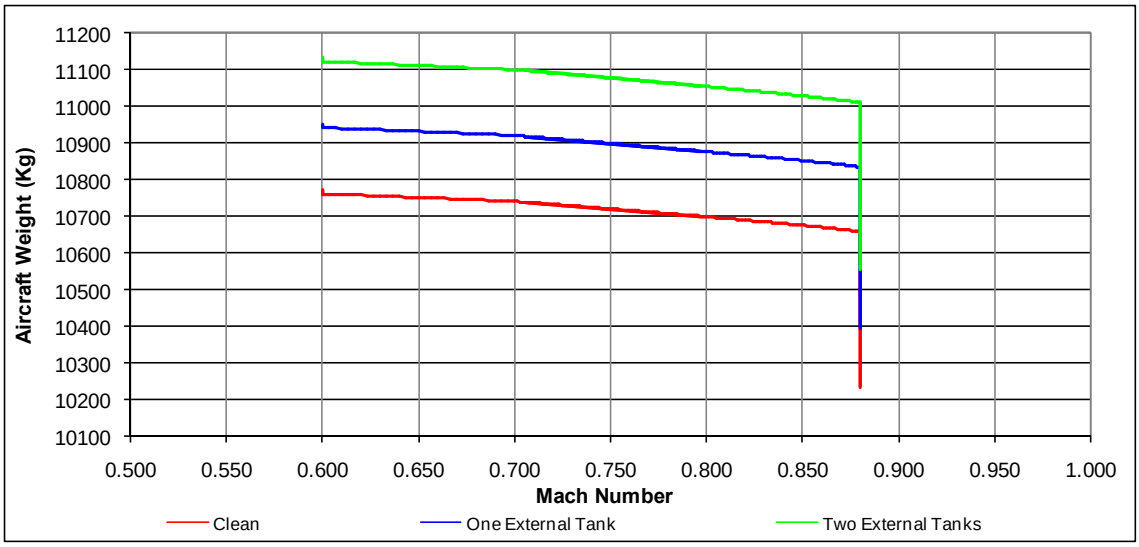

Figure 6-11: Aircraft weight vs. Mach number

According to ARES calculations the maximum amount of fuel was consumed during the mission with the third configuration (two external wing tanks) is at about 577 Kg. This fact was expected because as illustrated in Figure 6-5 the drag of this configuration is the higher. For the second configuration (one external wing tank) the amount of the consumed fuel calculated at about 556 Kg and for the first configuration (clean aircraft) at about 537 Kg. In Figure 6-12 is illustrated the variation of the consumed fuel with the external configuration.

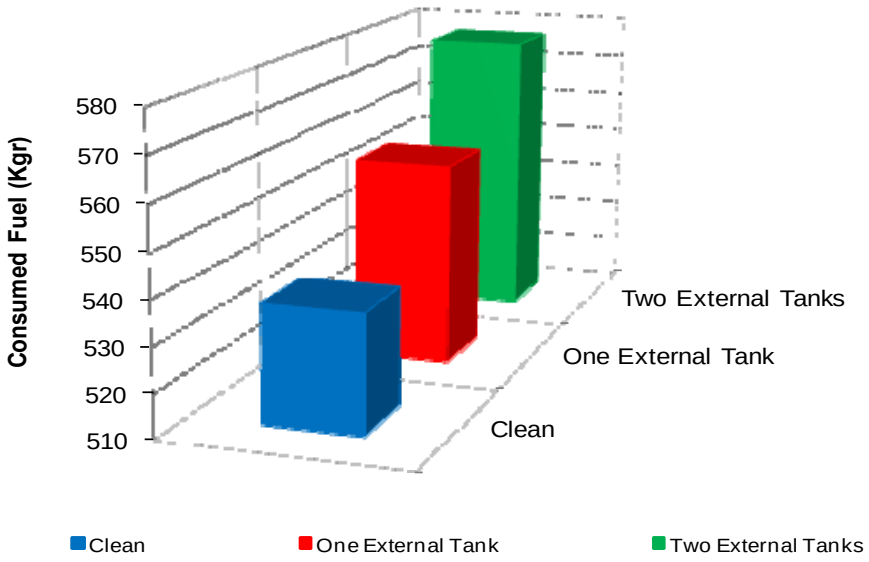

Figure 6-12: Consumed Fuel for each configuration

Based on ARES results, is extracted the conclusion that the addition of an external wing tank increase the amount of the consumed fuel at least 3.5 %. This conclusion is very significant because it can be used at the mission planning.

In Figures 6-13, 6-14 is depicted the fuel consumption. The maximum fuel consumption is observed in the third segment of the mission where there is combined climb from 17000 ft to 18000 ft and acceleration from 0.7M to 0.88 M. Also, as mentioned before, in this segment the total drag is maximum and this fact also affects the fuel consumption.

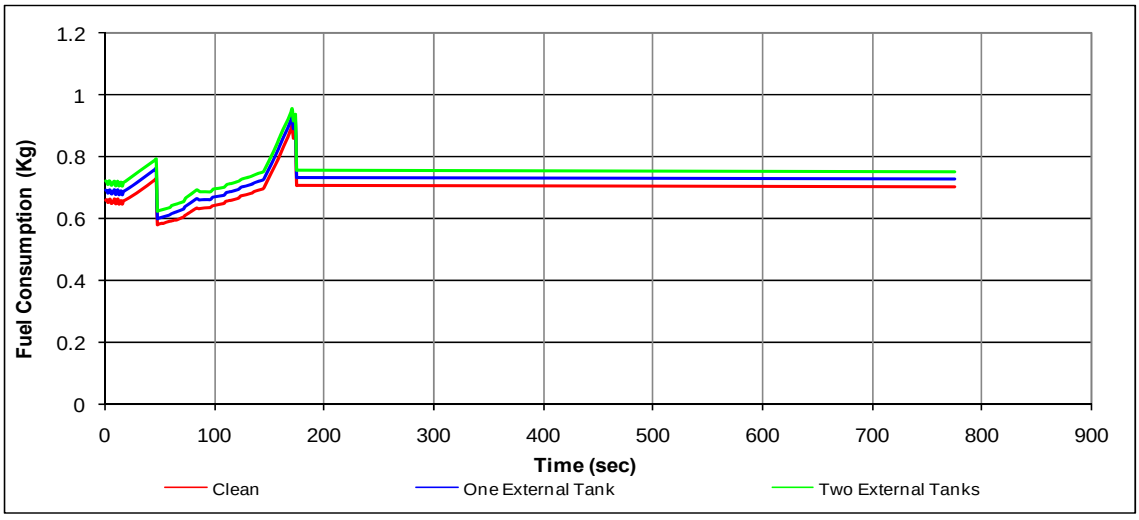

Figure 6-13: Fuel Consumption vs. Time

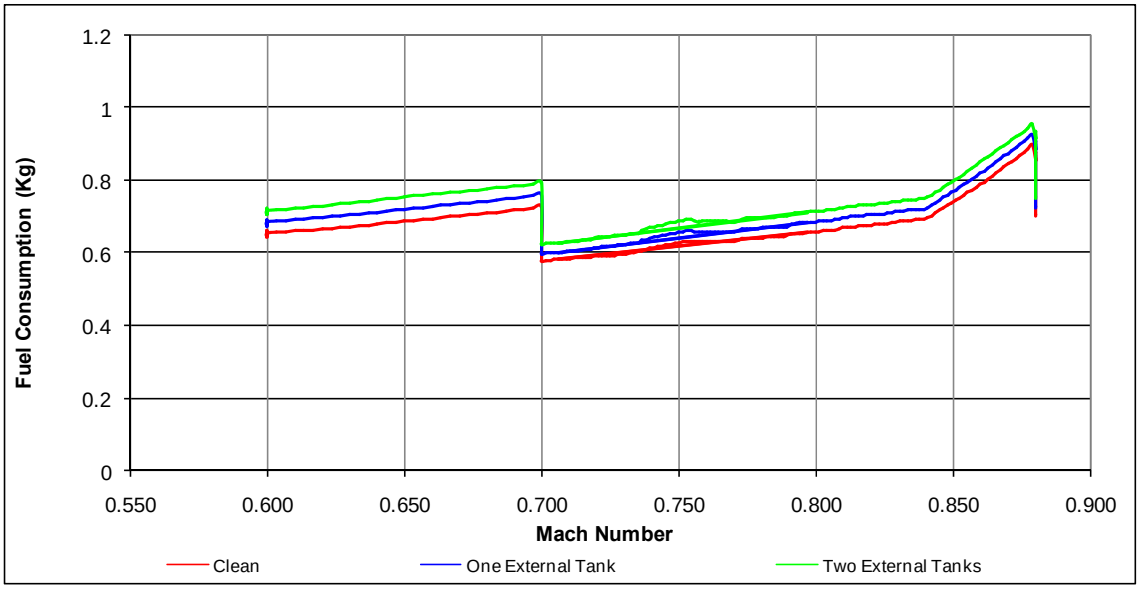

Figure 6-14: Fuel Consumption vs. Mach number

From the previous Figures is also observed a steep change in the fuel consumption in two points during the flight. The explanation is the same as in the case of the uninstalled net thrust and based on the fact that an occurred change in flight requirements affect directly the jet engine demands and consequently causes changes in the engine parameters (fuel consumption, thrust, TET etc).

An advantage of ARES method is the provision of valuable information that can be used for the component structural and thermal analysis and of course life consumption. Such information is the variation of the TET with time. The comparison of the Figures 6-6, 6-15 reveals that the TET changes proportional to the uninstalled net thrust and is higher when used external configuration. The range of the TET results that were calculated from ARES are summarised in Table 6-1 and are illustrated in Figure 6-16 (detailed calculations are included in the Appendix C). Based on calculated results is extracted the conclusion that the addition of an external wing tank increase the maximum TET at least 0.8 %.

	Clean	One External Tank	Two External Tanks
Max TET (K)	1682	1696	1710
Min TET (K)	1476	1509	1530

Table 6-1 Calculated TET Range

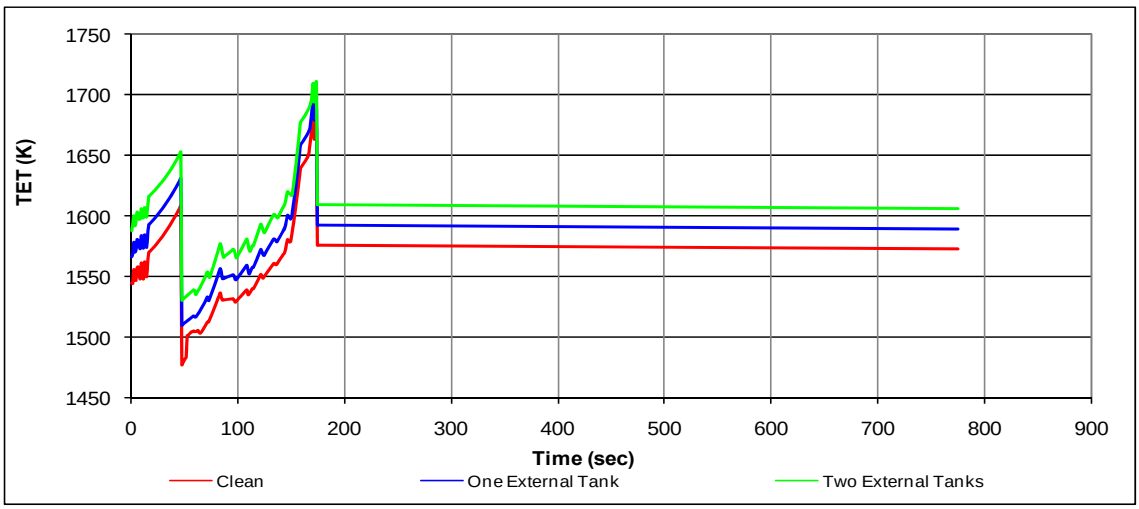

Figure 6-15: TET vs. Time

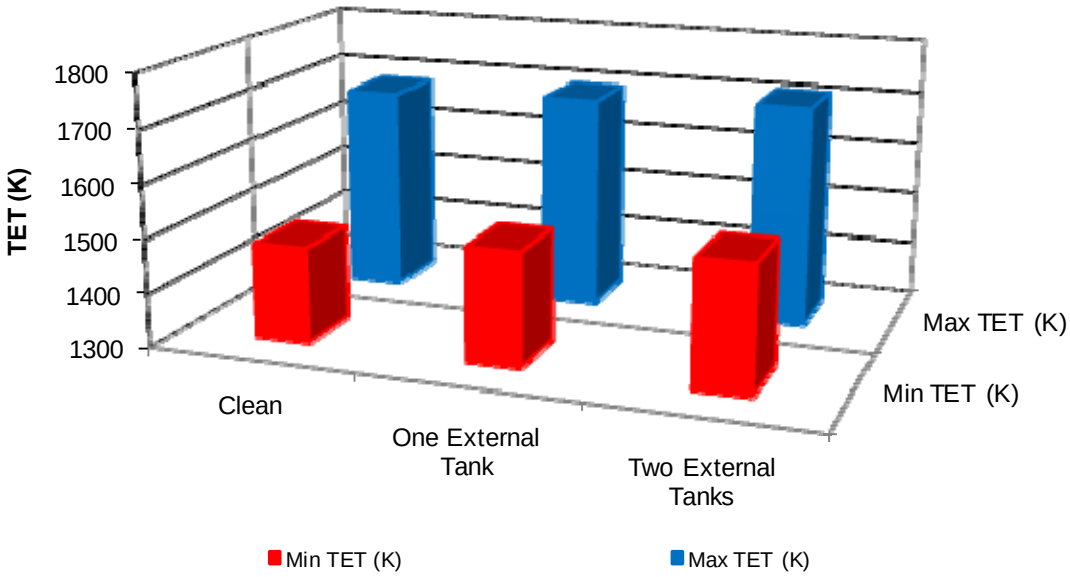

Figure 6-16: Maximum and Minimum TET for each configuration

6.5 Verification of the Calculated Results

The major issue in this study, as mentioned in previous chapter, is the verification of the calculated results. The collection of detailed information about specific parameters of a jet engine is very difficult. Data, such as temperature variation and limits, compressor map, pressure losses, combustion efficiency, the used material technology etc, are considered confidential by the engine manufacturer.

The creation of an engine model with the use of TURBOMATCH and PYTHIA softwares is based on parameters that were gathered from the literature survey, while others parameters, not available or not exactly defined, were based on default values of the software or appropriately guessed. The final results will be similar to the real ones but minor deviations are inevitable.

Moreover, as mentioned in the previous Chapter, the drag force was computed with the use of CFD software. The final outputs may differ from the real forces, but this difference as justified in §5.6 is considered as minor.

Although the initial verification of ARES method has been done (MSc Thesis), an extra validation is needed for the updated version with the new feature. For the accomplishment of this task, the change in a specific engine parameter for different external configurations was evaluated. The change of this parameter as calculated by ARES for an engine MT-200 which is similar to EJ-200 was compared to the change of the same parameter as estimated from data that were gathered from literature survey (private data) referring to the F-110-GE-100 engine. In both cases the host aircraft was the F-16 Fighting Falcon. Similarity of the magnitude of the change can prove the validity of ARES calculations.

The data that were used in this study are applicable to F-16 Fighting Falcon equipped with an F-110-GE-100 jet engine. The F-110-GE-100 which is illustrated in Figure 6-17 is a twin spool afterburning turbofan engine.

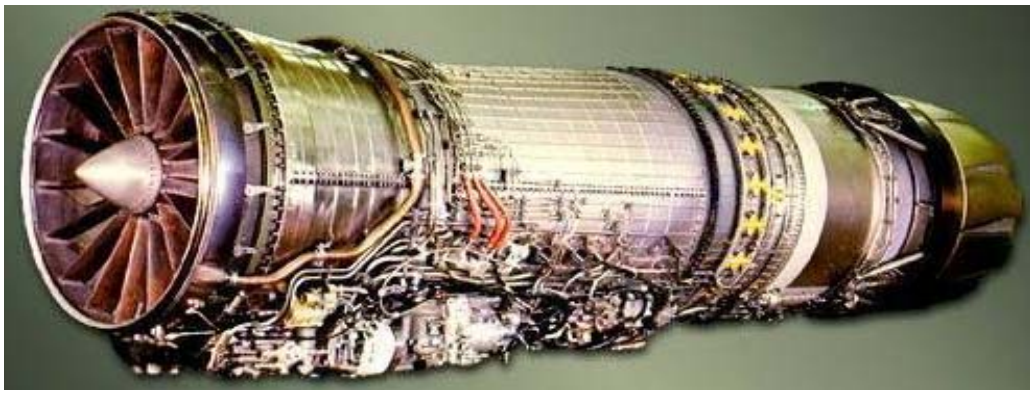

Figure 6-17: F-110-GE-100 aero engine [39]

It consists of a 3-stages Fan, 9-stages High Pressure Compressor, annular Combustors, 2-stages Low Pressure Turbine and a 1-stage High Pressure Turbine. The general characteristics of the engine are tabulated in Table 6-2.

General Characteristics F-110- GE-100	
Length (in)	182.3 – 232.3
Diameter (in)	46.5
Total Mass Flow (Kg/sec)	122
Thrust Maximum Dry (N)	74000
Thrust Maximum Afterburner (N)	120000
Overall Pressure Ratio (OPR)	29.9
TET (K)	1510

Table 6-2 General Characteristics F-110- GE-100 [41]

The engine parameter that was decided to be used in the aforementioned comparison is the fuel flow. The available performance data of the F-110-GE-100, allow the estimation of the engine fuel flow for various flight conditions and external configurations.

As a multirole aircraft, the F-16 can fly a wide range of missions with totally different weapon configurations and payload. It can carry many types of weapons (bombs, various missiles AAM, AGM, ASM) [36] and pods (navigation, ECM, targeting) and many types of external tanks (1 300gal, 2 370gal, 2 600gal). Because of the large number of external stores most of the available charts are presented in drag index format.

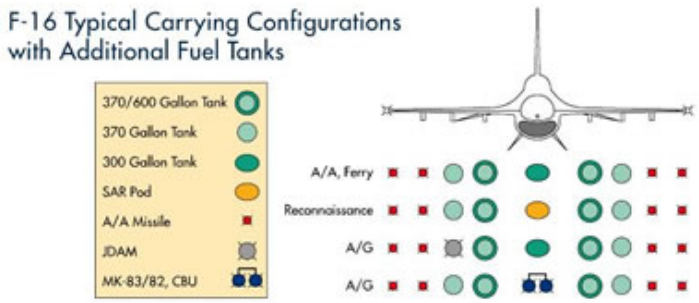

Figure 6-18: F-16 Typical Carrying Configurations [40]

The drag index is a numerical factor which provides a means for quantifying the effects on aircraft performance of adding stores to the basic aircraft. Each external store has a specific drag index.

The external configurations that were used in the study are the following:

- Clean aircraft
- Aircraft loaded with two external tanks.

The aircraft weight for both configurations is considered the same. All the parameters are the same in both cases because an objective of the study was the estimation of the fuel flow change which is caused only by altering the external stores.

The change in the fuel flow of an F-16 powered by an F-110-GE-100 for specific flight conditions when two wing tanks are added is estimated, based on literature data (private data), at about 11.5%. At this point must be mentioned that a slight higher velocity and a higher drag index was used for the aforementioned estimation. This fact was inevitable because there are not detailed data or detailed tables for each parameter. Consequently, the estimated change of the fuel flow must be slight lower.

The change of the Fuel flow that was calculated by ARES for an F-16 powered by an engine similar to MT- 200 is about 10.3%. The comparison between the estimated and calculated change of the fuel flow reveals that there is a deviation between the two values at about 10%.

Due to the fact that the estimated change of the fuel flow is lower, as mentioned before, for the specific flight conditions and external configuration of the study, is derived the conclusion that the final deviation will be definitely less than 10%. This deviation is acceptable considering that ARES method does not include the flow distortion effects in the engine performance calculations and also for the additional drag of the external tank uses data that in future can be more accurate.

In conclusion, an initial verification of the final results of the updated version of ARES method was provided by the aforementioned study. However, for an increased reliability of ARES a further validation is demanded.

Chapter 7 Conclusions and Future Work

7.1 General Conclusions

The main objective of this study was the modification of ARES method in order to integrate in the program calculations the additional drag of the external tanks. Additionally, as further requirements were the establishment of a procedure that can be used for the calculation of the additional drag that an external load (tanks, bombs, missiles, pods) contributes in the total aircraft drag and also the development of a procedure that will be used for the calculation of the thrust deductions due to installation effects.

As presented in the previous chapters, the trends of the final results of the updated ARES were as expected. The total aircraft drag and the demanded uninstalled net thrust were increased with the addition of external tanks in the aircraft. The fuel consumption was higher for the configuration with the two tanks and was noticed an increase of the TET which is proportional to the number of the used external tanks (maximum TET increases at least 0.8% per tank). Additionally was extracted the conclusion that the addition of an external wing tank increases the amount of the consumed fuel at least 3.5 %.

An initial verification of the updated version of ARES method was made. For the accomplishment of this task, the change of the fuel flow for different external configurations was evaluated. The change of this parameter as calculated by ARES for an engine MT-200 which is similar to EJ-200 was compared to the change of the same parameter as estimated from data that were gathered from literature survey referring to the F-110-GE-100 engine. In both cases the host aircraft was the F-16 Fighting Falcon. The comparison between the two changes of the fuel flow revealed that there is an acceptable deviation which is less than 10%. The further development of ARES method will cause a further reduction of this deviation.

The trends of the final results of the updated ARES combined with the initial verification that was made, lead to the conclusion that the accomplishment of the basic objective was achieved. However, for an increased reliability of ARES a further validation is demanded.

Moreover, a specific procedure that can be used for the calculation of the additional drag that an external load contributes in the total aircraft drag, was developed. The verification of the simulation results was almost impossible without test flights or experimental measurements. Nevertheless, the use of advanced computational tools which ensure the accuracy of the final output, the previous experience in similar cases, the validation of the simulation outputs through the initial verification of ARES results and the fact that the variation of the extracted quantities and forces, such as drag coefficient and drag, with velocity (Mach number) are similar to the generic curves (detailed analysis there is in §5.5), prove the reliability of the simulation results.

Furthermore, a procedure so as to be feasible for a researcher to illustrate, for different operating conditions (altitude, Mach number, angle of attack etc), the fluid path in the vicinity of the combat aircraft (especially in the intake and nozzle area) and to receive information about the main parameters (pressure, velocity, temperature etc) in the area of the engine face was developed. The CFD aircraft model, which is the final result of the aforementioned procedure, can be used as the basic tool for a future study which will focus mainly on the effect that a distorted air flow will have on the performance of the engine. The extra requirements of this study were covered with the development of these two procedures.

The current methods that are used for the performance assessment, as referred in the literature review, are firstly the ground and wind tunnel testing, where the main disadvantage is the fact that the study of the airframe/engine interaction effects is impossible or very difficult respectively and secondly the real flight testing which is the final stage, where the manufacturer foot the bill for the construction of the engine, check only one specific aircraft/engine configuration and have to deal with factors [12] such as space and weight limitations and installation problems (that prevent the use of extensive instrument packages), that lead to high measurement uncertainties.

The present study can give solutions to these problems. Firstly, ARES include in the calculations the way that the engine performance is affected by the airframe/propulsion system integration (thrust losses, spillage drag etc.) and the inlet/propulsion system compatibility (pressure recovery). Secondly, the software is built in such a way so as to model different combinations of combat aircraft/engine by simply altering the aircraft data, geometric characteristics and engine specifications. Thirdly, ARES can evaluate missions where the aircraft is loaded with external tanks and fourthly can use data from CFD simulations where there are not limitations in terms of space, weight, test facilities, scaling and geometry. The aforementioned characteristics transform ARES to an innovated and very useful integrated aircraft-engine performance tool for combat aircraft. However, the further development of the software will integrate new features that are necessary (flow distortion) and will improve the accuracy of the final results.

Finally, ARES is the method that was demanded for the completion of TERA. There was a significant gap in TERA concerning the study of the military aircraft/engine integration because the existing method- software (HERMES) referred only to civil aircraft and was taking into account the civil podded propulsion system. ARES as an integrated aircraft-engine performance tool for military aircraft can fill this gap and also can enforce TERA with a new and very significant ability.

7.2 Future Work

ARES can perform and evaluate all the segments of a flight mission (climb, descend, accelerated flights, accelerated climb or descend, loiter, decelerated flights) apart from the takeoff and landing. The first task that can be considered as future work is the development of FORTRAN modules for these two specific segments. The completed evaluation of a flight mission by ARES will be feasible after the integration of these two modules in the main FORTRAN code.

Moreover, as further update of ARES is considered the addition of a database with the drag which is contributed from all the external stores (bombs, various missiles,

pods and external tanks) and stores loading combinations that an combat aircraft is capable of carrying. For this specific work is demanded the development of CFD models for the external stores and the performance of many simulations so as to be coved the whole range of the flight missions.

Furthermore, a future work which will focus on the way that the performance of a fully integrated (buried) propulsion system is eroded by the loss of total pressure in the long and curved intake and by the effect of flow distortion on the engine in different operational conditions is demanded. The develop of a method to estimate the change in performance due to the aforementioned distortion and afterwards the integration of this method in ARES will transform the software in a completed integrated aircraft-engine performance tool for combat aircraft.

Finally, in the present study was made an effort for an initial verification of ARES but in the future after the final updates of the software an extra verification will be necessary. The new procedures that will be added and the accuracy of the CFD simulations data that will be used, will affect the final results. Considering that the evaluation of the aircraft/ engine performance is affected from these results, a further verification is demanded.

REFERENCES

1. Shaw, C.T., (1992), *Using Computational Fluid Dynamics,* Prentice Hall, Hemel Hempstead, UK.

2. Tu, J., Yeoh, G.H., Liu, C. (2008), *Computational Fluid Dynamics A Practical Approach,* Butterworth- Heinemann, Oxford, UK.

3. Oates, G.C. (1989), *Aircraft Propulsion Systems Technology and Design,* American Institute of Aeronautics and Astronautics Inc., Washington.

4. Raymer, D.P. (2006), *Aircraft Design: A Conceptual Approach,* 4th ed., American Institute of Aeronautics and Astronautics Inc. , Virginia.

5. Goldsmith, E.L., Seddon, J. (1993), *Practical Intake Aerodynamic Design,* Blackwell Scientific Publications.

6. Williams, D. (2008), *Airframe Engine Integration,* (MSc course notes, Volume two), Cranfield University, School of Engineering, Cranfield.

7. Seddon, J., Goldsmith, E.L. (1993), *Intake Aerodynamics,* 2nd ed, Blackwell Scientific Publications.

8. Fowler, T.W. (1989), *Jet Engines and Propulsion Systems for Engineers,* Training and Educational Development and the University of Cincinnati, GE Aircraft Engines.

9. Tsentseris, M. (2009), *Development of ARES: Method for Military Aircraft/Engine Integration,* Cranfield University, MSc Thesis.

10. Oates, G.C. (1989), *Aircraft Propulsion Systems Technology and Design,* American Institute of Aeronautics and Astronautics Inc., Washington.

11. Benek, J.A., Kraft, E.M., Lauer, R.F., (1996), *Validation Issues for Engine/Airframe Integration*, AIAA Report, AIAA 96-2031, New Orleans, LA.

12. Covert, E.E. (1985), *Trust and Drag: Its Prediction and Verification*, American Institute of Aeronautics and Astronautics Inc..

13. Cranfield University (1999), *The TURBOMATCH Scheme - For Aero/Industrial Gas Turbine Engine Design Point/Off Design Performance Calculation,* Cranfield University, School of Engineering, Cranfield.

14. Society of Automotive Engineers (1985), *In-flight Thrust Determination,* AIR 1703.

15. Overall, B.W., *Distortion Screen and Airjet Distortion Generator,* AEDC-TR.

16. Aerospace Recommended Practice, *Gas Turbine Engine Inlet Flow Distortion Guidelines,* ARP-1420.

17. *Air Intakes for High Speed Vehicles,* AGARD AR 270, September 1991.

18. Risk, Y.M., Gee, K. (1991), *Numerical Prediction of the Unsteady Flowfield Around the F-18 Aircraft at Large Incidence,* AIAA 91-0020.

19. Degani, D., Schiff, L.B. (1991), *Numerical Simulations of the Effect of Spatial Disturbances on Vortex Asymmetry,* AIAA Journal Vol. 29.

20. Sickles, W.L., Erickson, J.J.C. (1990), *Wall Interference Corrections for Three Dimensional Flows,* AIAA 90-1408.

21. Cumpsty, N.A., (1989), *Compressors Aerodynamics,* Longman.

22. Ghate, D., Isaacs, A., Sudhakar, K., Mujumdar, P.M., Marathe, A.G., *3d Duct Design Using Variable Fidelity Method,* American Institute of Aeronautics and Astronautics.

23. Laskaridis , P., (2004), *Performance Investigations and Systems Architectures for the More Electric Aircraft,* Cranfield University, PhD Thesis.

24. Williams, D. (1986), *Review of Current Knowledge on Engine Response to Distorted Inflow Conditions,* AGARD CP-400.

25. *Guide for Verification for Verification and Validation of Computational Fluid Dynamics Simulation,* AIAA/G-077/1998.

26. Borg, R., (1981), *A Synthesis Method for Estimating Maximum Inlet Distortion*, Paper 19, AGARD CP 301.

27. Seldock, D. (1984), *Improved Statistical Analysis Method for Prediction of Maximum Inlet Distortion,* AIAA 84-1274.

28. Hercock, R., G., (1982), *Effects on Intake Flow on Engine Stability,* Paper 20, AGARD CP 324.

29. Mazzwy, R., S., (1977), *Multiple Segment Parallel Compressor model,* ASME Journal of Engineering of Power 99.

30. Bowdtich, D., N., Coltrin, R., E. (1983), *A Survey of Inlet/Engine Distortion Compatibility*, AIAA 83-1166.

31. Burstadt, P., L.,Wenzel, L.,M., (1976), *A Method to Account for Variations of Average Compressor Inlet Pressure During Instantaneous Distortion Analysis,* AIAA 76-703.

32. Anderson, J., (1999), *Aircraft Performance and Design,* McGraw Hill International Editions, United States.

33. *Inclination Effects on Drag,* Glenn Research Center, National Aeronautics and Space Administration.

34. *Size Effects on Drag,* Glenn Research Center, National Aeronautics and Space Administration.

35. *Boundary Layer,* Glenn Research Center, National Aeronautics and Space Administration.

36. F-16 Armament at http://www.f-16.net/f-16_armament.html (accessed 20-7-09)

37. http://images.rcuniverse.com/forum/upfiles/479050/Eb86728.jpg (accessed 21-1-13)

38. http://greenairdesigns.com/ejcgallery/displayimage.php?album=60&pid=2324

#top_display_media (accessed 21-1-13)

39. http://club.china.com/data/thread/1013/2710/21/80/8_1.html (accessed 21-1-13)

40. http://defense-update.com/20060728_f-16-fuel.html (accessed 21-1-13)

41. http://en.wikipedia.org/wiki/General_Electric_F110 (accessed 21-1-13)

BIBLIOGRAPHY

1. Jenkinson, L.R., Simpkin, P., Rhodes, D. (1999), *Civil Jet Aircraft Design,* Arnold, London.

2. Laskaridis, P. (2004), *Performance Investigations and System Architectures for the More Electrical Aircraft,* PhD Thesis, Cranfield University.

3. Roskam, J. (1985), *Airplane Design*, Roskam Aviation and Engineering Corporation.

4. Torenbeek, E. (1982), *Synthesis of subsonic airplane design: an introduction to the preliminary design, of subsonic general aviation and transport aircraft, with emphasis on layout, aerodynamic design, propulsion and performance,* The Hague; Hingham, MA.

5. Howe, D., *Aircraft Conceptual Design Synthesis,* Professional Engineering Publishing Ltd., London and Bury St. Edmunds, UK.

6. Oliveira, G.L., Trapp, L G., Antonini, P.M. (2003), *Engine – Airframe Integration Methodologies for Regional Jet Aircraft with Underwing Engines*, In: 41st Aerospace Sciences Meeting & Exhibition 6-9 January 2003, Reno, Nevada, AIAA 2003-0934.

7. Nichols, M.R. (1966), *Aerodynamics of Airframe - Engine Integration of Supersonic Aircraft,* NASA TN D-3390.

8. Liu, H. (2008), *Aircraft Engine Performance and Integration in Flying Crane Aircraft Conceptual Design,* Cranfield University, MSc Thesis.

9. Vicente, E. (1994), *Effect of Bypass Ratio on Long Range Subsonic Engines,* Cranfield University, MSc Thesis.

Appendix A: Design point performance simulation of the MT-200

```
TURBOMATCH SCHEME - Windows NT version (October 1999)
 LIMITS: 100 Code words, 800 Brick Data Items, 50 Station Vector
 15 BD Items printable by any call of:-
 OUTPUT, OUTPBD, OUTPSV, PLOTIT, PLOTBD or PLOTSV
  Input "Program" follows
 !TURBOMATCH SCHEME DESIGN FILE
 !ENGINE TYPE: MT-200
 ////
 DP SI KE VA FP
  -1
  -1
 INTAKE  S1,2       D1,2,3,4,5,6                        R300
 COMPRE  S2,3       D7,8,9,10,11,12,13,14,15,16,17          R301 V7 V8
 PREMAS  S3,4,20    D18,19,20,21                            V18
 COMPRE  S4,5       D22,23,24,25,26,27,28,29,30,31,32       R302 V22 V23
 PREMAS  S5,6,21    D33,34,35,36
 PREMAS  S6,7,22    D37,38,39,40
 PREMAS  S7,8,23    D41,42,43,44
 BURNER  S8,9       D45,46,47,48,49,50,51                   R303
 MIXEES  S9,21,10
 TURBIN  S10,11     D52,53,54,55,56,57,58,59,60,61,62,63          V53
 MIXEES  S11,22,12
 TURBIN  S12,13     D64,65,66,67,68,69,70,71,72,73,74,75          V65
 DUCTER  S20,14     D76,77,78,79                            R304
 MIXFUL  S13,14,15  D80,81,82
 DUCTER  S15,16     D83,84,85,86                            R305
 NOZDIV  S16,17,1   D87,88,89                              R306
 PERFOR  S1,0,0     D90,91,92,93,306,300,303,0,0,304,0,0,305
 CODEND
```

```
1    0.0                    ! INTAKE - Altitude
2    0.0                    ! ISA Deviation
3    0.0                    ! Flight Mach number
4   -1.0                    ! Pressure recovery - USAF standard
5    0.0                    ! Pressure deviation
6    60.0                   ! Relative humidity (%)

7   0.7                     ! LP COMPRESSOR - Surge margin
8  -1                       ! PCN Rotational speed ratio
9   4.2                     ! Pressure ratio
10   0.86                   ! Isentropic efficiency
11   1.0                    ! Error selection
12   2.0                    ! Compressor map
13   1.0                    ! Shaft number
14   1.0                    ! PR Degradation factor
15   1.0                    ! WAC Degradation factor
16   1.0                    ! ETA Degradation factor
17   0.0                    ! Stator Angle

18   0.7142857              ! Lambda (W)
19   0.0                    ! Delta (W)
20   1.0                    ! Lambda (P)
21   0.0                    ! Delta (P)

22   0.7                    ! HP COMPRESSOR - Surge margin
23  -1                      ! PCN Rotational speed ratio
24   6.2                    ! Pressure ratio
25   0.85                   ! Isentropic efficiency
26   1.0                    ! Error selection
27   4.0                    ! Compressor map
28   2.0                    ! Shaft number
29   1.0                    ! PR Degradation factor
30   1.0                    ! WAC Degradation factor
31   1.0                    ETA Degradation factor
32   0.0                    ! Stator Angle

33   0.94                   ! Lambda (W)
34   0.0                    ! Delta (W)
35   1.0                    ! Lambda (P)
36   0.0                    ! Delta (P)

37   0.94                   ! Lambda (W)
38   0.0                    ! Delta (W)
39   1.0                    ! Lambda (P)
40   0.0                    ! Delta (P)
```

```
41   0.93          ! Lambda (W)
42    0.0          ! Delta (W)
43    1.0          ! Lambda (P)
44    0.0          ! Delta (P)


45   0.05          ! Pressure loss
46   0.99          ! Combustion efficiency
47  -1.0           ! Fuel flow
48   0.0           ! Injected water/steam flow
49  340.0          ! Temperature of injected water or steam
50   0.0           ! Steam quality


51    1.0          ! ETA Degradation factor
52   0.0           ! HP TURBINE - Auxiliary work
53   0.7           ! Inlet ND mass flow
54   0.7           ! Relative ND speed
55   0.87          ! Isentropic efficiency
56  -1.0           ! Relative rotational speed
57   2.0           ! Shaft number
58   4.0           ! Turbine map
59  -1.0           ! Power law index
60    1.0          ! TF Degradation factor
61    1.0          ! DH Degradation factor
62    1.0          ! ETA Degradation factor
63   0.0           ! NGV Angle


64    0.0          ! LP TURBINE - Auxiliary work
65   0.7           ! Inlet ND mass flow
66   0.7           ! Relative ND speed
67   0.87          ! Isentropic efficiency
68  -1.0           ! Relative rotational speed
69   1.0           ! Shaft number
70   4.0           ! Turbine map
71  -1.0           ! Power law index
72    1.0          ! TF Degradation factor
73    1.0          ! DH Degradation factor
74    1.0          ! ETA Degradation factor
75   0.0           ! NGV Angle

76   0.0           ! Reheat/ Intercooling Switch
77   0.032         ! Pressure Loss
78   0.0           ! Combustion Efficiency
79   1000000.0     ! Limiting Value of fuel Flow

80   1.0                    ! Compressor Providing Bypass Stream
81   1.0           ! Match Number /Static Pressure Switch
82   0.4           ! Match Number or Static Pressure
```

```
83    0.0                          ! Reheat/ Intercooling Switch
84     0.01                        ! Pressure Loss
85     0.85                        ! Combustion Efficiency
86     1000000.0                   ! Limiting Value of fuel Flow

87    1.0                          ! Switch Set
88    -1.0                         ! Throat Area
89     1.0                         !P Degradation Factor

90   -1.0                          ! Power Output
91    -1.0                         ! Propeller efficiency
92     0.0                         ! Scaling index
93     0.0                         ! Design point net thrust


-1

1 2 77

9 6 1820

16 6 2000.0

-1

            The Units for this Run are as follows:-

Temperature = K   Pressure = Atmospheres   Length = metres

Area = sq metres  Mass Flow = kg/sec       Velocity = metres/sec

Force = Newtons   s.f.c.(Thrust) =  mg/N sec   s.f.c.(Power) = mug/J

Sp. Thrust =    N/kg/sec     Power =   Watts

 ***** DESIGN POINT ENGINE CALCULATIONS *****

***** AMBIENT AND INLET PARAMETERS *****

Alt. =      0.0     I.S.A. Dev. =    0.000       PDev. =    0.000

Mach No. =  0.00     Etar = 1.0000        Momentum Drag =      0.00

Rel.Humidity = 60.00
```

***** COMPRESSOR 1 PARAMETERS *****

PRSF = 0.63855E+01 ETASF = 0.10044E+01 WASF = 0.24936E+00

DGPRSF = 0.10000E+01 DGETASF = 0.10000E+01 DGWASF = 0.10000E+01

Z = 0.70000 PR = 4.200 ETA = 0.86000

PCN = 1.0000 CN = 1.00000 COMWK = 0.13370E+08

STATOR ANGLE = 0.00

***** COMPRESSOR 2 PARAMETERS *****

PRSF = 0.63016E+01 ETASF = 0.10271E+01 WASF = 0.88887E-01

DGPRSF = 0.10000E+01 DGETASF = 0.10000E+01 DGWASF = 0.10000E+01

Z = 0.70000 PR = 6.200 ETA = 0.85000

PCN = 1.0000 CN = 1.00000 COMWK = 0.20682E+08

STATOR ANGLE = 0.00

***** COMBUSTION CHAMBER PARAMETERS *****

ETASF = 0.99000E+00 DGETASF = 0.10000E+01

ETA = 0.99000 DLP = 1.3219 WFB = 1.3492 WWB = 0.00000

***** TURBINE 1 PARAMETERS *****

CNSF = 0.97314E+02 ETASF = 0.10224E+01 TFSF = 0.47225E+01

DHSF = 0.17870E+05

DGETASF = 0.10000E+01 DGTFSF = 0.10000E+01 DGDHSF = 0.10000E+01

TF = 393.111 ETA = 0.87000 CN = 2.320

AUXWK = 0.00000E+00 NGV ANGLE = 0.00

***** TURBINE 2 PARAMETERS *****

CNSF = 0.86909E+02 ETASF = 0.10224E+01 TFSF = 0.17341E+01

DHSF = 0.13635E+05

DGETASF = 0.10000E+01 DGTFSF = 0.10000E+01 DGDHSF = 0.10000E+01

TF = 392.828 ETA = 0.87000 CN = 2.320

AUXWK = 0.00000E+00 NGV ANGLE = 0.00

***** MIXING MACH NUMBERS *****

Station 13, M= 0.401 Station 14,M = 0.422 Station 15,M = 0.421

***** CONVERGENT/DIVERGENT NOZZLE 1 PARAMETERS *****

NDISF = 0.10000E+01 DGNDISF = 0.10000E+01

Throat Area = 0.1481 Throat Velocity = 575.47 Throat Mach No. = 1.0000

Exit Area = 0.1817 Exit Velocity = 819.21 Exit Mach No. = 1.5594

Nozzle Coeff. = 0.9780 Gross Thrust = 60048.77

Nozzle exit and throat areas are floating.

AREA RATIO (EXIT/THROAT): 1.23

Scale Factor on above Mass Flows, Areas, Thrusts & Powers = 1.0000

Station	F.A.R.	Mass Flow	Pstatic	Ptotal	Tstatic	Ttotal	Vel	Area	W.A.R.	X
1	0.00000	77.000	1.00000	1.00000	288.15	288.15	0.0	******	0.00637	1.000
2	0.00000	77.000	******	1.00000	******	288.15	******	******	0.00637	1.000
3	0.00000	77.000	******	4.21000	******	457.84	******	******	0.00637	1.000
4	0.00000	55.000	******	4.21000	******	457.84	******	******	0.00637	1.000
5	0.00000	55.000	******	26.43880	******	808.56	******	******	0.00637	1.000
6	0.00000	51.700	******	26.43880	******	808.56	******	******	0.00637	1.000
7	0.00000	48.598	******	26.43880	******	808.56	******	******	0.00637	1.000
8	0.00000	45.196	******	26.43880	******	808.56	******	******	0.00637	1.000
9	0.03004	46.545	******	25.11686	******	1820.00	******	******	0.00637	1.000
10	0.02800	49.845	******	25.11686	******	1759.43	******	******	0.00637	1.000

11	0.02800	49.845	******	8.75577	******	1436.95	******	******	0.00637	1.000
12	0.02631	52.947	******	8.75577	******	1403.30	******	******	0.00637	1.000
13	0.02631	52.947	3.60679	4.00124	1171.46	1200.45	266.6	0.1838	0.00637	1.000
14	0.00000	22.000	3.60679	4.07528	442.32	457.84	179.0	0.0434	0.00637	1.000
15	0.01845	74.947	3.55423	3.99047	971.40	999.49	257.0	0.2272	0.00637	1.000
16	0.01845	74.947	******	3.95056	******	999.49	******	******	0.00637	1.000
17	0.01845	74.947	1.00000	3.95056	705.59	999.49	819.2	0.1817	0.00637	1.000
18	0.00000	0.000	******	0.00000	******	0.00	******	******	0.00000	0.000
19	0.00000	0.000	******	0.00000	******	0.00	******	******	0.00000	0.000
20	0.00000	22.000	******	4.21000	******	457.84	******	******	0.00637	1.000
21	0.00000	3.300	******	26.43880	******	808.56	******	******	0.00637	1.000
22	0.00000	3.102	******	26.43880	******	808.56	******	******	0.00637	1.000

Gross Thrust = 60048.77
Momentum Drag = 0.00
Net Thrust = 60048.77
Fuel Flow = 1.3492
s.f.c. = 22.46759
Sp. Thrust = 779.854

Appendix B: Intake sizing and Spillage Drag calculation of the MT-200

Intake sizing

Design point flight condition: Altitude 4870 m and Mach number 0.6
Ambient static pressure **pso** =0.5424 Atm or **pso** =7.971psi
Total pressure **Ptotal** =0.69197 Atm
Non-dimensional total pressure **δt,ef**= $P_{t,\text{engine face}}$/ 1 =0.69197
Total temperature **Ttotal** =275.02 K
Non-dimensional total temperature **θt= Ttotal**/288.15 = **0.9544**
Mass flow **W**=58.238 Kg/sec or 128.3928 lb/sec
Inlet diameter D_{ef} =0.74 m or 29.13 in

Engine face area **Aef**=$\frac{\pi D^2}{4} = \frac{\pi 0.74^2}{4}$=0.43 m^2 or 666.63 in^2

Engine corrected mass-flow $\mathbf{Wc_{ef}} = \frac{W\sqrt{\theta t}}{\delta_{t,ef}} = \frac{128.3928\sqrt{0.9544}}{0.69197} = 181.27\ \frac{lb}{\sec}$

Qef'=$\frac{W\sqrt{\theta t}}{\delta_{t,ef} A_{ef}} = \frac{128.3929\sqrt{0.9544}}{0.69197 x 666.63} = 0.2719$

Intake total pressure recovery $\frac{Pt_{ef}}{Pt_0}$ =1 - 0.328x(Qef')^2 =1 - 0.328x(0.2719)^2 = 0.9757

Corrected throat flow $Wc_{th} = \frac{W\sqrt{\theta t}}{\delta_{t,th}}$ = Wc_{ef} x 0.9757= 181.27 x 0.9757= 176.87 $\frac{lb}{\sec}$

Design Throat Mach number chosen, M_{th} = 0.75

$\frac{W\sqrt{\theta t}}{\delta_{t,th} A_{th}} = \frac{0.5931 M_{th}}{(1+0.2M_{th}^2)^3} = \frac{0.5931 x 0.75}{(1+0.2x0.75^2)^3}$ =0.32306

Hence Throat area Ath = $\frac{176.87}{0.32306}$ = 547.49 in^2

Diffuser area ratio, $\frac{A_{ef}}{A_{th}} = \frac{666.63}{547.49}$ = 1.2176

Intake contraction ratio, $\frac{A_H}{A_{th}}$ = 1.14

Hence Highlight area $\mathbf{A_H}$ = 1.14x 547.49 = 624.14 in^2

Capture Ratio, $\frac{A_C}{A_{th}} = 1.3$

Hence Capture area **AC** = 1.3 x 547.49 = 711.73 in^2

Diffuser Length/ Engine Face Gross Area $\frac{L_{duct}}{D_{ef}} = 5.6$

Hence L_{duct} =5.6x D_{ef} =5.6x 29.13=163.128 in

$$\frac{W\sqrt{\theta t}}{\delta_0 A_0} = \frac{0.5931 M_0}{(1+0.2M_0^2)^3} = \frac{0.5931x0.6}{(1+0.2x0.6^2)^3} = 0.2888$$

For subsonic flight $\frac{\delta_{t,th}}{\delta_{t0}} = \frac{Pt_{th}}{Pt_0} = 1.0$

$$\text{Ao} = \frac{\frac{W\sqrt{\theta_t}}{\delta_{t,th}}\frac{\delta_{t,th}}{\delta_{t0}}}{Q'_0} = \frac{176.87x1.0}{0.2888} = 612.43 \text{ in}^2$$

$$\text{MFR} = \frac{A_0}{A_C} = \frac{\frac{W\sqrt{\theta_t}}{\delta_{t,th}}\frac{\delta_{t,th}}{\delta_{t0}}}{Q'_0 A_C} = \frac{176.87x1.0}{0.2888x711.73} = 0.86$$

Spillage drag calculation for MT-200

Altitude 4870 m and Mach number 0.6

The the MFR and the AC for altitude 4870 m and Mach number 0.6 and the values were **MFR**= 0.86 and **AC** = 711.73 in^2 .
Additionally at this flight condition the ambient static pressure **pso** =0.5424 Atm or **pso** =7.971 psi .
Furthermore the flight dynamic head which can be estimated from the equation (6.9)

qo = 0.7 $p_{so}M_o^2$ = 0.7x 7.971x 0.6^2= 2.01 $\frac{lbf}{ft^2}$

From the Figure J-1 is obvious that the incremental spillage drag **ΔCD** is zero at Mo=0.6 and MFR= 0.86.

Therefore from the equation (6.8) the spillage drag is
ΔDspill = qo ΔCD Ac =2.01x 0 x 711.73 = 0 lbf

In the same way, the spillage drag for different altitudes and Mach numbers was calculated and the results are tabulated below:

ALTITUDE (m):	4870								
Mach Number	**δt,ef**	**θt**	**Wc,ef**	**Ao**	**Pt,ef / Pto**	**MFR**	**qo**	**ΔC_D**	**ΔD_{spill} (N)**
0.6	0.69	0.95	181.27	612.31	0.976	0.86	2.01	0	0
0.65	0.72	0.97	178.93	578.04	0.976	0.81	2.357	0	0
0.7	0.75	0.98	176.42	549.6	0.977	0.77	2.734	0	0
0.75	0.79	0.99	173.47	525.03	0.978	0.74	3.139	0	0
0.8	0.83	1	170.22	503.89	0.979	0.71	3.571	0.006	67.83
0.88	0.9	1.03	162.25	469.54	0.981	0.66	4.321	0.045	615.6
ALTITUDE (m):	5000								
Mach Number	**δt,ef**	**θt**	**Wc,ef**	**Ao**	**Pt,ef / Pto**	**MFR**	**qo**	**ΔC_D**	**ΔD_{spill} (N)**
0.6	0.68	0.95	181.94	614.45	0.976	0.86	1.974	0	0
0.65	0.71	0.96	179.62	580.13	0.976	0.82	2.317	0	0
0.7	0.74	0.97	177.11	551.63	0.977	0.78	2.687	0	0
0.75	0.77	0.99	174.25	527.29	0.978	0.74	3.085	0	0
0.8	0.81	1	171.02	506.15	0.978	0.71	3.51	0.006	66.67
0.88	0.88	1.02	163.5	473	0.98	0.66	4.247	0.045	605.01
ALTITUDE (m):	5250								
Mach Number	**δt,ef**	**θt**	**Wc,ef**	**Ao**	**Pt,ef / Pto**	**MFR**	**qo**	**ΔC_D**	**ΔD_{spill} (N)**
0.6	0.66	0.95	183.23	618.6	0.975	0.87	1.909	0	0
0.65	0.68	0.96	180.94	584.2	0.976	0.82	2.241	0	0
0.7	0.72	0.97	178.45	555.62	0.976	0.78	2.598	0	0
0.75	0.75	0.98	175.77	531.66	0.977	0.75	2.983	0	0
0.8	0.79	0.99	172.58	510.55	0.978	0.72	3.394	0.004	42.98
0.88	0.85	1.02	166.04	480.06	0.98	0.67	4.107	0.042	546.06
ALTITUDE (m):	5500								
Mach Number	**δt,ef**	**θt**	**Wc,ef**	**Ao**	**Pt,ef / Pto**	**MFR**	**qo**	**ΔC_D**	**ΔD_{spill} (N)**
0.6	0.64	0.94	184.49	622.63	0.975	0.87	1.846	0	0
0.65	0.66	0.95	182.31	588.39	0.975	0.83	2.166	0	0
0.7	0.69	0.96	179.78	559.55	0.976	0.79	2.512	0	0
0.75	0.72	0.97	177.12	535.56	0.977	0.75	2.884	0	0
0.8	0.76	0.99	174.11	514.88	0.978	0.72	3.281	0.004	41.55
0.88	0.83	1.01	168.58	487.07	0.979	0.68	3.97	0.039	490.24

Table B-1: Spillage drag calculation for the MT-200

Appendix C: Aircraft/Engine Performance of MT-200 with Thrust losses and Drag contribution

Clean

Climb in 15 sec. from 16000 ft to 17000 ft with constant Mach number 0.6.

Mach Number	Altitude (ft)	Uninstalled Thrust (N)	TET (K)	Uninstalled SFC (mg/Nsec)	Drag (N)	Aircraft Weight (Kg)	Fuel Consumption (Kg)
0.600	16000	24224.91	1543.92	27.15	11395.84	10772	0.6578175
0.600	16067	24231.74	1543.67	27.19	11382.84	10771.34	0.6589533
0.600	16133	24238.7	1555.16	26.82	11369.97	10770.68	0.6501813
0.600	16200	24245.74	1547.96	27.13	11357.16	10770.03	0.6579025
0.600	16267	24252.82	1546.33	27.24	11344.41	10769.38	0.6605663
0.600	16333	24259.96	1556.47	26.69	11331.71	10768.71	0.6475888
0.600	16400	24267.18	1557.39	26.73	11319.09	10768.07	0.6486925
0.600	16467	24253.5	1552.77	27.01	11306.6	10767.42	0.6551096
0.600	16533	24238.46	1547.54	27.30	11294.17	10766.76	0.6615977
0.600	16600	24223.46	1560.55	26.67	11281.79	10766.1	0.6460048
0.600	16667	24208.55	1553.70	26.97	11269.48	10765.46	0.6528203
0.600	16733	24193.71	1547.47	27.35	11257.24	10764.8	0.6615969
0.600	16800	24178.96	1561.31	26.69	11245.11	10764.14	0.6452443
0.600	16867	24164.31	1556.08	26.90	11233.05	10763.5	0.6500698
0.600	16933	24149.71	1549.30	27.17	11221.04	10762.85	0.6562358
0.600	17000	24135.15	1561.16	26.72	11209.09	10762.19	0.6450034
0.600	17000	24470.69	1569.2	26.8	11248.86	10762.19	0.6549575

Table C-1: Performance calculations for the first segment of the mission

Aircraft acceleration in 30sec. from Mach number 0.6 to 0.7 at constant altitude 17000ft.

Mach Number	Altitude (ft)	Uninstalled Thrust (N)	TET (K)	Uninstalled SFC (mg/Nsec)	Drag (N)	Aircraft Weight (Kg)	Fuel Consumption (Kg)
0.603	17000	24508.57	1570.12	26.8	11295.18	10761.54	0.6568591
0.607	17000	24547.58	1571.045	26.8	11342.63	10760.88	0.6587981
0.610	17000	24587.7	1572.002	26.9	11391.19	10760.22	0.6607713
0.613	17000	24628.9	1572.975	26.9	11440.85	10759.56	0.662779
0.617	17000	24671.19	1573.967	26.9	11491.59	10758.9	0.6648212
0.620	17000	24714.54	1574.978	27.0	11543.41	10758.23	0.6668984
0.623	17000	24758.94	1576.005	27.0	11596.28	10757.56	0.6690089
0.627	17000	24804.39	1577.049	27.1	11650.2	10756.9	0.6711547
0.630	17000	24850.85	1578.108	27.1	11705.16	10756.22	0.6733437
0.633	17000	24898.33	1579.217	27.1	11761.13	10755.55	0.6756336
0.637	17000	24946.82	1580.349	27.2	11818.12	10754.88	0.6779785
0.640	17000	24996.29	1581.518	27.2	11876.11	10754.2	0.6803747
0.643	17000	25046.75	1582.727	27.3	11935.08	10753.52	0.6828247
0.647	17000	25098.18	1583.959	27.3	11995.03	10752.83	0.6853294
0.650	17000	25150.57	1585.24	27.4	12055.96	10752.15	0.6878872
0.653	17000	25204.69	1586.585	27.4	12117.83	10751.46	0.6903156
0.657	17000	25259.54	1587.957	27.4	12180.66	10750.77	0.6927562
0.660	17000	25315.11	1589.34	27.5	12244.43	10750.08	0.695243
0.663	17000	25371.37	1590.739	27.5	12309.12	10749.38	0.6977464
0.667	17000	25428.31	1592.16	27.5	12374.74	10748.68	0.7002649
0.670	17000	25485.9	1593.592	27.6	12441.27	10747.98	0.7028
0.673	17000	25544.12	1595.047	27.6	12508.7	10747.28	0.7053483
0.677	17000	25603.01	1596.519	27.6	12577.02	10746.58	0.707914
0.680	17000	25665.16	1598.074	27.7	12646.23	10745.87	0.7105812
0.683	17000	25728.45	1599.623	27.7	12716.32	10745.16	0.7133005
0.687	17000	25792.83	1601.195	27.8	12787.28	10744.45	0.7160567
0.690	17000	25858.26	1602.794	27.8	12859.1	10743.73	0.7188449
0.693	17000	25924.73	1604.404	27.8	12931.78	10743.01	0.7216683
0.697	17000	25992.2	1606.051	27.9	13005.3	10742.29	0.7245229
0.700	17000	26060.66	1607.72	27.9	13079.67	10741.56	0.7274086

Table C-2: Performance calculations for the second segment of the mission

Climb from 17000 ft to 18000 ft with aircraft acceleration from Mach number 0.7 to 0.88 in 125 sec

Mach Number	Altitude (ft)	Uninstalled Thrust (N)	TET (K)	Uninstalled SFC (mg/Nsec)	Drag (N)	Aircraft Weight (Kg)	Fuel Consumption (Kg)
0.700	17000	20768.45	1476.38	27.9	13079.37	10741.56	0.5785586
0.701	17008	20803.52	1478.053	27.9	13109.52	10740.98	0.5798349
0.703	17016	20838.96	1479.733	27.9	13139.8	10740.4	0.5811228
0.704	17024	20874.77	1481.399	27.9	13170.2	10739.82	0.582423
0.706	17032	20910.96	1482.703	27.9	13200.72	10739.24	0.5830486
0.707	17040	20947.53	1500.235	27.8	13231.38	10738.66	0.5823256
0.709	17048	20984.48	1501.068	27.8	13262.16	10738.07	0.5835845
0.710	17056	21021.81	1501.93	27.8	13293.08	10737.49	0.5848655
0.712	17064	21059.54	1502.796	27.8	13324.12	10736.9	0.5861695
0.713	17072	21097.62	1503.691	27.8	13355.29	10736.32	0.5874963
0.715	17080	21136.08	1503.668	27.8	13386.58	10735.73	0.5884437
0.716	17088	21174.91	1504.408	27.8	13417.99	10735.14	0.5897111
0.718	17096	21214.11	1503.868	27.8	13449.52	10734.55	0.589982
0.719	17104	21253.68	1503.938	27.8	13481.17	10733.96	0.5908005
0.720	17112	21293.63	1503.994	27.8	13512.94	10733.37	0.591478
0.722	17120	21333.94	1504.881	27.8	13544.83	10732.78	0.5928056
0.723	17128	21374.62	1503.444	27.8	13576.84	10732.19	0.5935691
0.725	17136	21415.67	1502.493	27.7	13608.97	10731.59	0.593362
0.726	17144	21457.1	1503.091	27.7	13641.22	10731	0.5942065
0.728	17152	21498.88	1504.415	27.7	13673.59	10730.41	0.5957432
0.729	17160	21541.04	1505.797	27.7	13706.07	10729.81	0.597291
0.731	17168	21583.55	1507.245	27.7	13738.67	10729.21	0.5988492
0.732	17176	21626.45	1508.763	27.8	13771.38	10728.61	0.6004169
0.734	17184	21669.69	1510.355	27.8	13804.21	10728.01	0.6019922
0.735	17192	21713.32	1511.761	27.8	13837.16	10727.41	0.6038233
0.737	17200	21757.29	1511.841	27.9	13870.21	10726.81	0.607753
0.738	17208	21801.63	1513.838	28.0	13903.39	10726.2	0.6100587
0.739	17216	21846.33	1515.921	28.0	13936.67	10725.59	0.6124026
0.741	17224	21891.4	1518.075	28.1	13970.07	10724.98	0.6147902
0.742	17232	21930.91	1520.187	28.1	14003.58	10724.36	0.6170266
0.744	17240	21970.01	1522.358	28.2	14037.2	10723.74	0.6192794
0.745	17248	22009.02	1524.587	28.2	14070.93	10723.12	0.6215611
0.747	17256	22047.91	1526.896	28.3	14104.77	10722.5	0.6238754
0.748	17264	22086.71	1529.281	28.4	14138.72	10721.88	0.6262252
0.750	17272	22125.39	1531.734	28.4	14172.78	10721.25	0.6286108
0.751	17280	22151.22	1533.826	28.5	14206.96	10720.62	0.6305943
0.753	17288	22174.27	1535.822	28.5	14241.24	10719.99	0.6325206
0.754	17296	22197.58	1532.086	28.4	14275.63	10719.36	0.6309691
0.756	17304	22221.16	1529.904	28.4	14310.13	10718.73	0.6302456
0.757	17312	22245.01	1530.04	28.4	14344.74	10718.1	0.6308264
0.759	17320	22269.12	1530.167	28.4	14379.45	10717.47	0.631357
0.760	17328	22293.51	1530.281	28.3	14414.28	10716.84	0.6318337
0.761	17336	22318.16	1530.402	28.3	14449.21	10716.21	0.6322579
0.763	17344	22343.08	1530.51	28.3	14484.25	10715.57	0.6326278
0.764	17352	22368.26	1530.62	28.3	14519.39	10714.94	0.632943
0.766	17360	22393.71	1530.718	28.3	14554.64	10714.31	0.633203
0.767	17368	22419.42	1530.818	28.3	14589.99	10713.67	0.6334082
0.769	17376	22445.4	1530.91	28.2	14625.45	10713.04	0.6335574
0.770	17384	22471.63	1530.988	28.2	14661.01	10712.41	0.6336551
0.772	17392	22498.12	1529.702	28.3	14696.67	10711.77	0.6357813
0.773	17400	22524.89	1528.178	28.4	14732.44	10711.14	0.6390343
0.775	17408	22551.9	1529.091	28.4	14768.31	10710.5	0.6398418
0.776	17416	22579.19	1530.014	28.4	14804.28	10709.86	0.6406395
0.778	17424	22606.73	1530.946	28.4	14840.36	10709.22	0.6414276
0.779	17432	22634.53	1531.897	28.4	14876.53	10708.58	0.6422054
0.780	17440	22662.6	1532.854	28.4	14912.81	10707.94	0.6429729
0.782	17448	22690.92	1533.835	28.4	14949.19	10707.29	0.6437289
0.783	17456	22719.5	1534.822	28.4	14985.67	10706.65	0.6444736
0.785	17464	22748.34	1535.826	28.4	15022.25	10706	0.645207
0.786	17472	22777.44	1536.853	28.4	15058.94	10705.36	0.6459281
0.788	17480	22806.8	1537.886	28.4	15095.72	10704.71	0.6466369
0.789	17488	22836.41	1538.236	28.4	15132.6	10704.07	0.6479384

Mach Number	Altitude (ft)	Uninstalled Thrust (N)	TET (K)	Uninstalled SFC (mg/Nsec)	Drag (N)	Aircraft Weight (Kg)	Fuel Consumption (Kg)
0.791	17496	22866.29	1534.355	28.6	15169.58	10703.42	0.652892
0.792	17504	22896.42	1534.932	28.6	15206.65	10702.76	0.6544126
0.794	17512	22926.79	1536.346	28.6	15243.83	10702.11	0.6553068
0.795	17520	22957.44	1537.81	28.6	15281.1	10701.46	0.6562031
0.797	17528	22988.33	1539.321	28.6	15318.47	10700.8	0.6571005
0.798	17536	23019.49	1540.871	28.6	15355.94	10700.14	0.6579995
0.799	17544	23050.89	1542.48	28.6	15393.51	10699.48	0.6589009
0.801	17552	23078.92	1544.23	28.6	15431.17	10698.83	0.659887
0.802	17560	23105.28	1546.017	28.6	15468.92	10698.17	0.6609198
0.804	17568	23131.89	1547.771	28.6	15506.78	10697.5	0.6619598
0.805	17576	23158.73	1549.482	28.6	15544.73	10696.84	0.6630101
0.807	17584	23185.81	1551.165	28.6	15582.77	10696.18	0.6641024
0.808	17592	23213.13	1549.681	28.8	15620.91	10695.51	0.667708
0.810	17600	23240.69	1547.983	28.9	15659.15	10694.85	0.6713375
0.811	17608	23268.48	1549.208	28.9	15697.47	10694.18	0.6721226
0.813	17616	23296.51	1550.441	28.9	15735.89	10693.5	0.6729332
0.814	17624	23324.78	1551.677	28.9	15774.41	10692.83	0.6737675
0.816	17632	23353.28	1552.906	28.9	15813.01	10692.16	0.6746274
0.817	17640	23382.02	1554.134	28.9	15851.71	10691.48	0.6755124
0.819	17648	23410.99	1555.361	28.9	15890.51	10690.81	0.6764235
0.820	17656	23440.2	1556.577	28.9	15929.39	10690.13	0.6773573
0.821	17664	23469.65	1557.788	28.9	15968.37	10689.45	0.6783142
0.823	17672	23499.33	1558.974	28.9	16007.44	10688.77	0.679297
0.824	17680	23529.25	1560.152	28.9	16046.6	10688.09	0.680306
0.826	17688	23559.41	1560.081	29.0	16085.85	10687.41	0.6823204
0.827	17696	23589.79	1559.114	29.0	16125.19	10686.73	0.6850114
0.829	17704	23620.43	1559.557	29.1	16164.66	10686.05	0.6866702
0.830	17712	23651.35	1560.99	29.1	16204.24	10685.36	0.6876308
0.832	17720	23682.5	1562.394	29.1	16243.92	10684.67	0.6886122
0.833	17728	23713.88	1563.767	29.1	16283.69	10683.98	0.6896145
0.835	17736	23745.5	1565.092	29.1	16323.54	10683.29	0.6906379
0.836	17744	23777.34	1566.395	29.1	16363.49	10682.6	0.6916821
0.838	17752	23809.43	1567.65	29.1	16403.52	10681.91	0.692748
0.839	17760	23841.73	1568.859	29.1	16443.64	10681.22	0.6938332
0.841	17768	23931.94	1571.369	29.1	16541.51	10680.53	0.6968145
0.842	17776	24125.96	1576.346	29.1	16743.07	10679.83	0.7032652
0.843	17784	24321.21	1579.921	29.2	16945.7	10679.12	0.7101234
0.845	17792	24517.66	1578.867	29.3	17149.4	10678.42	0.7179592
0.846	17800	24715.34	1577.833	29.4	17354.19	10677.7	0.7256023
0.848	17808	24914.24	1578.581	29.4	17560.06	10676.97	0.7328725
0.849	17816	25114.35	1584.268	29.4	17767	10676.24	0.739549
0.851	17824	25315.71	1590.107	29.5	17975.05	10675.5	0.7462297
0.852	17832	25518.28	1596.174	29.5	18184.17	10674.75	0.7529545
0.854	17840	25722.09	1602.446	29.5	18394.38	10674	0.7598218
0.855	17848	25927.1	1609.013	29.6	18605.67	10673.24	0.7668279
0.857	17856	26133.38	1615.901	29.6	18818.08	10672.47	0.7739921
0.858	17864	26340.86	1623.098	29.7	19031.54	10671.7	0.7813352
0.860	17872	26549.58	1630.608	29.7	19246.12	10670.92	0.7889245
0.861	17880	26759.54	1638.468	29.8	19461.79	10670.13	0.7967629
0.863	17888	26970.75	1640.161	29.9	19678.57	10669.33	0.805126
0.864	17896	27183.17	1641.471	29.9	19896.43	10668.53	0.8134563
0.865	17904	27396.84	1642.782	30.0	20115.4	10667.71	0.8216323
0.867	17912	27611.76	1644.128	30.0	20335.47	10666.89	0.829677
0.868	17920	27827.92	1645.503	30.1	20556.65	10666.06	0.8375904
0.870	17928	28045.33	1646.967	30.1	20778.95	10665.23	0.8454069
0.871	17936	28264	1648.514	30.2	21002.34	10664.38	0.8531536
0.873	17944	28483.91	1651.553	30.2	21226.85	10663.53	0.8611578
0.874	17952	28705.06	1658.77	30.3	21452.46	10662.67	0.8702065
0.876	17960	28927.48	1666.206	30.4	21679.2	10661.8	0.8794782
0.877	17968	29151.12	1673.817	30.5	21907.04	10660.92	0.8888943
0.879	17976	29376.05	1681.619	30.6	22136.01	10660.03	0.8984704
0.880	17984	28165.14	1663.107	30.5	22366.09	10659.13	0.8586326
0.880	17992	28394.24	1671.117	30.6	22597.3	10658.27	0.868567
0.880	18000	28624.48	1679.231	30.7	22829.63	10657.4	0.8785626

Table C-3: Performance calculations for the third segment of the mission

Flight of 600 seconds (10 minutes) at constant altitude 18000 ft with constant Mach number 0.88.

Because of the restriction that there is for the total number of the pages, below are listed only the first and last 10 of the 600 iterations of this segment.

Mach Number	Altitude (ft)	Uninstalled Thrust (N)	TET (K)	Uninstalled SFC (mg/Nsec)	Drag (N)	Aircraft Weight (Kg)	Fuel Consumption (Kg)
0.880	18000	23773.93	1575.326	29.7	22332.72	10657.4	0.7055639
0.880	18000	23773.7	1575.326	29.7	22332.49	10656.69	0.7055563
0.880	18000	23773.46	1575.316	29.7	22332.25	10655.99	0.7055486
0.880	18000	23773.23	1575.312	29.7	22332.02	10655.28	0.7055408
0.880	18000	23772.99	1575.306	29.7	22331.78	10654.58	0.7055328
0.880	18000	23772.75	1575.302	29.7	22331.54	10653.87	0.705525
0.880	18000	23772.52	1575.296	29.7	22331.31	10653.17	0.7055175
0.880	18000	23772.28	1575.292	29.7	22331.07	10652.46	0.7055097
0.880	18000	23772.04	1575.286	29.7	22330.83	10651.75	0.7055016
0.880	18000	23771.81	1575.282	29.7	22330.6	10651.05	0.705494
0.880	18000	23637.51	1572.28	29.7	22196.3	10241.75	0.7010793
0.880	18000	23637.29	1572.28	29.7	22196.08	10241.05	0.701072
0.880	18000	23637.06	1572.27	29.7	22195.85	10240.35	0.7010646
0.880	18000	23636.83	1572.27	29.7	22195.62	10239.65	0.701057
0.880	18000	23636.61	1572.26	29.7	22195.4	10238.95	0.7010498
0.880	18000	23636.39	1572.26	29.7	22195.18	10238.24	0.7010425
0.880	18000	23636.16	1572.25	29.7	22194.95	10237.54	0.701035
0.880	18000	23635.93	1572.246	29.7	22194.72	10236.84	0.7010275
0.880	18000	23635.71	1572.24	29.7	22194.5	10236.14	0.7010203
0.880	18000	23635.48	1572.236	29.7	22194.27	10235.44	0.7010127

Table C-4: Performance calculations for the fourth segment of the mission

One External Tank

Climb in 15 sec. from 16000 ft to 17000 ft with constant Mach number 0.6.

Mach Number	Altitude (ft)	Uninstalled Thrust (N)	TET (K)	Uninstalled SFC (mg/Nsec)	Drag (N)	Aircraft Weight (Kg)	Fuel Consumption (Kg)
0.600	16000	25224.25	1566.05	27.35	12207.94	10953	0.689774
0.600	16067	25231.38	1568.66	27.28	12195.22	10952.31	0.6882447
0.600	16133	25238.64	1578.09	26.95	12182.63	10951.62	0.680274
0.600	16200	25245.98	1570.09	27.32	12170.11	10950.94	0.6896255
0.600	16267	25253.35	1571.34	27.32	12157.64	10950.25	0.6898255
0.600	16333	25260.8	1580.27	26.85	12145.23	10949.56	0.6782503
0.600	16400	25268.33	1579.69	26.88	12132.89	10948.88	0.6790934
0.600	16467	25254.96	1575.12	27.19	12120.69	10948.21	0.6866424
0.600	16533	25240.21	1572.97	27.37	12108.55	10947.52	0.6909248
0.600	16600	25225.53	1583.56	26.80	12096.46	10946.83	0.6759216
0.600	16667	25210.93	1576.24	27.14	12084.44	10946.15	0.6842286
0.600	16733	25196.39	1573.44	27.42	12072.49	10945.47	0.6908535
0.600	16800	25181.95	1584.12	26.81	12060.65	10944.78	0.6751668
0.600	16867	25167.61	1578.66	27.08	12048.88	10944.1	0.6816504
0.600	16933	25153.32	1573.91	27.33	12037.17	10943.42	0.6873322
0.600	17000	25139.07	1584.71	26.85	12025.52	10942.73	0.6749305
0.600	17000	25480.92	1592.53	26.89	12066.63	10942.73	0.6852565

Table C-5: Performance calculations for the first segment of the mission

Aircraft acceleration in 30sec. from Mach number 0.6 to 0.7 at constant altitude 17000ft.

Mach Number	Altitude (ft)	Uninstalled Thrust (N)	TET (K)	Uninstalled SFC (mg/Nsec)	Drag (N)	Aircraft Weight (Kg)	Fuel Consumption (Kg)
0.603	17000	25517.42	1593.422	26.93	12111.6	10942.05	0.6872898
0.607	17000	25555.07	1594.339	26.98	12157.73	10941.36	0.6893754
0.610	17000	25593.85	1595.288	27.02	12204.98	10940.67	0.6915123
0.613	17000	25633.74	1596.262	27.06	12253.36	10939.98	0.6937021
0.617	17000	25674.73	1597.277	27.11	12302.84	10939.28	0.6959459
0.620	17000	25716.8	1598.304	27.15	12353.41	10938.59	0.6982446
0.623	17000	25759.94	1599.359	27.20	12405.06	10937.89	0.7005933
0.627	17000	25804.15	1600.427	27.24	12457.77	10937.19	0.7029961
0.630	17000	25849.4	1601.532	27.29	12511.54	10936.49	0.7054568
0.633	17000	25895.68	1602.667	27.34	12566.35	10935.78	0.7079757
0.637	17000	25942.98	1603.819	27.39	12622.19	10935.07	0.7105546
0.640	17000	25991.29	1605.014	27.44	12679.05	10934.36	0.7131929
0.643	17000	26040.6	1606.233	27.49	12736.91	10933.65	0.7158926
0.647	17000	26090.9	1607.479	27.54	12795.77	10932.93	0.7186533
0.650	17000	26142.18	1608.72	27.60	12855.61	10932.21	0.721467
0.653	17000	26195.19	1609.987	27.63	12916.43	10931.49	0.7238504
0.657	17000	26248.96	1611.265	27.67	12978.21	10930.77	0.7262597
0.660	17000	26303.47	1612.576	27.70	13040.95	10930.04	0.7286927
0.663	17000	26358.68	1613.923	27.74	13104.63	10929.31	0.7311486
0.667	17000	26414.59	1615.287	27.77	13169.25	10928.58	0.733628
0.670	17000	26471.16	1616.688	27.81	13234.79	10927.85	0.7361296
0.673	17000	26528.37	1618.1	27.84	13301.25	10927.11	0.7386488
0.677	17000	26586.26	1619.532	27.88	13368.62	10926.37	0.7411728
0.680	17000	26647.45	1621.028	27.91	13436.89	10925.63	0.7438009
0.683	17000	26709.77	1622.567	27.95	13506.05	10924.89	0.7464659
0.687	17000	26773.2	1624.15	27.98	13576.09	10924.14	0.7491666
0.690	17000	26837.7	1625.756	28.02	13647.02	10923.39	0.7519027
0.693	17000	26903.24	1627.4	28.05	13718.81	10922.64	0.7546728
0.697	17000	26969.81	1629.065	28.09	13791.46	10921.89	0.7574681
0.700	17000	27037.37	1630.75	28.12	13864.96	10921.13	0.7602846

Table C-6: Performance calculations for the second segment of the mission

Climb from 17000 ft to 18000 ft with aircraft acceleration from Mach number 0.7 to 0.88 in 125 sec

Mach Number	Altitude (ft)	Uninstalled Thrust (N)	TET (K)	Uninstalled SFC (mg/Nsec)	Drag (N)	Aircraft Weight (Kg)	Fuel Consumption (Kg)
0.700	17000	21655.61	1509.46	27.62	13864.66	10921.13	0.5981468
0.701	17008	21690.27	1510.23	27.62	13894.46	10920.53	0.5991933
0.703	17016	21725.31	1510.984	27.63	13924.38	10919.93	0.6002482
0.704	17024	21760.73	1511.734	27.63	13954.44	10919.33	0.6013095
0.706	17032	21796.52	1512.442	27.64	13984.62	10918.73	0.6023771
0.707	17040	21832.71	1513.149	27.64	14014.94	10918.13	0.6034513
0.709	17048	21869.26	1513.846	27.64	14045.38	10917.53	0.6045287
0.710	17056	21906.2	1514.542	27.65	14075.96	10916.92	0.6056095
0.712	17064	21943.54	1515.223	27.65	14106.67	10916.32	0.6066926
0.713	17072	21981.23	1515.892	27.65	14137.5	10915.71	0.6077755
0.715	17080	22019.31	1516.566	27.65	14168.46	10915.1	0.6088579
0.716	17088	22057.76	1517.233	27.65	14199.54	10914.49	0.6099386
0.718	17096	22096.58	1516.345	27.71	14230.74	10913.88	0.6122788
0.719	17104	22135.77	1516.318	27.75	14262.07	10913.27	0.6143643
0.720	17112	22175.34	1517.501	27.76	14293.51	10912.66	0.6156577
0.722	17120	22215.28	1518.758	27.77	14325.08	10912.04	0.6169657
0.723	17128	22255.58	1520.084	27.78	14356.77	10911.42	0.6182871
0.725	17136	22296.26	1521.48	27.79	14388.58	10910.8	0.6196222
0.726	17144	22337.31	1522.94	27.80	14420.51	10910.18	0.6209707
0.728	17152	22378.73	1524.476	27.81	14452.55	10909.56	0.622333
0.729	17160	22420.51	1526.075	27.82	14484.72	10908.94	0.623696
0.731	17168	22462.67	1527.731	27.83	14517.01	10908.32	0.6250682
0.732	17176	22505.19	1529.459	27.84	14549.41	10907.69	0.6264477
0.734	17184	22548.08	1531.258	27.84	14581.93	10907.07	0.6278342
0.735	17192	22591.33	1532.873	27.86	14614.57	10906.44	0.6294758
0.737	17200	22634.95	1529.858	28.09	14647.32	10905.81	0.6358368
0.738	17208	22678.93	1531.563	28.16	14680.19	10905.17	0.6386888
0.739	17216	22723.27	1533.889	28.21	14713.17	10904.54	0.6411257
0.741	17224	22767.99	1536.293	28.27	14746.26	10903.89	0.6436155
0.742	17232	22807.15	1538.661	28.32	14779.47	10903.25	0.6459701
0.744	17240	22845.89	1541.092	28.38	14812.79	10902.6	0.6483579
0.745	17248	22884.55	1543.603	28.44	14846.23	10901.96	0.6507952
0.747	17256	22923.1	1546.181	28.50	14879.77	10901.3	0.653282
0.748	17264	22961.54	1548.846	28.56	14913.43	10900.65	0.6558201
0.750	17272	22999.88	1551.577	28.63	14947.2	10900	0.6584145
0.751	17280	23025.37	1553.986	28.69	14981.08	10899.34	0.6605778
0.753	17288	23048.07	1556.313	28.75	15015.08	10898.68	0.662688
0.754	17296	23071.04	1553.157	28.66	15049.18	10898.01	0.6612822
0.756	17304	23094.28	1548.108	28.52	15083.39	10897.35	0.6585684
0.757	17312	23117.8	1548.026	28.49	15117.72	10896.69	0.6586277
0.759	17320	23141.58	1548.421	28.47	15152.15	10896.04	0.6589234
0.760	17328	23165.63	1548.798	28.45	15186.7	10895.38	0.6591595
0.761	17336	23189.96	1549.172	28.43	15221.35	10894.72	0.6593414
0.763	17344	23214.55	1549.542	28.41	15256.11	10894.06	0.6594629
0.764	17352	23239.4	1549.902	28.38	15290.98	10893.4	0.6595246
0.766	17360	23264.53	1550.255	28.35	15325.96	10892.74	0.6595266
0.767	17368	23289.92	1550.586	28.32	15361.04	10892.08	0.6594662
0.769	17376	23315.58	1550.896	28.28	15396.23	10891.42	0.659341
0.770	17384	23341.49	1551.217	28.24	15431.52	10890.76	0.6591707
0.772	17392	23367.67	1550.15	28.29	15466.92	10890.1	0.6611018
0.773	17400	23394.11	1547.357	28.46	15502.42	10889.44	0.6656995
0.775	17408	23420.82	1547.189	28.51	15538.03	10888.77	0.667644
0.776	17416	23447.79	1548.361	28.50	15573.73	10888.11	0.6682289
0.778	17424	23475.02	1549.544	28.49	15609.55	10887.44	0.6688066
0.779	17432	23502.51	1550.747	28.48	15645.46	10886.77	0.6693782
0.780	17440	23530.27	1551.969	28.47	15681.48	10886.1	0.6699454
0.782	17448	23558.29	1553.205	28.46	15717.61	10885.43	0.6705065
0.783	17456	23586.57	1554.459	28.45	15753.83	10884.76	0.6710639
0.785	17464	23615.11	1555.741	28.44	15790.16	10884.09	0.6716173
0.786	17472	23643.91	1557.04	28.43	15826.59	10883.42	0.6721675
0.788	17480	23672.97	1558.365	28.42	15863.12	10882.74	0.6727163
0.789	17488	23702.28	1558.961	28.43	15899.75	10882.07	0.6738392

Mach Number	Altitude (ft)	Uninstalled Thrust (N)	TET (K)	Uninstalled SFC (mg/Nsec)	Drag (N)	Aircraft Weight (Kg)	Fuel Consumption (Kg)
0.791	17496	23731.86	1554.999	28.59	15936.48	10881.4	0.6783909
0.792	17504	23761.7	1551.903	28.72	15973.31	10880.72	0.6823384
0.794	17512	23791.78	1553.65	28.72	16010.24	10880.04	0.6831824
0.795	17520	23822.13	1555.465	28.72	16047.27	10879.35	0.6840544
0.797	17528	23852.73	1557.351	28.72	16084.39	10878.67	0.6849558
0.798	17536	23883.6	1559.318	28.72	16121.62	10877.98	0.6858881
0.799	17544	23914.71	1561.371	28.72	16158.95	10877.3	0.6868547
0.801	17552	23942.45	1563.586	28.73	16196.37	10876.61	0.6879051
0.802	17560	23968.53	1565.811	28.75	16233.89	10875.92	0.6890007
0.804	17568	23994.85	1567.987	28.76	16271.5	10875.23	0.6901123
0.805	17576	24021.4	1570.113	28.78	16309.21	10874.54	0.6912389
0.807	17584	24048.2	1572.176	28.79	16347.03	10873.85	0.6923804
0.808	17592	24075.24	1570.328	28.88	16384.93	10873.16	0.6951944
0.810	17600	24102.52	1567.951	28.97	16422.93	10872.46	0.6981577
0.811	17608	24130.03	1567.163	29.02	16461.03	10871.77	0.7002201
0.813	17616	24157.79	1568.762	29.02	16499.22	10871.07	0.7010346
0.814	17624	24185.78	1570.349	29.02	16537.51	10870.37	0.7018846
0.816	17632	24214.01	1571.916	29.02	16575.89	10869.66	0.7027661
0.817	17640	24242.48	1573.456	29.03	16614.36	10868.96	0.7036813
0.819	17648	24271.18	1574.974	29.03	16652.93	10868.26	0.7046276
0.820	17656	24300.12	1576.469	29.04	16691.59	10867.55	0.7056074
0.821	17664	24329.3	1577.928	29.04	16730.35	10866.85	0.7066175
0.823	17672	24358.71	1579.364	29.05	16769.19	10866.14	0.7076566
0.824	17680	24388.37	1580.759	29.06	16808.13	10865.43	0.7087243
0.826	17688	24418.25	1580.619	29.09	16847.17	10864.72	0.7104348
0.827	17696	24448.37	1579.387	29.15	16886.29	10864.01	0.7125866
0.829	17704	24478.76	1578.439	29.19	16925.54	10863.3	0.7145959
0.830	17712	24509.41	1579.798	29.20	16964.91	10862.59	0.7157424
0.832	17720	24540.3	1581.481	29.21	17004.37	10861.87	0.7167687
0.833	17728	24571.42	1583.104	29.21	17043.92	10861.16	0.717812
0.835	17736	24602.78	1584.668	29.22	17083.56	10860.44	0.7188723
0.836	17744	24634.37	1586.171	29.23	17123.3	10859.72	0.7199491
0.838	17752	24666.2	1587.602	29.23	17163.12	10859	0.7210418
0.839	17760	24698.25	1588.97	29.24	17203.04	10858.28	0.7221519
0.841	17768	24788.24	1591.64	29.26	17300.74	10857.56	0.725205
0.842	17776	24982.14	1596.723	29.29	17502.21	10856.83	0.7317484
0.843	17784	25177.26	1600.343	29.33	17704.77	10856.1	0.7385454
0.845	17792	25373.58	1599.272	29.40	17908.38	10855.36	0.7459822
0.846	17800	25571.14	1598.273	29.46	18113.09	10854.61	0.7533493
0.848	17808	25769.92	1597.304	29.52	18318.88	10853.86	0.7606634
0.849	17816	25969.91	1599.95	29.56	18525.75	10853.1	0.7676721
0.851	17824	26171.14	1606.108	29.59	18733.71	10852.33	0.774431
0.852	17832	26373.59	1612.486	29.62	18942.76	10851.56	0.7812601
0.854	17840	26577.28	1619.173	29.66	19152.9	10850.78	0.7882728
0.855	17848	26782.17	1626.166	29.70	19364.11	10849.99	0.7954733
0.857	17856	26988.34	1633.555	29.75	19576.44	10849.19	0.8030319
0.858	17864	27195.69	1641.347	29.82	19789.84	10848.39	0.8109257
0.860	17872	27404.3	1649.468	29.89	20004.34	10847.58	0.8191181
0.861	17880	27614.14	1657.96	29.97	20219.94	10846.76	0.8276336
0.863	17888	27825.22	1659.66	30.04	20436.64	10845.93	0.8358373
0.864	17896	28037.53	1660.888	30.10	20654.43	10845.1	0.8438864
0.865	17904	28251.09	1662.196	30.15	20873.32	10844.25	0.8518947
0.867	17912	28465.89	1663.576	30.21	21093.32	10843.4	0.8598402
0.868	17920	28681.94	1665.032	30.25	21314.43	10842.54	0.8676513
0.870	17928	28899.24	1666.536	30.29	21536.66	10841.67	0.8753358
0.871	17936	29117.79	1668.165	30.32	21759.99	10840.8	0.8829562
0.873	17944	29337.58	1669.942	30.36	21984.43	10839.92	0.8905495
0.874	17952	29558.63	1672.621	30.39	22209.97	10839.02	0.8983698
0.876	17960	29780.93	1680.234	30.48	22436.64	10838.13	0.9077746
0.877	17968	30004.47	1687.994	30.57	22664.42	10837.22	0.9172795
0.879	17976	30229.28	1695.819	30.66	22893.32	10836.3	0.9268124
0.880	17984	29018.27	1679.176	30.61	23123.33	10835.38	0.8883653
0.880	17992	29247.27	1687.216	30.71	23354.48	10834.49	0.8981649
0.880	18000	29477.4	1695.411	30.80	23586.75	10833.59	0.9080333

Table C-7: Performance calculations for the third segment of the mission

Flight of 600 seconds (10 minutes) at constant altitude 18000 ft with constant Mach number 0.88.

Because of the restriction that there is for the total number of the pages, below are listed only the first and last 10 of the 600 iterations of this segment.

Mach Number	Altitude (ft)	Uninstalled Thrust (N)	TET (K)	Uninstalled SFC (mg/Nsec)	Drag (N)	Aircraft Weight (Kg)	Fuel Consumption (Kg)
0.880	18000	24531.2	1592.252	29.79	23089.99	10833.59	0.730697
0.880	18000	24530.95	1592.248	29.79	23089.74	10832.86	0.7306889
0.880	18000	24530.7	1592.242	29.79	23089.49	10832.13	0.7306805
0.880	18000	24530.45	1592.238	29.79	23089.24	10831.4	0.7306721
0.880	18000	24530.21	1592.234	29.79	23089	10830.67	0.7306643
0.880	18000	24529.96	1592.228	29.79	23088.75	10829.94	0.7306558
0.880	18000	24529.71	1592.224	29.79	23088.5	10829.21	0.7306476
0.880	18000	24529.46	1592.218	29.79	23088.25	10828.48	0.7306392
0.880	18000	24529.21	1592.208	29.79	23088	10827.75	0.7306308
0.880	18000	24528.96	1592.208	29.79	23087.75	10827.02	0.7306226
0.880	18000	24387.65	1589.08	29.77	22946.44	10403.17	0.7259084
0.880	18000	24387.41	1589.08	29.77	22946.2	10402.45	0.7259006
0.880	18000	24387.17	1589.07	29.77	22945.96	10401.72	0.7258924
0.880	18000	24386.94	1589.07	29.77	22945.73	10400.99	0.7258848
0.880	18000	24386.7	1589.06	29.77	22945.49	10400.27	0.7258767
0.880	18000	24386.46	1589.06	29.77	22945.25	10399.54	0.7258689
0.880	18000	24386.23	1589.05	29.77	22945.02	10398.82	0.725861
0.880	18000	24385.99	1589.05	29.77	22944.78	10398.09	0.7258531
0.880	18000	24385.75	1589.04	29.77	22944.54	10397.37	0.725845
0.880	18000	24385.51	1589.034	29.77	22944.3	10396.64	0.7258371

Table C-8: Performance calculations for the fourth segment of the mission

Two External Tanks

Climb in 15 sec. from 16000 ft to 17000 ft with constant Mach number 0.6.

Mach Number	Altitude (ft)	Uninstalled Thrust (N)	TET (K)	Uninstalled SFC (mg/Nsec)	Drag (N)	Aircraft Weight (Kg)	Fuel Consumption (Kg)
0.600	16000	26225.49	1587.66	27.54	13021.93	11134	0.7223334
0.600	16067	26232.92	1592.69	27.36	13009.5	11133.28	0.7178279
0.600	16133	26240.49	1600	27.09	12997.2	11132.56	0.7108302
0.600	16200	26248.13	1591.79	27.51	12984.97	11131.85	0.7221884
0.600	16267	26255.81	1595.46	27.41	12972.79	11131.13	0.7196143
0.600	16333	26263.56	1602.87	26.98	12960.67	11130.41	0.7087182
0.600	16400	26271.41	1601.73	27.07	12948.63	11129.7	0.711068
0.600	16467	26258.33	1597.02	27.38	12936.72	11128.99	0.7190536
0.600	16533	26243.89	1597.54	27.46	12924.86	11128.27	0.7207746
0.600	16600	26229.52	1605.81	26.93	12913.07	11127.55	0.7063612
0.600	16667	26215.23	1598.32	27.33	12901.35	11126.84	0.7165112
0.600	16733	26201.01	1598.49	27.50	12889.69	11126.12	0.7206582
0.600	16800	26186.89	1606.76	26.96	12878.15	11125.4	0.7059585
0.600	16867	26172.86	1601.28	27.29	12866.68	11124.7	0.7141877
0.600	16933	26158.88	1599.09	27.44	12855.27	11123.98	0.7177429
0.600	17000	26144.95	1607.7	26.98	12843.91	11123.26	0.7054006
0.600	17000	26493.12	1615.86	27.04	12886.39	11123.26	0.716503

Table C-9: Performance calculations for the first segment of the mission

Aircraft acceleration in 30sec. from Mach number 0.6 to 0.7 at constant altitude 17000ft.

Mach Number	Altitude (ft)	Uninstalled Thrust (N)	TET (K)	Uninstalled SFC (mg/Nsec)	Drag (N)	Aircraft Weight (Kg)	Fuel Consumption (Kg)
0.603	17000	26528.21	1616.737	27.09	12929.99	11122.54	0.718766
0.607	17000	26564.48	1617.629	27.14	12974.76	11121.82	0.7210764
0.610	17000	26601.9	1618.536	27.19	13020.69	11121.1	0.7234342
0.613	17000	26640.45	1619.479	27.25	13067.76	11120.38	0.7258747
0.617	17000	26680.12	1620.437	27.30	13115.95	11119.65	0.7283665
0.620	17000	26720.89	1621.416	27.35	13165.26	11118.93	0.7308962
0.623	17000	26762.76	1622.403	27.41	13215.67	11118.2	0.7334645
0.627	17000	26805.71	1623.41	27.46	13267.16	11117.46	0.7360717
0.630	17000	26849.72	1624.432	27.51	13319.72	11116.73	0.7387161
0.633	17000	26894.77	1625.463	27.57	13373.35	11115.99	0.7413981
0.637	17000	26940.87	1626.519	27.62	13428.02	11115.25	0.7441173
0.640	17000	26988	1627.578	27.67	13483.72	11114.5	0.7468737
0.643	17000	27036.14	1628.642	27.73	13540.46	11113.75	0.7496603
0.647	17000	27085.29	1629.702	27.78	13598.2	11113	0.7524743
0.650	17000	27135.43	1630.76	27.84	13656.95	11112.25	0.7553217
0.653	17000	27187.33	1632.034	27.87	13716.68	11111.5	0.7576312
0.657	17000	27240	1633.337	27.90	13777.4	11110.74	0.7599663
0.660	17000	27293.42	1634.66	27.93	13839.09	11109.98	0.7623249
0.663	17000	27347.57	1635.997	27.96	13901.74	11109.22	0.7647073
0.667	17000	27402.43	1637.377	27.99	13965.34	11108.45	0.7671105
0.670	17000	27457.96	1638.76	28.03	14029.88	11107.68	0.7695324
0.673	17000	27514.16	1640.164	28.06	14095.36	11106.92	0.7719483
0.677	17000	27571.04	1641.57	28.09	14161.76	11106.14	0.7743641
0.680	17000	27631.23	1643.066	28.12	14229.07	11105.37	0.7769001
0.683	17000	27692.58	1644.603	28.15	14297.29	11104.59	0.7794863
0.687	17000	27755.05	1646.184	28.18	14366.41	11103.81	0.7821212
0.690	17000	27818.59	1647.804	28.21	14436.41	11103.03	0.7848045
0.693	17000	27883.2	1649.425	28.24	14507.3	11102.25	0.7875426
0.697	17000	27948.84	1651.067	28.28	14579.06	11101.46	0.7903314
0.700	17000	28015.49	1652.74	28.31	14651.69	11100.67	0.7931684

Table C-10: Performance calculations for the second segment of the mission

Climb from 17000 ft to 18000 ft with aircraft acceleration from Mach number 0.7 to 0.88 in 125 sec

Mach Number	Altitude (ft)	Uninstalled Thrust (N)	TET (K)	Uninstalled SFC (mg/Nsec)	Drag (N)	Aircraft Weight (Kg)	Fuel Consumption (Kg)
0.700	17000	22544.18	1530.13	27.71	14651.38	11100.67	0.6246111
0.701	17008	22578.44	1530.93	27.71	14680.82	11100.04	0.625633
0.703	17016	22613.06	1531.717	27.71	14710.39	11099.42	0.6266595
0.704	17024	22648.07	1532.492	27.71	14740.09	11098.79	0.627684
0.706	17032	22683.46	1533.265	27.72	14769.92	11098.17	0.6287059
0.707	17040	22719.23	1534.037	27.72	14799.88	11097.54	0.6297228
0.709	17048	22755.38	1534.809	27.72	14829.97	11096.91	0.6307341
0.710	17056	22791.92	1535.58	27.72	14860.21	11096.28	0.6317382
0.712	17064	22828.86	1536.347	27.72	14890.57	11095.64	0.632734
0.713	17072	22866.16	1537.115	27.71	14921.07	11095.01	0.6337191
0.715	17080	22903.83	1537.889	27.71	14951.68	11094.38	0.6346914
0.716	17088	22941.89	1538.665	27.71	14982.42	11093.74	0.6356503
0.718	17096	22980.32	1537.989	27.76	15013.29	11093.11	0.6379259
0.719	17104	23019.13	1534.793	27.91	15044.29	11092.47	0.6425579
0.720	17112	23058.31	1536.118	27.92	15075.4	11091.83	0.6436787
0.722	17120	23097.86	1537.566	27.92	15106.64	11091.18	0.6447805
0.723	17128	23137.78	1539.084	27.92	15138	11090.54	0.6458997
0.725	17136	23178.07	1540.674	27.92	15169.48	11089.89	0.6470355
0.726	17144	23218.74	1542.348	27.92	15201.08	11089.25	0.6481857
0.728	17152	23259.79	1544.084	27.92	15232.81	11088.6	0.6493492
0.729	17160	23301.2	1545.897	27.92	15264.65	11087.95	0.6505234
0.731	17168	23342.98	1547.775	27.92	15296.62	11087.3	0.6517075
0.732	17176	23385.13	1549.718	27.92	15328.71	11086.65	0.6529
0.734	17184	23427.65	1551.744	27.92	15360.91	11085.99	0.6540995
0.735	17192	23470.54	1553.57	27.93	15393.24	11085.34	0.6555481
0.737	17200	23513.79	1550.692	28.15	15425.68	11084.68	0.6618711
0.738	17208	23557.41	1548.842	28.34	15458.23	11084.02	0.6676455
0.739	17216	23601.39	1551.443	28.40	15490.91	11083.35	0.6701747
0.741	17224	23645.74	1554.13	28.45	15523.69	11082.68	0.6727805
0.742	17232	23684.54	1556.813	28.51	15556.6	11082.01	0.6752706
0.744	17240	23722.93	1559.556	28.57	15589.62	11081.33	0.6778166
0.745	17248	23761.23	1562.392	28.64	15622.75	11080.66	0.680433
0.747	17256	23799.42	1565.314	28.70	15655.99	11079.98	0.6831236
0.748	17264	23837.53	1568.32	28.77	15689.36	11079.29	0.6858887
0.750	17272	23875.52	1571.422	28.85	15722.83	11078.61	0.6887283
0.751	17280	23900.64	1574.209	28.92	15756.41	11077.92	0.6910935
0.753	17288	23923	1576.92	28.99	15790.11	11077.23	0.6934111
0.754	17296	23945.62	1574.039	28.90	15823.92	11076.53	0.6920274
0.756	17304	23968.52	1569.217	28.76	15857.85	11075.84	0.6892452
0.757	17312	23991.7	1565.637	28.64	15891.88	11075.15	0.6870098
0.759	17320	24015.14	1566.321	28.61	15926.03	11074.47	0.6871221
0.760	17328	24038.85	1567.01	28.59	15960.29	11073.78	0.687201
0.761	17336	24062.85	1567.713	28.56	15994.66	11073.09	0.6872403
0.763	17344	24087.1	1568.432	28.53	16029.14	11072.4	0.6872458
0.764	17352	24111.63	1569.165	28.50	16063.73	11071.72	0.6872167
0.766	17360	24136.42	1569.904	28.47	16098.43	11071.03	0.6871526
0.767	17368	24161.49	1570.666	28.44	16133.24	11070.34	0.6870571
0.769	17376	24186.82	1571.443	28.40	16168.15	11069.65	0.6869287
0.770	17384	24212.41	1572.236	28.36	16203.17	11068.97	0.6867658
0.772	17392	24238.27	1571.333	28.40	16238.3	11068.28	0.6883656
0.773	17400	24264.39	1568.264	28.52	16273.53	11067.59	0.6921405
0.775	17408	24290.78	1565.154	28.65	16308.87	11066.9	0.6958339
0.776	17416	24317.43	1566.41	28.64	16344.31	11066.21	0.6965001
0.778	17424	24344.35	1567.943	28.63	16379.86	11065.51	0.6970067
0.779	17432	24371.53	1569.501	28.62	16415.51	11064.81	0.697528
0.780	17440	24398.97	1571.1	28.61	16451.26	11064.11	0.6980636
0.782	17448	24426.68	1572.729	28.60	16487.13	11063.42	0.6986145
0.783	17456	24454.65	1574.396	28.59	16523.09	11062.72	0.6991799
0.785	17464	24482.88	1576.095	28.58	16559.16	11062.02	0.6997582
0.786	17472	24511.37	1577.827	28.57	16595.33	11061.32	0.700345
0.788	17480	24540.13	1579.602	28.56	16631.61	11060.62	0.7009591
0.789	17488	24569.14	1580.569	28.57	16667.98	11059.92	0.702042

Mach Number	Altitude (ft)	Uninstalled Thrust (N)	TET (K)	Uninstalled SFC (mg/Nsec)	Drag (N)	Aircraft Weight (Kg)	Fuel Consumption (Kg)
0.791	17496	24598.42	1576.259	28.69	16704.46	11059.21	0.7056515
0.792	17504	24627.96	1571.804	28.80	16741.04	11058.51	0.7091646
0.794	17512	24657.74	1570.506	28.85	16777.72	11057.8	0.7114291
0.795	17520	24687.79	1572.783	28.86	16814.5	11057.09	0.7123679
0.797	17528	24718.1	1575.142	28.86	16851.38	11056.38	0.7133439
0.798	17536	24748.67	1577.59	28.86	16888.36	11055.66	0.7143567
0.799	17544	24779.49	1580.121	28.87	16925.44	11054.95	0.7154074
0.801	17552	24806.94	1582.806	28.88	16962.62	11054.23	0.7165321
0.802	17560	24832.73	1585.489	28.90	16999.89	11053.52	0.7176934
0.804	17568	24858.76	1588.1	28.92	17037.26	11052.8	0.7188656
0.805	17576	24885.02	1590.642	28.94	17074.74	11052.08	0.7200483
0.807	17584	24911.54	1593.085	28.95	17112.31	11051.36	0.7212426
0.808	17592	24938.29	1591.036	29.01	17149.98	11050.64	0.7234942
0.810	17600	24965.29	1588.382	29.07	17187.75	11049.92	0.7258473
0.811	17608	24992.52	1585.973	29.13	17225.61	11049.19	0.7280936
0.813	17616	25020	1586.609	29.15	17263.56	11048.46	0.7294021
0.814	17624	25047.71	1588.579	29.16	17301.62	11047.73	0.7303136
0.816	17632	25075.65	1590.514	29.16	17339.77	11047	0.7312479
0.817	17640	25103.85	1592.391	29.17	17378.01	11046.27	0.7322083
0.819	17648	25132.28	1594.223	29.17	17416.35	11045.54	0.733187
0.820	17656	25160.94	1595.999	29.18	17454.78	11044.81	0.7341892
0.821	17664	25189.85	1597.717	29.19	17493.31	11044.07	0.7352139
0.823	17672	25218.98	1599.374	29.19	17531.93	11043.34	0.7362593
0.824	17680	25248.37	1600.969	29.20	17570.65	11042.6	0.7373264
0.826	17688	25277.99	1600.869	29.23	17609.46	11041.86	0.7388668
0.827	17696	25307.84	1599.572	29.27	17648.37	11041.12	0.7407266
0.829	17704	25337.96	1598.573	29.30	17687.39	11040.38	0.7424929
0.830	17712	25368.35	1598.266	29.33	17726.54	11039.64	0.7440791
0.832	17720	25398.97	1600.234	29.34	17765.79	11038.9	0.7451357
0.833	17728	25429.83	1602.118	29.34	17805.12	11038.15	0.7462056
0.835	17736	25460.93	1603.918	29.35	17844.55	11037.41	0.7472885
0.836	17744	25492.25	1605.627	29.36	17884.07	11036.66	0.7483831
0.838	17752	25523.82	1607.249	29.36	17923.68	11035.91	0.7494907
0.839	17760	25555.62	1608.752	29.37	17963.38	11035.16	0.750613
0.841	17768	25645.4	1611.448	29.39	18060.92	11034.41	0.7536732
0.842	17776	25839.17	1616.377	29.42	18262.31	11033.66	0.7602137
0.843	17784	26034.16	1619.88	29.46	18464.77	11032.9	0.7669794
0.845	17792	26230.36	1618.961	29.52	18668.31	11032.13	0.7742596
0.846	17800	26427.78	1618.154	29.57	18872.93	11031.35	0.781494
0.848	17808	26626.44	1617.429	29.62	19078.65	11030.57	0.7887226
0.849	17816	26826.31	1616.804	29.67	19285.43	11029.78	0.7958827
0.851	17824	27027.42	1621.559	29.70	19493.32	11028.99	0.8028393
0.852	17832	27229.75	1628.405	29.74	19702.29	11028.19	0.8099347
0.854	17840	27433.3	1635.583	29.79	19912.34	11027.38	0.8172995
0.855	17848	27638.08	1643.123	29.85	20123.48	11026.56	0.8249525
0.857	17856	27844.12	1650.997	29.91	20335.74	11025.73	0.8328917
0.858	17864	28051.36	1659.235	29.99	20549.05	11024.9	0.8411357
0.860	17872	28259.84	1667.835	30.07	20763.48	11024.06	0.8497965
0.861	17880	28469.57	1676.828	30.17	20979	11023.21	0.8589204
0.863	17888	28680.52	1678.555	30.23	21195.63	11022.35	0.8670689
0.864	17896	28892.72	1679.73	30.28	21413.34	11021.48	0.8749415
0.865	17904	29106.16	1680.989	30.33	21632.17	11020.61	0.8826871
0.867	17912	29320.84	1682.349	30.37	21852.1	11019.73	0.8903349
0.868	17920	29536.77	1683.864	30.40	22073.13	11018.83	0.8979769
0.870	17928	29753.95	1685.507	30.44	22295.29	11017.94	0.9055695
0.871	17936	29972.39	1687.286	30.46	22518.55	11017.03	0.9131035
0.873	17944	30192.07	1689.207	30.49	22742.92	11016.12	0.9206535
0.874	17952	30413	1691.281	30.52	22968.39	11015.2	0.9282382
0.876	17960	30635.19	1693.695	30.55	23195	11014.27	0.9359394
0.877	17968	30858.62	1701.406	30.64	23422.7	11013.33	0.9454328
0.879	17976	31083.33	1709.328	30.72	23651.54	11012.39	0.9550151
0.880	17984	29872.21	1694.213	30.70	23881.48	11011.43	0.9171826
0.880	17992	30101.1	1702.216	30.79	24112.57	11010.52	0.9268641
0.880	18000	30331.12	1710.288	30.88	24344.78	11009.59	0.9365609

Table C-11: Performance calculations for the third segment of the mission

Flight of 600 seconds (10 minutes) at constant altitude 18000 ft with constant Mach number 0.88.

Because of the restriction that there is for the total number of the pages, below are listed only the first and last 10 of the 600 iterations of this segment.

Mach Number	Altitude (ft)	Uninstalled Thrust (N)	TET (K)	Uninstalled SFC (mg/Nsec)	Drag (N)	Aircraft Weight (Kg)	Fuel Consumption (Kg)
0.880	18000	25289.37	1609.214	29.93	23848.16	11009.59	0.7570102
0.880	18000	25289.11	1609.214	29.93	23847.9	11008.83	0.7570009
0.880	18000	25288.85	1609.204	29.93	23847.64	11008.08	0.7569919
0.880	18000	25288.59	1609.204	29.93	23847.38	11007.32	0.7569826
0.880	18000	25288.33	1609.194	29.93	23847.12	11006.56	0.7569736
0.880	18000	25288.07	1609.194	29.93	23846.86	11005.81	0.7569643
0.880	18000	25287.8	1609.184	29.93	23846.59	11005.05	0.7569548
0.880	18000	25287.54	1609.178	29.93	23846.33	11004.29	0.7569456
0.880	18000	25287.28	1609.174	29.93	23846.07	11003.54	0.7569366
0.880	18000	25287.02	1609.164	29.93	23845.81	11002.78	0.7569273
0.880	18000	25138.33	1605.892	29.90	23697.12	10563.77	0.7517148
0.880	18000	25138.08	1605.886	29.90	23696.87	10563.02	0.751706
0.880	18000	25137.83	1605.882	29.90	23696.62	10562.26	0.7516973
0.880	18000	25137.58	1605.876	29.90	23696.37	10561.51	0.7516885
0.880	18000	25137.33	1605.872	29.90	23696.12	10560.76	0.7516795
0.880	18000	25137.08	1605.862	29.90	23695.87	10560.01	0.7516708
0.880	18000	25136.83	1605.862	29.90	23695.62	10559.26	0.7516621
0.880	18000	25136.58	1605.852	29.90	23695.37	10558.5	0.7516534
0.880	18000	25136.33	1605.846	29.90	23695.12	10557.75	0.7516446
0.880	18000	25136.08	1605.842	29.90	23694.87	10557	0.7516358

Table C-12: Performance calculations for the fourth segment of the mission